UNIVERSITÉ DE MONTRÉAL

FUSION OF HIGH DENSITY LOW PRECISION AND LOW DENSITY HIGH PRECISION DATA IN COORDINATE METROLOGY

MICHAŁ BARTOSZ RAK

DÉPARTEMENT DE GÉNIE MÉCANIQUE

ÉCOLE POLYTECHNIQUE DE MONTRÉAL

ET

FACULTY OF MECHATRONICS

WARSAW UNIVERSITY OF TECHNOLOGY

THÈSE EN COTUTELLE PRÉSENTÉE EN VUE DE L'OBTENTION

DU DIPLÔME DE PHILOSOPIAE DOCTOR

(GÉNIE MÉCANIQUE)

NOVEMBRE 2016

© Michał Bartosz Rak, 2016.

UNIVERSITÉ DE MONTRÉAL

ÉCOLE POLYTECHNIQUE DE MONTRÉAL

Cette thèse intitulée :

FUSION OF HIGH DENSITY LOW PRECISION AND LOW DENSITY HIGH PRECISION DATA IN COORDINATE METROLOGY

présentée par : RAK Michał Bartosz

en vue de l'obtention du diplôme de : Philosophiae Doctor

a été dûment acceptée par le jury d'examen constitué de :

M. ACHICHE Sofiane, Ph. D., président

M. MAYER René, Ph. D., membre et directeur de recherche

M. WOŹNIAK Adam, Ph. D., membre et codirecteur de recherche

M. FENG Hsi-Yung (Steve), Ph. D., membre

M. WALCZAK Krzysztof, Ph. D., membre externe

DEDICATION

I would like to thank my supervisors, Professor Adam Woźniak and Professor René Mayer, for their support and encouragement.

Dziękuję Profesorom Wydziału Mechatroniki a w szczególności Pani Dziekan, Profesor Natalii Golnik za otuchę i nadzieję.
(translation: I would like to thank professors of the Faculty of Mechatronics, in particular Dean Natalia Golnik for cheer and hope.)

Rodzicom i bratu dzięki którym bez obaw wyznaczam sobie kolejne cele, bo wiem, że są ze mną.
(translation: I would like to thank my parents and brother who are always with me so I can set new goals without fear.)

Ani za ogromną pomoc, motywację i wiarę, gdy mojej brakowało.
(translation: Ania thank you for the huge help, motivation and faith when mine was missing.)

Thank you Ania and Xavier for all these splendid days which I spent with you.

Najma, je te remercie infiniment pour avoir toujours réussi à me donner le sourire.
(translation: Thank you Najma for always making me smile.)

RÉSUMÉ

Dans les techniques de mesures tridimensionnelles, les dimensions et la géométrie des éléments sont déterminées sur la base des coordonnées de points. Ces points peuvent être recueillis à partir de méthodes avec ou sans contact. Malheureusement, toutes ces méthodes possèdent aussi bien des avantages que des inconvénients.

Les données issues de mesures sans contact comme la triangulation laser ou les techniques de projection de franges lumineuses se caractérisent par une précision faible, mais une forte densité de points. Les mesures avec contact, quant à elles, produisent des points de faible densité, mais avec une plus grande précision.

Ainsi, il est souhaitable de développer un procédé qui permet la fusion de deux ensembles de données, tout en conservant les avantages et en minimisant les inconvénients.

Cette thèse présente une méthode de fusion, insensible à les caractéristiques des données d'entrée, en particulier dans le cas de mesure sans contact où les propriétés des points recueillis dépendent à la fois de la méthode de mesure et de la stratégie choisie. Ce procédé est applicable pour les surfaces à forme libre.

Dans les méthodes présentées, deux ensembles de données, issues d'une surface, sont recueillis. Un premier ensemble provient de mesure sans contact et fournit des informations complètes sur l'objet mesuré. Le deuxième ensemble résulte de mesures avec contact et représente des points caractéristiques utilisés pour corriger le premier ensemble.

Deux méthodes de détermination des points caractéristiques sont proposées, appelées marqueurs matériels et virtuels. En ce qui concerne les marqueurs matériels, des éléments spéciaux, faits en billes en céramique, sont conçus, fabriqués et montés magnétiquement sur la surface où il est permis. Les centres de ces billes, déterminés à l'aide des données de mesures avec et sans contact, sont des paires de points caractéristiques correspondants, utilisés pour la fusion. Quant aux marqueurs virtuels, les points correspondants sont déterminés à partir de mesure sans contact, sur la base de points recueillis directement sur la surface mesurée, en utilisant la méthode de contact.

Ces deux méthodes sont testées sur des pièces industrielles réelles. Pour les marqueurs matériels d'un plan, une aube de turbine et un couvercle de moteur ont été utilisés. En plus, pour les marqueurs virtuels un réservoir de carburant d'un avion a été utilisé. Les résultats de marqueurs

virtuels sont similaires aux résultats de la simulation par ordinateur. De meilleurs résultats ont été obtenus lorsque la distance entre les points de caractéristique était plus bas. L'incertitude de la mesure a été diminuée de plus de 40%.

ABSTRACT

In coordinate measuring techniques dimensions and geometry of elements are determined on the basis of coordinates of points. These points can be collected using contact and non-contact methods. Unfortunately every method apart from its advantages has also disadvantages.

Data from non-contact measurements like laser triangulation or structured-light projection techniques is characterized by a low precision but high density of points. Contact measurements derive low density of points but with higher precision.

It is desirable to develop a method which allows merging two sets of data, maintaining the advantages and minimizing disadvantages. This thesis presents a method of data fusion insensitive to the characteristics of the input data, especially in case of non-contact measurements, where the properties of gathered points depend both on the measuring method and chosen strategy. The method is applicable for freeform surfaces.

In the presented method two sets of data from a surface are gathered. One set comes from non-contact measurements and provides complete information about the measured object. The second set comes from contact measurements and represents characteristic points used to correct the first set.

Two methods of characteristic points' determination were proposed called material and virtual markers. In material markers special features made of ceramic balls in magnetic mount were designed and manufactured. The centres of these balls were determined using data from non-contact measurements and contact measurements forming pairs of corresponding characteristic points used for fusion. For virtual markers corresponding points from non-contact measurements were determined based on points gathered directly from the measured surface using contact method.

Both methods were tested on real parts from the industry. For material markers a plane, a turbine blade and an engine cover were used. For virtual markers additionally a fuel tank of a plane was used.

Results from virtual markers are similar to results from computer simulation. Better results were obtained when the distance between characteristic points was lower. Uncertainty of the measurement was decreased by more than 40 %.

TABLE OF CONTENTS

DEDICATION III

RÉSUMÉ IV

ABSTRACT VI

TABLE OF CONTENTS VII

LIST OF TABLES IX

LIST OF FIGURES XI

LIST OF SYMBOLS AND ABBREVIATIONS XIV

LIST OF APPENDICES XVII

CHAPTER 1 INTRODUCTION 1

1.1 Description of the problem 1

1.2 General objectives 9

1.3 Hypothesis 9

CHAPTER 2 LITERATURE REVIEW 10

2.1 Coordinate measuring technique 10

2.2 Contact versus non-contact measurements 11

2.3 Part in the coordinate system 11

2.4 Measuring plan 12

2.5 Triangulation scanning 15

2.6 Registration process 17

2.7 Data processing 18

2.8 Measuring accuracy 18

2.9 Error compensation of laser scanning and system calibration 19

2.10 Multisensory architectures and data fusion 20

2.11 Iterative closest point algorithm 23

2.12 Frontier of knowledge 25

2.13 Objectives 26

CHAPTER 3 METROLOGICAL CHARACTERISTICS OF NON-CONTACT TRIANGULATING LASER SCANNING MEASUREMENTS 28

CHAPTER 4 PROPOSED METHOD OF DATA FUSION 38

4.1 Theory 38

4.1.1 Determination of characteristic points using material markers 40

4.1.2 Determination of characteristic points using virtual markers 50

4.1.3 Description of the data fusion method 53

4.1.4 The reliability function 59

4.1.5 Determination of λ parameter 60

4.1.6 Uncertainty analysis 69

4.2 Methodology 73

4.3 Results and discussion 76

4.3.1 Results and discussion for material markers 76

4.3.2 Results and discussion for virtual markers 81

CHAPTER 5 CONCLUSIONS 98

BIBLIOGRAPHY 105

APPENDICES 112

LIST OF TABLES

Table 1.1 : Geometrical parameters of the plano-parallel plate. 5

Table 3.1 : The values of the determined radius for different ways of data processing [42].....32

Table 3.2 : The values of sphericity error for the point clouds [42] 33

Table 3.3 : Selected standards of roughness [43].....34

Table 3.4 : Straightness of cross-sections for reflective surfaces [43].....35

Table 3.5: Straightness of cross-sections for scattering surfaces [43] 36

Table 4.1 : Results of measurements of balls made of different materials [44].....42

Table 4.2 : Parameters of the measured ball - data coverage [46] 46

Table 4.3 : Total deviations for each strategy [49] 50

Table 4.4 : Results of data fusion for a line 67

Table 4.5 : Results of data fusion for an arc.....69

Table 4.6 : The specification of Legex 9106.....73

Table 4.7 : The specification of Accura 7 73

Table 4.8 : The specification of REVscan.....74

Table 4.9 : The specification of MMC80.....74

Table 4.10 : The cube - results of data fusion with material markers 77

Table 4.11 : Turbine blade - results of data fusion with material markers 79

Table 4.12 : Engine cover - results of data fusion with material markers.....80

Table 4.13 : Planar surface - comparison of point clouds with data from the CMM [48].....84

Table 4.14 : Turbine blade - comparison of point clouds with data from the CMM [48] 86

Table 4.15 : Engine cover - comparison of point clouds with data from the CMM [48].....88

Table 4.16 : Plane part - comparison of point clouds with data from the CMM 90

Table 4.17 : Comparison of geometrical parameters for the plano-parallel plate.....95

Table 4.18 : Range of points coordinates for fitted features 97

LIST OF FIGURES

Fig. 1.1: Contact and non-contact measurements of a curve 2

Fig. 1.2: Measuring strategies 3

Fig. 1.3: Cross-sections of point clouds along the scanning direction for all strategies 4

Fig. 1.4: Plano-parallel plate 5

Fig. 1.5: Cross-section of CT data.....6

Fig. 1.6: Comparison between CT measurement and CAD model 7

Fig. 1.7: Traction network.....8

Fig. 2.1: Working principle of laser triangulation [36] 15

Fig. 2.2: Application of ICP algorithm to HDLP and LDHP data 25

Fig. 3.1: Test stand for examination of factors affecting accuracy of laser scanning 29

Fig. 3.2: Influence of the scanning depth 29

Fig. 3.3: Influence of the external lighting on the results, the whiskers represent max/min values 30

Fig. 3.4: Halogen lamp: a) range of results, b) RMS error, the whiskers represent max/min values 31

Fig. 3.5: The number of measurement points for the halogen lamp - different powers, the whiskers represent max/min values.....31

Fig. 3.6: Measuring strategies: a) parallel, b) cross, c) chaotic [46] 32

Fig. 3.7: Sample standards of roughness.....34

Fig. 3.8: Straightness of cross-sections for reflective surfaces 36

Fig. 3.9: Straightness of cross-sections for scattering surfaces.....37

Fig. 4.1: General idea of data fusion method 39

Fig. 4.2: Simulation of systematic errors from non-contact measurements.....40

Fig. 4.3: Different materials of ceramic balls: a) silicon nitride, b) tungsten carbide, c) zirconium oxide, d) aluminium oxide 41

Fig. 4.4: Sphericity error for different diameters [44].....43

Fig. 4.5: Determination of ball's position [44] 44

Fig. 4.6: Metal sleeve for material markers 45

Fig. 4.7: Material markers 45

Fig. 4.8: Ball's data coverage (2D view) 46

Fig. 4.9: Artefact with material markers 47

Fig. 4.10: Measuring strategies: a) single scan, b) perpendicular scans, c) chaotic scan, d) single scan with intensive work of joints, e) high coverage scan [41] 48

Fig. 4.11: 3D and 2D deviation diagrams for strategies: a) single scan, b) perpendicular scans, c) chaotic scan, d) single scan with intensive work of joints, e) high coverage scan [41].....49

Fig. 4.12: Flowchart of virtual markers method [48].....51

Fig. 4.13: Determination of a characteristic point pair: a) • - point cloud from laser scanner, • - point from the CMM; b) determination of virtual sphere around the point from the CMM; c) selection of points inside the sphere (•); d) average of points from inside the sphere • - characteristic point, corresponding to the point from the CMM (•) [48] 52

Fig. 4.14: Pairs of corresponding points 53

Fig. 4.15: Inverse-variance weighting method for a pair of points 54

Fig. 4.16: Concept of correcting vectors [47] 55

Fig. 4.17: Test on different methods of weight determination.....56

Fig. 4.18: Reliability function 60

Fig. 4.19: Research on λ determination on the example of a line 61

Fig. 4.20: Research on λ determination on the example of an arc 63

Fig. 4.21: Data fusion for a line - different density of markers.....66

Fig. 4.22: Data fusion for an arc - different density of markers.....68

Fig. 4.23: Data fusion with uncertainties of characteristic points 71

Fig. 4.24: Results of data fusion taking expanded uncertainty into account 72

Fig. 4.25: The cube with material markers [47] 77

Fig. 4.26: Turbine blade with material markers [47] 78

Fig. 4.27: Engine cover with material markers [47] 80

Fig. 4.28: Planar test part. White markers are used for self-positioning. They enable to determine scanner's relative position to the part [48] 82

Fig. 4.29: Principle of CMM measurements of the part (the actual number of points varies for different part geometry). • - reference data for evaluation of the method, • - characteristic points used for data fusion [48] 83

Fig. 4.30: Comparison between data from a CMM and a point cloud [48] 83

Fig. 4.31: Turbine blade with the 3CB for referencing [48] 85

Fig. 4.32: Comparison of cross-sections of point clouds before and after fusion with reference data [48] 86

Fig. 4.33: Engine cover with the 3CB [48] 87

Fig. 4.34: Measurand – plane part 89

Fig. 4.35: Distances between point cloud from non-contact measurement and reference data before data fusion 91

Fig. 4.36: Distances between point cloud from non-contact measurement and reference data after data fusion 91

Fig. 4.37: Cross section of a point cloud - plane part 92

Fig. 4.38: The magnified edge from Fig. 4.38 93

Fig. 4.39: The curve characterization using characteristic points from contact method 94

Fig. 4.40: Comparison of cross-sections before and after data fusion 95

Fig. 4.41: Comparison between data after fusion and CAD model 96

LIST OF SYMBOLS AND ABBREVIATIONS

3D_dev	tridimensional centre deviation;
a	signal peak on the CCD array;
b	systematic error;
$B_{i,p}(u), B_{j,q}(v)$	normalized B-splines of degree p and q for the u and v directions;
C	constant;
Cor_vect_j	correction vectors;
d	triangulation base;
dist	distance between characteristic points;
$dist_{after}$	mean distance after application of the ICP algorithm;
$dist_{before}$	mean distance before application of the algorithm;
D_i	distances from each characteristic point to the points from the cloud;
E	alignment error in the ICP algorithm;
f	focal length;
F	rigid transformation function;
k	number of pair points;
K	coverage factor;
m	mean time between failures;
max. dev.	maximal difference between position from contact and non-contact measurement;
mean of dev.	mean difference between position from contact and non-contact measurement;
min. dev.	minimal difference between position from contact and non-contact measurement;
n_i	normal vector of plane passing through q_i;

N	number of measurements for weighted average calculation;
p_i, q_i	point-pairs from moving and fixed mesh respectively;
p_{ij}	*j*th measurement coordinate on the *i*th surface patch;
P_{a_f}	position of a point from the point cloud after fusion;
P_{AVE}	weighted average position calculated from P_{CMM} and P_{LS};
P_{b_f}	position of a point from the point cloud before fusion;
P_{CMM}	position of characteristic point from LDHP method;
P_{LS}	position of characteristic point from HDLP method;
q_{ij}	corresponding nearest point to p_{ij};
$r(x)$	vector of the correlation values between the predicted point x and all points of the design of experiments;
$ratio_{imp}$	ratio of improvement;
R	distance between optical centre and measured surface;
R_m	rotation matrix;
$Re(t)$	reliability function;
R_θ	correlation matrix of the design points;
$s(u, v)$	B-spline function;
t	time;
t_m	translation matrix;
T	matrix for rigid body transformation;
$u(x)$	uncertainty of x;
U	expanded uncertainty;
w_i	weights to calculate weighted average;
Vc_i	correcting vectors at characteristic points;

x	any predicted point;
x_{avg}	weighted average of N measurements;
x_{ij}, y_{ij}, z_{ij}	coordinates of the B-spline surface control points ϕ_{ij};
y	corresponding response at points belonging or not to the designed experiment;
σ_a	uncertainty of the photodetector array;
σ_{ave}	uncertainty of the weighted average;
σ_i^2	variance of ith measurement;
σ_R	uncertainty of distance between optical centre and measured surface;
σ_x, σ_y, σ_z	standard deviations of position determination for each direction;
n_u, n_v	number of control points in the u and v directions in B-spline function;
θ	incident angle;
λ	sole distribution parameter;
$\mu_{\hat{y}}(x)$	prediction value;
ϕ_{ij}	control points in B-spline function.

LIST OF APPENDICES

Appendix A – THE SPECIFICATION OF LEGEX 9106 112

Appendix B – THE SPECIFICATION OF ACCURA 7 113

Appendix C – THE SPECIFICATION OF REVSCAN 114

Appendix D – THE SPECIFICATION OF MMC80 115

CHAPTER 1 INTRODUCTION

In contrast to conventional metrology, coordinate measuring techniques rely on computer processing of point coordinates gathered on the part surface. These points are used to characterise measured surface or feature. When large number of points are measured more complex information about the measurand is provided.

Points can be collected using contact and non-contact sensors. In the case of contact measurements high precision coordinates are obtained. The main disadvantages of this approach are the small number of measurement points and the long measuring time. Industry seeks faster and more thorough inspection of machined parts in order to shorten product process development time. An attractive solution is applying non-contact methods where much data of the whole object is gathered in a short time albeit with lower precision.

Unfortunately, every method has its advantages and disadvantages. The complexity and requirements of modern products means that it is often desirable to combine data from two measuring techniques. Therefore, in my dissertation I elaborated a method which allows combining two sets of data, maintaining the advantages and minimizing disadvantages.

1.1 Description of the problem

Results from the measuring process represent the true value of the inspected diameter with some level of uncertainty. It is caused by accuracy of the used, environmental conditions, measuring process etc. Results are burdened with two types of errors: random, which are unpredictable and systematic which are repeatable.

In coordinate metrology there are two methods of points collection: contact and non-contact. Contact measurement provides high accuracy data but density of points is low. Non-contact measurements are less accurate than contact measurements due to the presence of both systematic and random errors. But measurement data covers the inspected part with high density point cloud. Properties of both methods of points collection are presented in Fig. 1.1.

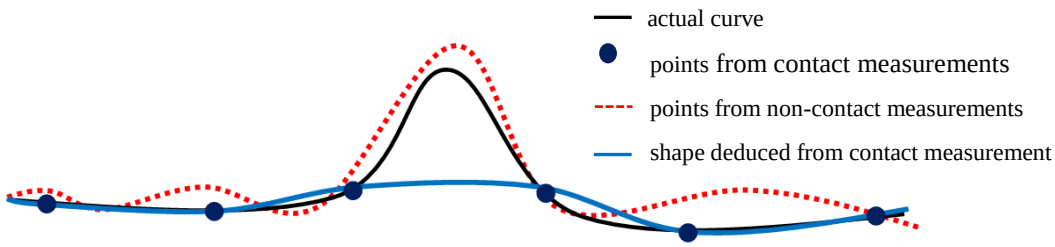

Fig. 1.1: Contact and non-contact measurements of a curve

As we can see from Fig. 1.1 measurement performed only in a non-contact way is characterized by high inaccuracy. Points from contact measurement are characterized by high accuracy, whereas a small number of points can make that the information deduced from them does not represent the actual state.

Inaccuracy of a measurement, which is much more significant in case of non-contact measurements, is caused by both systematic and random errors. Random errors are represented as noise in point cloud from non-contact measurement. Systematic errors are caused by measuring process and the non-contact device and increase the total inaccuracy of results.

As sample devices to present coexistence of measuring errors a measuring arm and a CT scanner were used. Below it is shown, how systematic errors affect the results.

The first system is a coordinate measuring arm equipped with a laser scanner. In [45] the effect of the measuring strategy on the measuring results was described. Five different measuring strategies were chosen (marks of the axes are presented in Fig. 1.2 (5)).

1) The rotary axes (“A”, “C”, “E”, “G”) were immobile, only tiltable axes (“B”, “D”, “F”) were used in the process of data acquisition.

2) Axis “A” was rotated by 180°, during the measurement only tiltable axes were moved.

3) Axes “A” and “G” were rotated by 180°, during the measurement only tiltable axes were moved.

4) The rotary axes were immobile, only tiltable axes were moved but the surface was measured three times in the row.

5) Movement in all seven axes.

The first strategy is the simplest one and can be used in a very limited number of cases, where a part can be measured with a single scanning path without employment of rotary axes. In the

second and third strategies before the measuring process one or two axes respectively were rotated by 180° but during the measurement their positions were not changed. In the fourth strategy the same surface was measured three times so individual scans overlapped. In many situations in real measurements it is impossible to avoid overlapping of scans which might be caused by the complex shape of the surface or unsuitable properties for optical measurements. The last strategy represents the situation in which big parts with quite complex shape are measured. Then all joints are rotated to cover the part with a laser beam.

These strategies are presented in Fig. 1.2

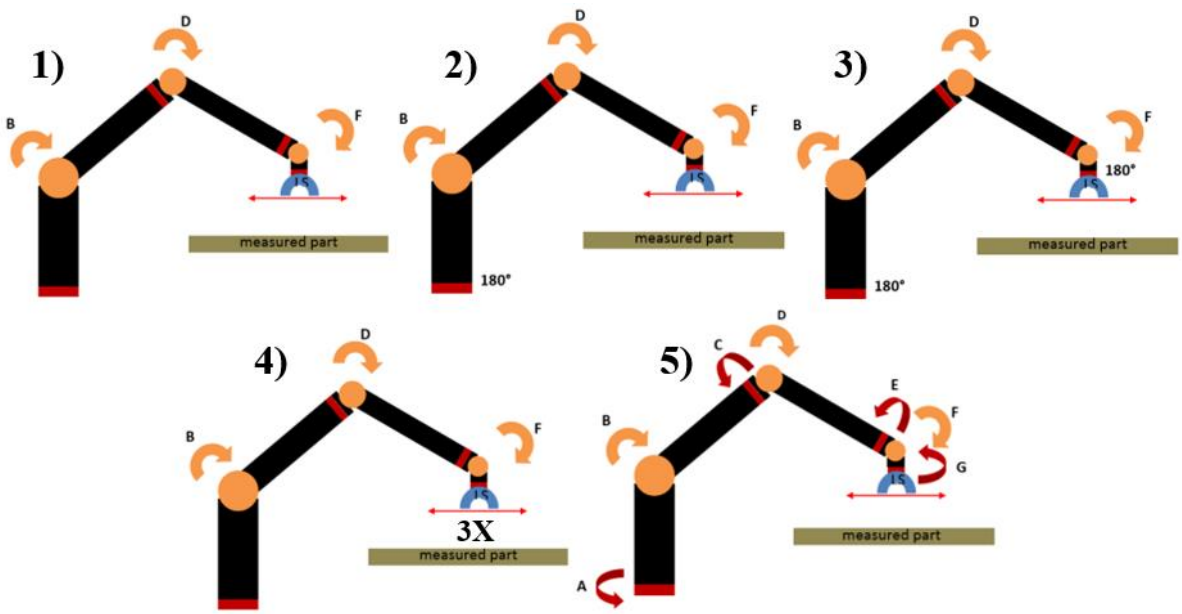

Fig. 1.2: Measuring strategies

Using these strategies a planar surface was measured and cross-sections of the resulting point clouds were analysed. The cross-sections are presented in Fig. 1.3.

Fig. 1.3: Cross-sections of point clouds along the scanning direction for all strategies

As can be seen from Fig. 1.3 results from a measurement using measuring arm equipped with a laser scanner are burdened with two types of errors: systematic and apparently, random. In Fig. 1.3 both types are visible and appear with the same order of magnitude. In Fig. 1.3a systematic error is marked with a black line. As it can be seen the value of systematic error is around 160 µm while random error is up to 40 µm. It means that systematic errors are the main component of the total error.

Another example in which a non-contact measurement provides systematic errors is computed tomography (CT). In computed tomography the part is placed on a rotary table and X-rayed by beam in the form of a line or a cone. Then for each rotation position of the part its 2D image is collected by the detector. From all images the data is processed to create 3D volume rendering of the part. The results depend on many factors. Important factors are: proper positioning of the part on rotary table, set voltage and current of the X-ray tube and also the algorithm used to detect the border between the material and the air.

To show how the CT measurement process introduces systematic errors affecting results the plano-parallel plate presented in Fig. 1.4 was used.

Fig. 1.4: Plano-parallel plate

The plate was measured on a CT scanner and an STL file of the outer surface was created as the internal structure is not an object of my concerns. Then the plate was calibrated on a coordinate measuring machine (CMM) using a high density of points. These points were used to create a CAD model of the plano-parallel plate.

The mesh of triangles (STL) was transformed to the coordinate system of the reference CAD model, created using CMM data, using best-fit algorithms.

Table 1.1 presents geometrical parameters of the used plano-parallel plate computed for CMM reference data and from CT measurement.

Table 1.1 : Geometrical parameters of the plano-parallel plate.

Characteristic	**Reference (CMM)**	**CT measurement**
distance between planes, mm	16.139	16.745
radius of the cylinder, mm	23.417	22.436

Table 1.1 shows how non-contact measurement differs from the reference. The distance between two planes is here defined as a mean value from two distances for two directions - between a plane and centre of gravity of the other plane. A plane is calculated by Gaussian fitting to the measured points while centre of gravity is calculated as average value of coordinates of all points.

The radius has the value of Gauss cylinder fitted to data. For CT measurement this is about 0.6 mm higher while the radius is almost 1 mm lower, which shows that only scaling is not adequate. In order to present the nature of the distortion introduced by the measurement process a cross-section was extracted. It is presented in Fig. 1.5.

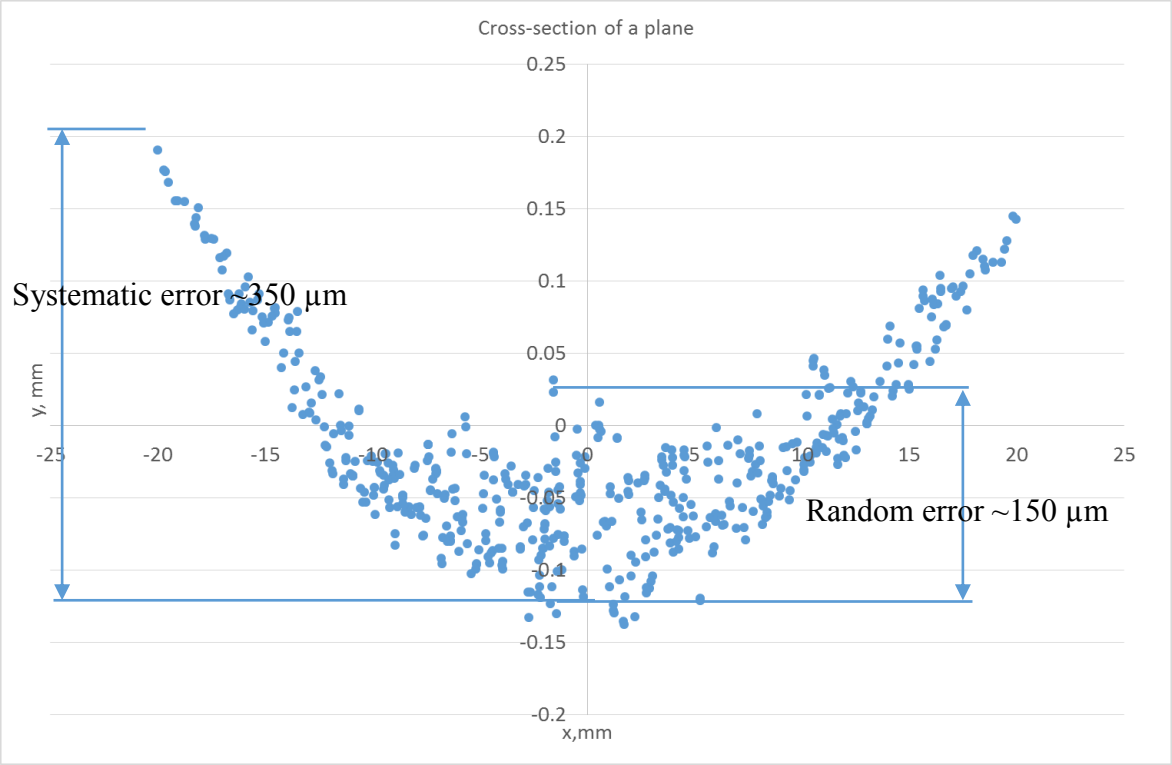

Fig. 1.5: Cross-section of CT data

As can be seen, results are affected by systematic and random errors. The cross-section should be linear, at that scale, while it appears concave. According to manufacturer specification flatness is of 63.3 nm which is negligible. When a line is fitted to this data using Gaussian method its position relative to the true value is incorrect. For this reason the measured height of the plate is also different from the reference. Fig. 1.6 shows a graphic comparison of the CT measurement minus the CAD model.

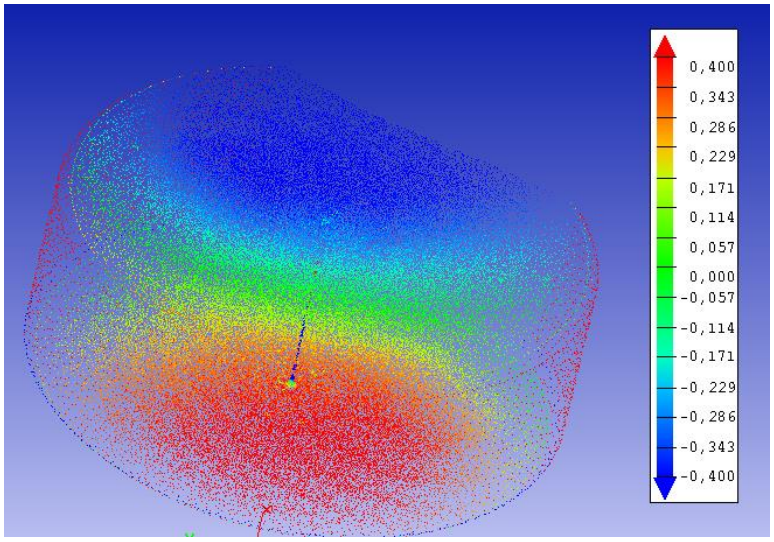

Fig. 1.6: Comparison between CT measurement and CAD model

As presented results showed, non-contact measurements introduce two types of error to the result – systematic and random. So why would not the operator use only contact method which are not susceptible to measurement conditions and provide more accurate data?

In almost all branches of industry, the production of parts requires thorough inspection of the first article and to some extent also every part made. Often, manufactured parts have to be assembled with others so their dimensions should conform to specific tolerances. Depending on the industry and function of the part, tolerances can have different values so inspection should be performed with proportional uncertainty.

On the other hand, measurement should be conducted as quickly as possible to decrease the total time and thereby the cost of the part production. Fast inspection is often contrary to the high accuracy measurement, which is time-consuming.

To solve this problem and to overcome limitations, an accurate and fast inspection method is needed. An idea is to combine data from two measuring methods that have different properties. The first method is accurate but rather slow. The second one is very quick but its accuracy is lower. Fusion of these two methods would provide high accuracy data in relatively short time. The contact measurement may be conducted only periodically if the non-contact method is found to have repeatable systematic errors.

Furthermore, time and costs of the measurements are not the only issues. There are some parts which cannot be measured using only contact methods. The sample part is a membrane keyboard

where areas around pads can be measured using contact methods while pads cannot. Their typical activation force is of 0.4 N. For example the pad would move during measurement with a TP20 Renishaw probe, which trigger force in Z direction is 0.75 N, and the measurement would be disrupted.

Another example is a traction network depicted in Fig. 1.7 for trams.

Fig. 1.7: Traction network

We can observe increase in the power of traction vehicles and an increase of their speed. This causes increase of technical requirements that traction network contact line must meet. Traction network must hang at a certain height. Too big a sag results in an incorrect cooperation between bow collector (pantograph) and the network which is particularly important at high speeds. Therefore, the height of traction network is controlled. Previously, it was measured using a contact measurement with special collector mounted on a traction vehicle but pressure on the traction line affects results. A recently developed method for this height control involves the use of vision systems. As it was shown non-contact methods provide two types of errors – systematic and random. Systematic errors can significantly change the results. In this case the use of two types of measurements, contact and non-contact, could also help. The whole traction network could be measured using the vision system and the result could be corrected using points gathered in contact way in places of network fastening – traction poles.

These examples showed that sometimes fusion of data from two measuring systems is a necessity not dictated solely by time or economic reasons. This makes the subject of data fusion relevant for research.

1.2 General objectives

The main objective of the present research is to fuse data of the same surface but obtained from different measuring methods. Some data may be derived from non-contact measurements like laser triangulation or structured-light projection technique and is characterized by a low precision but high density of points (HDLP). Other data may come from contact measurements and has low density of points but also higher precision (LDHP). The proposed approach is mainly suitable for freeform surfaces because in this case compensation of systematic errors is more complicated and standard methods cannot be used. The main goal is to increase the precision of one set of data, using the HDLP and LDHP sets.

1.3 Hypothesis

The precision of non-contact measurements can be increased by modelling point cloud on the basis of information from more accurate device. Using the proposed methods complex surfaces as well as simple ones with complex dimensions can be treated.

CHAPTER 2 LITERATURE REVIEW

2.1 Coordinate measuring technique

Coordinate measuring techniques are going through rapid developments thanks to the automation of measurements, the integration with CAD / CAM systems and the use of computer analysis and archiving of results. The first and still most common device used in coordinate metrology is the coordinate measuring machine (CMM). The accuracy of a CMM depends on the type of construction and on the measuring head. It is in the range of tens of microns, down to tenths of a micron. For part inspection two technologies can be used: contact and non-contact [27, 37].

In contact measurements high accuracy points from a surface are acquired by physical contact with the surface. The most obvious advantages are a lack of susceptibility to viewpoint or lighting conditions and an ability to inspect regions that cannot be reached by light beam. Another advantage is that CMM equipped with a contact probe can be used to extract features information from a small number of points [26]. The disadvantages are slower measuring speed than in case of non-contact measurements, limitations in the size of the part and the necessity to fasten the measured object [33], which is particularly significant for freeform surfaces [7] and big parts, which require much surface coverage and mechanical motion respectively. Note that when measuring a part with a CMM there are different sources of error like machine and part errors but also triggering probe and probe tip errors [39] . And also there are many factors affecting accuracy of touch trigger probes. Some of them were analysed in [64].

It is worth noticing that the set of measured points only constitute a small sample of the measured feature or surface. For this reason the quality and quantity of information obtained from a CMM depend on the number and distribution of measuring points [34]. Also as CMM software does not detect discontinued areas some information can be lost [63]. There is a need to find a compromise between the number of measuring points and measuring time. From an economic point of view the smallest sample should be chosen, but form errors require finding the maximum values of form deviations from a full-field inspection [40]. Depending on the task, point acquisition by CMM can be conducted in point-to-point and continuous scanning ways [37]. When points are collected in continuous mode, the density of points for a given time is higher, but so is uncertainty [62].

Nowadays faster and more thorough inspection of machined parts in order to shorten product development and production time is requested. An attractive solution is applying optical methods where data from the whole object is gathered in a short time. Unfortunately in optical methods larger uncertainty of points appears that reduces the benefit from higher density of points [37]. Optical methods include: triangulation, ranging, interferometry, structured lighting and image analysis.

A short comparison of contact and non-contact measuring methods was presented in the following subchapter.

2.2 Contact versus non-contact measurements

Both contact and non-contact measuring systems have their pros and cons. Contact systems give accurate data. Moreover scanning and routine operations can be repeated by using created measuring programmes. On the other hand, programming of measurement for complex components is tedious and the digitization is time-consuming. Non-contact scanning is fast and generates high density point cloud but resolution is limited and noise appears. Large memory is required to process the data [27].

In order to compare data from contact and non-contact measurements, both should be put into the same coordinate system. A common method of alignment is the use of three spheres located in the measuring space. They are measured together with the inspected part by all sensors. Then relation between centres of balls from different systems is calculated. Subsequently rotation and translation matrices are computed to minimize distances between these points [27]. To improve this kind of matching, spheres should have high diameters and should be as far as possible from each other [37]. There are also other methods to align part in the coordinate system. They are described below.

2.3 Part in the coordinate system

As in the process of measurement, the important issue is the location of the measuring part. There are a number of methods to define the position of the part in the coordinate system of the measuring device. The first type of alignment is by using some initial points and then by minimizing distances between measured and design points. This method is often called Best Fit Alignment. Another solution is the 3-2-1 approach where six points on three mutually

perpendicular planes are measured [51, 52]. Alas this method is only applicable for parts with plane surfaces [38]. There is also a method similar to the first one but where features are used instead of points. For the location of part in the measuring space dedicated tools and features can be used [38].

There are some problems with CAD-directed dimensional measurements. The first one is that actual measured point can be different from the intended ones. This is because of the lack of knowledge about the exact transformation between the device and the measured object and also due to dimensional errors of the part [38]. Uncertainty of the part's localization is small relative to the size of the part, but more than one order of magnitude than the tolerances allowed by the manufacturing operation [21].

When the part is correctly localized in the measuring volume measuring plan shall be created. The process is described in the following subchapter.

2.4 Measuring plan

A serious limitation in coordinate measurements is the need for skilled workers to prepare the measuring plan. When defining the measurement plan, a basic problem is the selection of the number and location of the measuring points. The three most common methods are blind sampling: uniform sampling (not efficient, especially when small number of points is measured), Latin Hypercube Sampling (uniform projection of the samples on each of the axis of the hyperplane) and Hammersley sequence (compared to the first method, this approach gives a pleasant, less clumped pattern) [14]. The measuring plan is crucial to avoid false conformity positives [1].

In order to design the measuring plan, two kinds of information can be used: a priori information from the machining process or measurement of similar part and in-process information called adaptive measuring plan [40, 1].

There are three factors important in the process of optimization a sampling plan: time, accuracy and completeness of the measurement. For economic reasons, the number of measuring points should be limited but it is highly probable that a small number of points cannot adequately represent the inspected feature [15].

For contact measurements, a sampling strategy presented by Colosimo et al. in [9] can be chosen. The authors suggested choosing measuring points in the areas, where according to the construction requirements, deviation from the nominal value is the most important. This reduces the time and the cost of the measurement while providing crucial information.

For freeform surfaces, because it is not always clear where control points should be located, the conventional method is to create a grid of measuring points on 2D plane and project it on the surface. Subsequently, the obtained structure/pattern or only nodes of the grid are measured with the CMM. The disadvantage of this approach is that it is not relevant for complex shapes [33].

Also the best strategies for optical measurements were analysed. A procedure was presented for creating automatic scanning plan. First, an initial plan is generated and tested. Then it is verified whether all points can be measured with this initial plan and then if necessary, it is modified. Next, on the basis of critical points, scan directions and paths are generated. Finally, depth of field and occlusions are checked [32].

Another approach was presented by Seokbae et al. in [51]. At the beginning, a complex part is divided into some functional surfaces. This is performed on the basis of distances between critical points obtained from the initial scanning. The existence of critical points simply means that the surface on which they appear cannot be measured by a single pass of the scanner. Distances between these points are longer than the length of the laser stripe or the angles between their normal vectors are bigger than doubled the view angle. After these operations a scan path is generated. Finally, depth of field and occlusions are checked. This way, scan directions can be modified or added to generate a final scan path.

When a laser scanning plan is generated, a few constraints need to be satisfied. The first one is the angle between the surface normal and incident laser beam called view angle. It should be less than the value set for a given sensor. The part should also be within the length of the stripe generated by the laser emitter. Measured points need to be on a certain range of distance from the laser source. Determination of the measuring plan should take into account the lack of interference with the measurand and proper preparation of the surface being measured [66].

As was mentioned earlier, from the engineering point of view the number of measuring points should be limited [40]. This speeds up the inspection time of the part.

Edgeworth et al. [15] presented the iterative sampling method to determine a measuring plan on the basis of surface normal measurements. To this end, deviations of points' location and surface normal from the nominal values were used. Afterwards, they created interpolating curves to predict the form error appearing between pairs of measuring points. This curve allows deciding whether the next measuring points are required to complete, within desired confidence limits, the measurement and selecting locations for the next sample. Their algorithm can also be used to identify outliers in a scanned surface data, because outliers can affect significantly the accuracy of the measurement. The limitation of this method is the necessity of having the nominal geometry which prevents its use, for example, in reverse engineering.

To create an adaptive measuring plan a curvature-based approach can be adapted. In this strategy points are concentrated in the areas with higher curvature [60].

Recently, to automate the measuring plan Kriging model began to be used. This model was developed based on works of G. Krige and initially used in mining. Kriging model allows interpolating the response at any location. This is performed by having design of experiment, where stochastic parameters are defined. Prediction value $\mu_{\hat{y}}(x)$ can be expressed by the equation [14]:

$$\mu_{\hat{y}}(x) = \beta + r(x)R_{\theta}^{-1}(y - \beta 1) \qquad 2.1$$

where x is any predicted point, y is a corresponding response at points belonging or not to the designed experiment, r(x) is a vector of the correlation values between the predicted point x and all points of the design of experiments and R_{θ} is the correlation matrix of the design points, β is a set of coefficients. Basically Kriging model is used to iteratively update a measuring plan [40].

In [14] authors presented a strategy for adaptive inspection of parts to limit the number of measuring points. Their method can be adapted for big freeform surfaces, which makes it useful in various industries. The procedure starts with the measurement of initial points which are determined by the Hammersley sequence. Then, first a Kriging model is built. The model allows for iterative addition of points to the design of the experiment. Points are chosen on the areas at risk. The loop is ended when probability of the surface conformity is not smaller than a required confidence interval. Authors tested their algorithm for big parts from the aeronautic industry like: forward pressure bulkhead, upper part of a cockpit and landing gear compartment. Similar

approaches were presented also in [40] and [1]. Unfortunately, it is still time-consuming contact inspection.

Based on developed measuring plan the inspection is performed using selected measuring method.

2.5 Triangulation scanning

As it was mentioned there are few non-contact measuring methods. They include: triangulation, ranging, interferometry, structured lighting and image analysis. In my dissertation I focused mainly on laser scanners based on triangulation because of their broad use in industry. Triangulation scanners are more accurate and cheaper [37] than other non-contact measuring techniques and are faster than tactile methods [57]. Regrettably the uncertainty of laser scanners results is one order of magnitude higher than for contact probes [17]. The working principle of triangulation is as follows. A laser plane is sent by the transmitter to the measured part. The illumination by the laser of the inspected surface is observed by a CCD (charge-coupled device) camera. This gives 2D coordinates of points that are the intersection of the laser beam and the measured surface. The distance between optical centre and measured surface can be calculated from following equation [36]:

$$R = \frac{fd}{a} \cos\theta + d \sin\theta \qquad 2.2$$

where f is the focal length, d is the triangulation base, a is the signal peak on the CCD array and θ is the incident angle. The geometric dependencies are presented in Fig. 2.1.

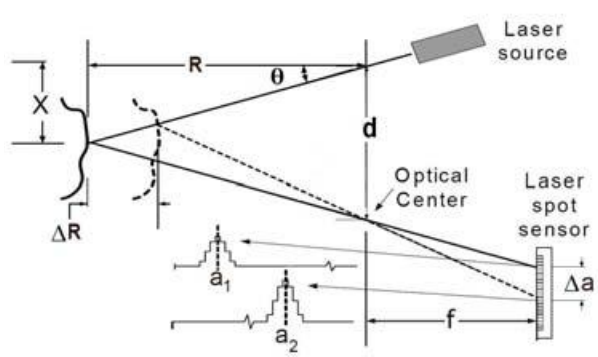

Fig. 2.1: Working principle of laser triangulation [36]

The uncertainty can be computed from the above equation and not including external factors (apart from incident angle) like for instance environmental conditions [36]:

$$\sigma_R \approx \frac{R^2}{fd}\sigma_a \qquad 2.3$$

where σ_a is the uncertainty of the photodetector array.

For the uncertainty calculation, the use of a sensor precision as a sensor accuracy is common and accurate if the variance of the sensor does not change around the measuring range, as it is most influencing factor [36].

The third coordinate value is determined on the basis of the position of the scanner in determined coordinate system or in the coordinate system of the device moving the scanner [11, 57, 18].

Apart from advantages of laser scanning like high speed, high-resolution and non-contact sensing, this method has also some limitations. There are many factors affecting laser scanning accuracy. The most important seems to be the properties of the measured surface like reflection, chemical composition of the material, microstructure and roughness. The best measurement results can be obtained with surfaces that produce a good diffuse reflection at the same wavelength as the laser source [57]. Therefore, a special preparation of the part is necessary in some instances. For example specular or transparent surfaces should be covered for example with special layers [57, 51] of white powder. Moreover geometric obstruction, like relative position between the sensor and the measured surface can affect laser scanning measurement [57, 61, 49]. Ultimately, the combined effects of environment, operation error, data processing, fitting and transformation error must be considered [61].

There are two main strategies when laser scanning is conducted. The first is a global strategy where orientation changes of the scanner during the measurement are minimized. In the second one, called multi-oriented strategy, the laser scanner passing over the surface is swivelling to maintain the laser beam normal to the surface during the entire measurement. However, it was proved that differences between both strategies are insignificant [37].

The most important disadvantage of optical measurements seem to be the lack of knowledge about the measurement uncertainty [37] and how to determine the best methodology for the measurement. To this end, factors affecting the accuracy of laser scanning were widely analysed and discussed by many authors.

In [12] it was shown that when the laser beam is perpendicular to the surface the highest number of points is acquired. Equally important are the distance between the surface and the device and the angle between the laser beam and the normal vector to the surface. A higher resolution is obtained when the sensor is close to the measured surface [57] and at small incident angles [59]. It was also showed that the intensity of the laser should be specified according to the surface colour, shape and roughness. Concerning the surface colour, for most common lasers with red colour of the beam, the best results are obtained for red surface, then for green and blue respectively [58]. Experimental equation used to calculate number of acquired points according to sensor-to-surface distance, longitudinal angle of measurement and relative reflection rate of the measured surface can be determined and then used to correct the measurement [58].

It is important to acquire points over the entire surface. It seems to be obvious that if fewer points are acquired, the quality of scanning is poorer. Additionally, gaps appear in the data that need to be filled by mathematical calculations on the basis of existing points. Moreover, filling gaps is performed according to user-defined parameters. This results in an unknown error.

Concerning illumination conditions, measurements should be conducted in the absence of external light. Although the best results are obtained with the absence of light, this approach is not convenient for many measuring tasks. For this reason often mercury vapour lamps (MVL) are used. This solution is better than halogen illumination regardless of the material of the measured part [3].

In [11] it was presented that errors in laser scanning are caused by two main sources. First is the influence of the laser interaction with the surface. Second are defects and distortions caused by the lenses.

2.6 Registration process

Results of laser triangulation measurement can be strongly affected by improper registration process. For instance, for large parts or objects with complex geometry it is impossible to measure the whole part with a single pass of the scanner. This is another inconvenience in triangulation based measurements.

An important issue in the registration process is that, all scans from different viewpoints need to be transformed into a common coordinate system [20].

There are different approaches to perform this task. The simplest approach seems to be the use of three coordinate balls (3CB) to calculate relations between paired merging views [26]. When using 3CB it is necessary to minimize obstruction of the part by the balls. In determination of rigid transformation following objective function is minimized [26]:

$$F = \sum_{i=1}^{n} \sum_{j=1}^{m} \left| T^{-1} p_{ij} - q_{ij} \right|^2 \qquad 2.4$$

where T is the matrix for rigid body transformation, p_{ij} is the *j*th measurement coordinate on the *i*th surface patch, and q_{ij} is the corresponding nearest point.

Another approach to provide a common coordinate system was presented by Kuang-Chao et al. [30]. In their method first a set of data is considered as fixed and to this data a surface is fitted. The second set is mobile and is transformed to the frame of the first set. Then a blending area is selected and the minimization function is applied in this area.

2.7 Data processing

Data from 3D optical digitization are known to be noisy, inaccurate and presenting gaps. Authors in [31] suggested adding quality indicators like complete "κ" and accurate "τ" to numerical representation of a point cloud. In previous works noisy "δ" and dense "ρ" indicators were listed. Noisy indicator δ is connected with sampling errors. Dense indicator ρ depends on user's scan planning and as the name suggests specifies the density of a point cloud. The completeness shows the importance of existing gaps and the accuracy is a notion of uncertainty.

The common approach to reducing noise is the use of a median filter where point coordinates are replaced by the median values of sets of points from the closest neighbourhood. The drawback is that it is not appropriate for sharp edge features [27]. In a similar way, average filter is also used, but in this case the average value is used instead of the median.

Also very important is the removal of outliers before the fitting process because they can affect the alignment [50]. They do not belong to the measured surface and should not be treated as such.

2.8 Measuring accuracy

Some terms can be presented concerning the quality and utility of measurements. Accuracy is defined by how well the measuring point agrees with the point which is the intersection between

laser beam and the measured surface. Precision is a variation from sets of measurements from the same intersection point [36]. Measurement error is defined by the difference between measured and true values. Uncertainty is defined as follows: non-negative parameter characterizing the dispersion of the quantity values being attributed to a measurand, based on the information used [29]. Uncertainty, in simplification, can also be defined as a collection of all measurement errors [16].

Generally, measurement error can be divided into two categories: systematic and random. The systematic one has always the same value under the same measuring conditions and random error depends on factors affecting laser scanning [57]. In some cases systematic error can be predicted. Ratio between random and systematic error should be small [17] so that compensation of systematic error will give desirable results.

Concerning errors in a laser scanning, it was noticed that, when the projected angle is around 0° the random error is the highest but when projected angle increases the systematic error increases. When scan depth is larger the influence of the projected angle is smaller [17].

A method intended to separate systematic from random error was presented in [56]. To this end a reference plane was measured with different scan depth. The distances between planes were considered to be systematic errors as a function of scanning depth and standard deviation on one plane indicated random error.

2.9 Error compensation of laser scanning and system calibration

In order to overcome the accuracy limitations of laser scanning, attempts to compensate the error were made.

In [5] Bracun et al. presented tests results of a one-shot triangulation system. They measured a surface illuminated by a number of light sheets and observed that the curvature of the stripe increases for stripes further from the central one.

Xi et al. [65] presented a method for laser scanner's error compensation. For this purpose an artefact composed of a ball fastened at a constant distance from a reference plane was used. They observed that measurement error, calculated from the distance between the centre of the ball and the plane, depends on angle and scan depth so an empirical formula for error estimation was determined and used to compensate the errors in actual measurements.

Common approach to calibrate vision systems uses the tip of a CMM probe as a target. The positions of the tip, from optical measurement are determined in various locations in space and are compared with positions indicated by the readout system of the CMM. The ball is used because its view is circular from all angles and its centre position can be calculated easily [52]. A similar approach is also presented in [58].

Santolaria et al. [49] presented another method for camera calibration. For this purpose they created an artefact in the form of an artefact with a set of calibration points. Positions of points from optical measurement were compared with calibrated values and analysed for different positions and angles of the camera.

To obtain knowledge about the measuring error of a particular device, a quick verification test can be performed as in [56] in which a reference plane was measured for different positions and orientations of the laser scanner. Then, a least squares plane was fitted to all points. The fit residuals provide a value for the maximum expected measurement error.

2.10 Multisensory architectures and data fusion

Another approaches to overcome the accuracy limitations of non-contact measurements are multisensory architectures and data fusion. Multisensory architectures are applicable to reduce uncertainty, improve reliability, increase coverage or decrease measuring time. Sensors can be integrated in different ways: mounting of contact and optical probes in the same frame or one measurand can be inspected by separate devices [62, 50]. Sensors registration is necessary.

A classification of data fusion methods was presented by Boudjemaa et al. in [4]. Authors named four methods of fusion: fusion across sensors, fusion across attributes, fusion across domains and fusion across time (filtering). In fusion across sensors the same property is measured by different sensors. In fusion across attributes different quantities, but connected with the same experimental situation, are measured by different sensors. In fusion across domains the same attribute over various ranges or domains are measured by different sensors. Finally, fusion across time, merges new data with historical information.

Representation of data from different measurement methods in the same coordinate system was the impetus that has triggered the researches on methods of fusion of these measurements [50]. The purpose was to take the most appropriate information from each of the method. That

improves the quality and completeness of the measurement. On one hand accuracy of laser scanners is one order of magnitude less than for tactile probe and with much noise but on the other hand triangulation scanning yields data with high density in a short time. That is why recently, integration of contact and non-contact systems is gaining attention [61]. Data fusion may overcome the limitations and drawbacks of the individual sensors like for instance low speed of CMMs [34]. Also, sometimes single sensor cannot derive complete information about the object [62].

Several methods for data fusion were presented. Many authors proposed to use information from non-contact device to create a coarse CAD model of the measured object. Then having a priori knowledge about the part, inspection is performed by contact probe [62, 52, 8, 35]. It is particularly important when the CAD model of the measured object is not available [27].

A similar approach was presented by Carbone et al. in [7]. The integration method is at the level of aggregation of the information, not a physical integration. First, a vision system digitizes the physical object with a structured light scanner, with a mean error within 0.1mm. Then, data is ordered and filtered. After these operations in the CAD environment, curves are reconstructed and a rough model is created. This model has an accuracy of 0.5 mm which is sufficient to create a collision-free measuring path. The rough model is used for digitization and inspection of the part with a CMM. The first digitization Bezier surfaces are created. Finally the created Bezier surfaces are used to perform the inspection again, until the required reconstruction accuracy is achieved.

Freeform surfaces can also be represented by a few parametric equations like Coons patches, B-splines and NURBS (Non-Uniform Rational B-Splines). B-spline can be expressed by the following equation [34]:

$$s(u,v) = \sum_{i=0}^{n_u-1} \sum_{j=0}^{n_v-1} B_{i,p}(u) \cdot B_{j,q}(v) \cdot \phi_{ij} \qquad 2.5$$

where: n_u, n_v are the number of control points in the u and v directions; ϕ_{ij} (i=0,1,…, n_{u-1}, j=0,1,…, n_{v-1} are the n (n=$n_u \times n_v$) control points and $B_{i,p}(u), B_{j,q}(v)$ are the normalized B-splines of degree p and q for the u and v directions respectively.

Measuring points with corresponding location parameters [u_k,v_k] can be represented by [34]:

$$x_k = \sum_{i=0}^{n_u-1} \sum_{j=0}^{n_v-1} B_{i,p}(u_k) \cdot B_{j,q}(v_k) \cdot x_{ij} \qquad 2.6$$

$$y_k = \sum_{i=0}^{n_u-1} \sum_{j=0}^{n_v-1} B_{i,p}(u_k) \cdot B_{j,q}(v_k) \cdot y_{ij} \qquad 2.7$$

$$z_k = \sum_{i=0}^{n_u-1} \sum_{j=0}^{n_v-1} B_{i,p}(u_k) \cdot B_{j,q}(v_k) \cdot z_{ij} \qquad 2.8$$

where: x_{ij}, y_{ij}, z_{ij} are the coordinates of the B-spline surface control points ϕ_{ij}.

In another approach for data fusion, during the measurement, large range devices are used first. Subsequently for specific features devices with smaller range but higher resolution are used. The objective is to limit measuring time. High-resolution measurements are applied only for a limited number of critical positions or features [62].

There are also methods [53, 54] in which data from non-contact sensor is used to determine a set of surface points that are re-measured in a tactile way.

A common approach is to measure the part with different devices and then replace features/surfaces which cannot be measured by one method by data from a more suitable one. For example, when a measured part has small cylindrical holes which cannot be measured by an optical system, the information about these features are obtained from contact measurement [62].

Another common approach to data fusion uses scanning of geometric surfaces with laser scanner and on measurement of accurate features by contact CMM. Then connection between both measurements is created [26]. For this case the mutual position of the sensors is calibrated [27]. For this purpose, calibration targets are used [52]. In [6] authors presented the most common method to calibrate integrated systems composed of CMM and laser scanner. In this method a ball is attached to the CMM's table and is measured by both contact and optical probes. The drawback of this method is that it is accurate only if measurement is performed in the vicinity of the calibration position.

Another method for high- and low-resolution data fusion was presented by Jamshidi et al. in [27] and [26]. CMM and Laser Scanner (LS) data registration uses three balls. Then both sets of data are converted to IGES format. Subsequently, data from CMM are used to reduce the data from LS. If features scanned by CMM are in the neighbourhood of the same features from LS, the LS data, within a desired tolerance, are wiped out and replaced by their CMM's equivalent. At the end, all features from contact measurement are attached to the mesh of triangles from optical measurement. Unfortunately their method can only be used to improve measurement of the part with precision features and is not suitable for freeform surfaces, as for research presented in [61].

There are also some commercial solutions for data fusion. One of them, called VAREA initially generates a triangular patch by the use of a vision system and then the digitization process is performed on a CMM. It cannot process freeform surfaces [34].

An interesting approach was presented in [55]. The authors proposed a method of data fusion from multi-resolution sensors. After measurement of a part using two types of devices features in both are detected. Then Points of Interest (POI) or Regions of Interest (ROI) are used to create the merged model. Points/regions from both methods that are closer to initial model are taken to create the merged model. Authors did not present how their algorithm would work for freeform surfaces without other features.

The subject of data fusion was also considered by Hannachi et al. [22]. In their approach the most accurate system reconstructs the outline of the object, while the less accurate one is used to characterize its 3D surfaces. In this approach distortions in measurements of the surfaces are not corrected.

Senin et al. in [50] used the ICP algorithm for data fusion. A point cloud from optical measurement is iteratively aligned to data from a CMM by finding corresponding points. They also augmented fixed point set to cope with the lack of point co-localization and so improved the registration result. The method requires having points arranged on a regular grid. Therefore as an optical measurement method only structured light scanning can be used. Triangulation laser scanners cannot be used because it is difficult to find specific point in the high density, unorganized point cloud that corresponds to point obtained with the use of CMM.

Colosimo et al. [10] proposed a method of data fusion via Gaussian models. This method uses kriging to predict the coordinates of points based on multiple measurements but putting different weights to data from different sensors.

2.11 Iterative closest point algorithm

In [27, 26] and [50] the merging process was performed by the use of the iterative closest point (ICP) algorithm, where points from overlapping areas are used to find transformation.

Generally in the ICP algorithm, an optimal transformation matrix to move one set of points relatively to another fixed point set is iteratively determined [50].

The ICP algorithm starts with two meshes between which the initial estimation of the rigid-body transformation is calculated. Subsequently, at each iteration the transformation is refined by the selection of new corresponding points in both meshes. Points are chosen from the overlapping areas. The best rotation and translation matrices are determined as to minimize the distance between both meshes [20, 19].

There are two approaches to the ICP algorithm: point-to-point (pt2pt) and point-to-plane (pt2pln). In the pt2pt algorithm, at each iteration, points from the moving set are associated with the closest points from the fixed set and transformation between corresponding points is calculated. In pt2pln algorithm instead of choosing a point from the fixed set, the new closest point is determined on the plane passing through the closest point from the fixed set. Authors proved that pt2pln gives better results [50].

The alignment error in the ICP algorithm is given by equation [19]:

$$E = \sum_{i=1}^{k} \left((R_m p_i + t_m - q_i) \cdot n_i \right)^2 \qquad 2.9$$

where (R_m, t_m) are rotation and translation respectively, (p_i, q_i) are point-pairs from moving and fixed mesh respectively from set of k pairs, n_i is a normal vector of plane passing through q_i (taking into account the points from nearest neighbourhood).

The main disadvantage of the ICP algorithm is that errors from each scans are cumulated [26]. The transform is calculated based on overlapping areas so if points from this region are burdened with error, position of mobile cloud is not optimal. This is particularly visible in the case of a merger of multiple scans. Another limitation of the ICP algorithm is that some features/surfaces need more constraints. In vision systems this problem can be avoided by the use of other constraints, such as colour [19].

In general the ICP algorithm is not matched to the specific problem. It is rather treated as a black box where implementation is not optimized regarding the form of the data. Therefore some points from different datasets cannot be found in exactly the same position of the measurand [50].

To sum up, the most important advantages of the ICP algorithm include: no pre-processing of data and features extraction are required, independency on the shape representation and it is handling all of six degrees of freedom. The disadvantages are, that the ICP cannot be easily

adapted to the weighted least squares extensions, uncertainties of points can be different and the ICP algorithm is sensitive to outliers [2].

Variations of the ICP algorithm exist. In [23] IRF (iterative registration and fusion) and pure ICP algorithms were compared. The IRF consists of two steps. First ICP is used to register data from different sensors or viewpoints, and then a Kalman filter is used to fuse aligned data. The Kalman filter uses a series of measurements that contain noise to estimate unknown variables with higher precision. It was proved that the IRF algorithm is less affected by the number of measurements than ICP but requires an initial estimation of the underlying surface.

2.12 Frontier of knowledge

Recent method of data fusion [50] dedicated to freeform surfaces has many limitations. One is the requirement for the data to follow a regular grid. When data from non-contact measurement is aligned to the data from contact measurements, the dimensional errors of measuring points have a significant influence on the accuracy of this transform. Thus it is impossible to map one set of points exactly to another [33]. ICP algorithm is a rigid transformation and it is only about getting more precise alignment sensitive to noise. There is also no scaling. This means that relations between points do not change, the whole point cloud is treated as a single object. Therefore point cloud modelling is not complete and no real improvement is obtained.

To show how ICP works the following simulation was performed and is presented in Fig. 2.2.

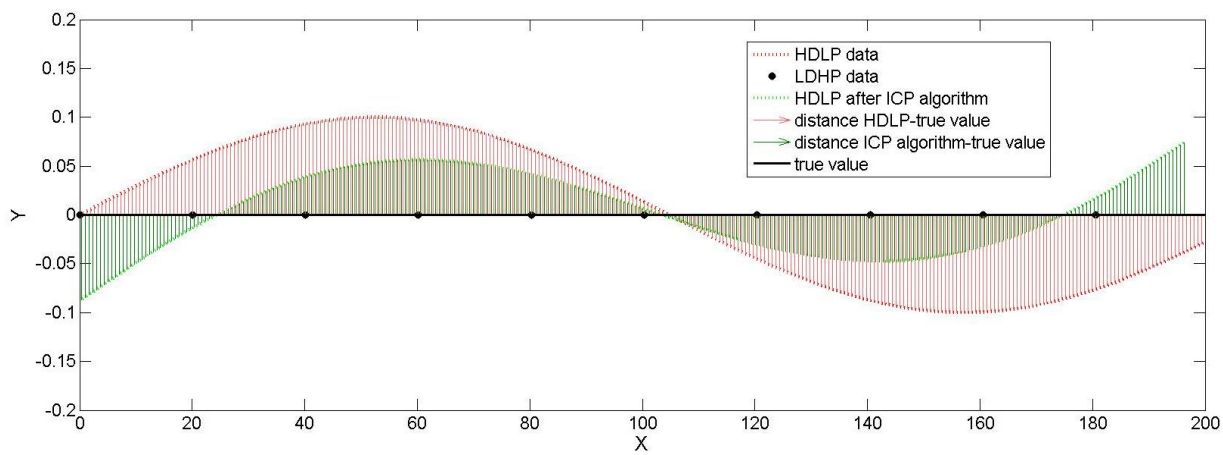

Fig. 2.2: Application of ICP algorithm to HDLP and LDHP data

The analysed curve is a straight line, so this is the true value. From this line high precision points were gathered. They are the LDHP data. The red dotted line is a representation on HDLP data. This type of data is distorted relative to the true curve/surface which will be shown based on real measurements later on. Red, thin arrows represent the distance between HDLP data and the true value. Then using HDLP and LDHP data the ICP algorithm was applied. In this algorithm, at each iteration, the error calculated from equation 2.9 is minimized [19].

The HDLP data after application of the ICP algorithm is transformed (rotated and translated) to the green dotted line presented in Fig. 2.2. The mean distance between the true value and HDLP before and after application of the ICP algorithm was calculated. Then the ratio of improvement was calculated from the equation 2.10

$$ratio_{imp} = \frac{dist_{before} - dist_{after}}{dist_{before}} \cdot 100\ \% \qquad 2.10$$

where $\mathrm{ratio_{imp}}$ is the ratio of improvement, $\mathrm{dist_{before}}$ is the mean distance before application of the ICP algorithm and $\mathrm{dist_{after}}$ is the mean distance after application of the ICP algorithm.

In the presented case the ratio of improvement was of 44.8 %.

The main drawbacks of the ICP algorithm is that the amplitude of initial distortion does not decrease. The HDLP data was only rotated and translated. Additionally HDLP data at X=0 having coordinates exactly the same as true value after application of the ICP algorithm is remote from the true value almost by the value of initial distortion's amplitude.

2.13 Objectives

The aim of the thesis is to develop a method for fusion of data from two measurements of fundamentally different nature: high density low precision (HDLP) and low density high precision (LDHP). In the research freeform surfaces were included due to the inconvenience of their inspection and description. The proposed method is insensitive to the nature of the input data. The method is to be treated on the basis of data from tactile method, laser triangulation (measuring arm equipped with a laser scanner and self-positioning laser scanner) and CT scanner to assess its versatility.

In the proposed method, the processing is carried out on a point cloud and not on surfaces as is used in computer graphics. The reason for this approach is that surface fitting to the point cloud is

somehow averaging or rounding. It is also important to properly choose the number of B-spline control points. To many control points make the surface over-fitting the noisy data and too small a number of points under-fits the data [34]. Therefore in this thesis any parametric surfaces were used because their form and shape depend on user-defined parameters. The human factor as the subjective factor should be avoided. There is also some probability that one operator, creating a surface from the same point cloud, will not do this in the same way every time, which shows the inconvenience of the method. It adds errors that cannot be estimated and included in the final result. In order to merge the measurements from two different methods, fusion at the level of data was done.

To sum up, the proposed method should enable improvement of point cloud from non-contact measurements based on some characteristic points from contact measurements.

CHAPTER 3 METROLOGICAL CHARACTERISTICS OF NON-CONTACT TRIANGULATING LASER SCANNING MEASUREMENTS

Triangulation scanners are more accurate and cheaper than other non-contact measuring techniques and are faster than tactile methods. As laser scanner is the main non-contact measuring method considered within this thesis, its properties were analysed. Some of the factors affecting its measurement accuracy are [61]:

1. projected angle;
2. laser scanning depth;
3. environmental effects;
4. operational error: influence of the operator and measuring strategy;
5. data processing;
6. surface properties: reflectivity, colour, chemical composition, microstructure and roughness.

The first two factors were widely examined by many authors. It has been shown that higher resolution is obtained when the distance between the laser scanner and the measured surface is shorter. As for the projected angle it is recommended to keep the triangulation plane orthogonal to the measured surface.

To examine the influence of the scanning depth a special test stand, presented in Fig. 3.1, was created. It allows testing only one factor at the time.

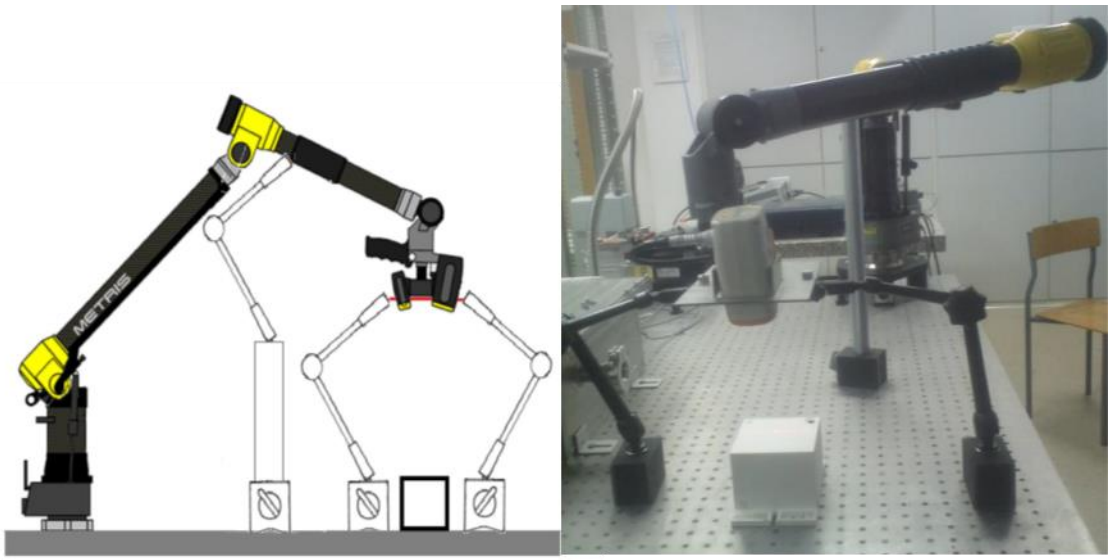

Fig. 3.1: Test stand for examination of factors affecting accuracy of laser scanning

On the test stand the influence of scanning depth was tested. A single line of a white reference cube was measured and a Gaussian line was fitted to data. In Fig. 3.2 the range of results for distances between measured line and the laser scanner for series of measurements depending on scanning depth is presented.

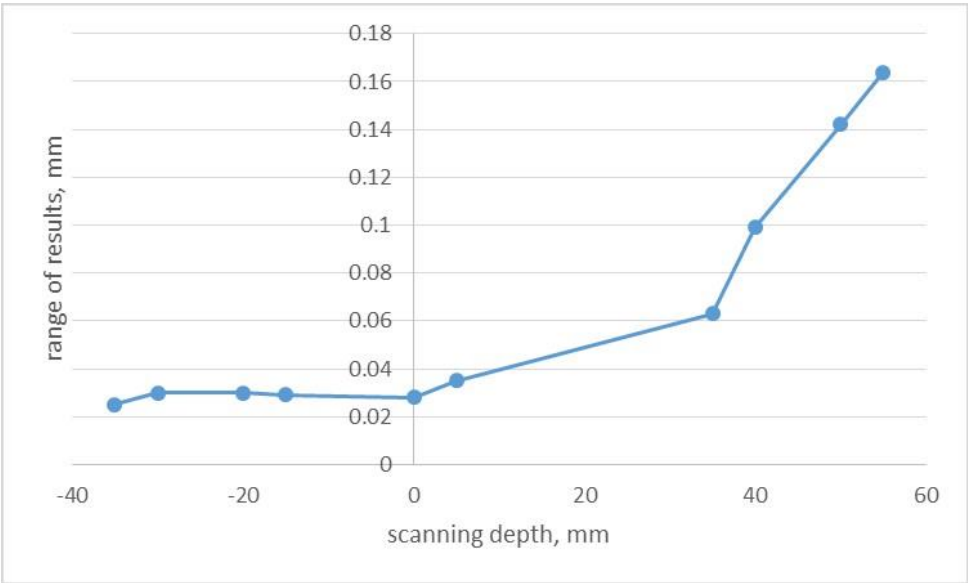

Fig. 3.2: Influence of the scanning depth

The "+" sign means higher scanning depth than nominal (described in the specification of the scanner) and "-" means lower scanning depth.

It is noted that an increase of the distance between the measured object and the laser scanner increases the range of results. Another situation occurs when the distance from the scanner to the plane has been reduced in relation to the optimal position, which depends on focal length and is provided by the manufacturer.

Regarding environmental effects, the impact of external illumination were tested. Different types and different intensities of lighting were used. The same test stand as for Fig. 3.1 was used. A single line, which straightness measured on a CMM was 7 µm, was measured using the laser scanner. The scanner was positioned perpendicular to the measured part and at the most optimal scanning depth, according to manufacturer's specification. Different types of lighting were used: darkness – absence of lighting, glow-tube lamp, halogen and mercury lamp. The illuminance was controlled by the use of a lux meter. The analysed parameters were: straightness of the measured line and number of gathered points. Results are presented in Fig. 3.3.

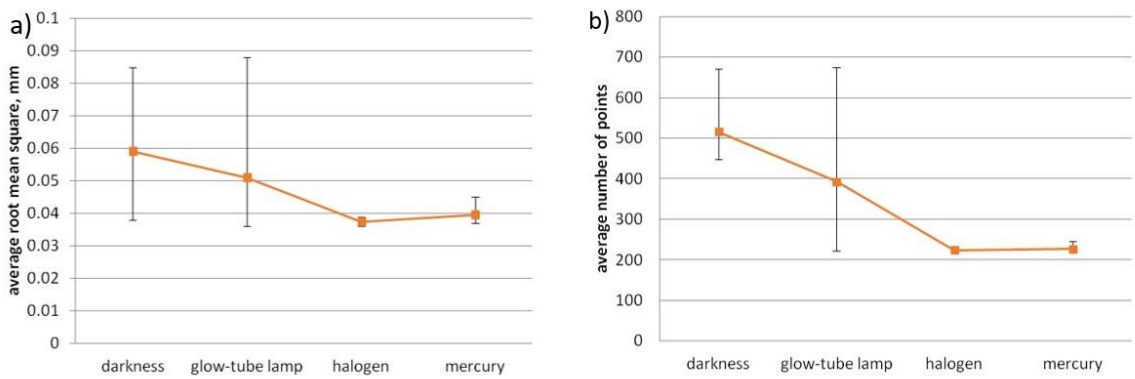

Fig. 3.3: Influence of the external lighting on the results, the whiskers represent max/min values

As can be inferred from the above figure, there is a correlation between lighting and the obtained results. In the absence of lighting RMS error of a line fitted to the data is the highest. It decreases with increasing light intensity. Stronger lighting allows obtaining better results from the same surface. This may be due to the fact that with higher lighting less data points is collected – less projected beam is reflected on the detector, and so an appearing noise is smaller.

In the next phase of the research a halogen lamp with adjustable lighting power was used. Three values were set: 31 lx, 370 lx and 520 lx. Results are presented in Fig. 3.4 and Fig. 3.5.

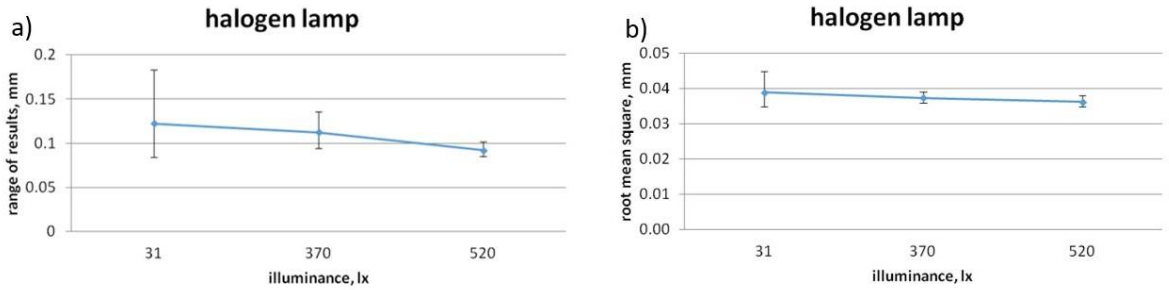

Fig. 3.4: Halogen lamp: a) range of results, b) RMS error, the whiskers represent max/min values

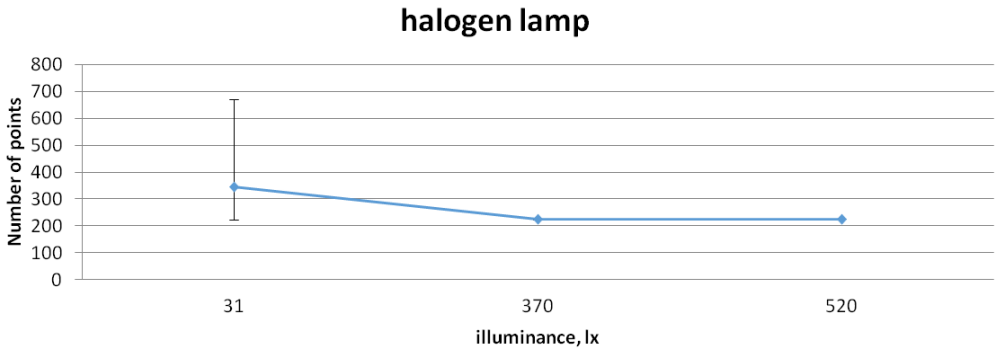

Fig. 3.5: The number of measurement points for the halogen lamp - different powers, the whiskers represent max/min values

As can be sees better results are obtained for higher power of the halogen lamp.

The influence of the measuring strategy was tested and described in details in [46]. Five strategies were chosen: parallel, cross, chaotic, parallel with joints and parallel-roll. The basic ones are presented in Fig. 3.6. In the parallel strategy, scanning of the plane is performed along one direction, so with minimal overlap. In cross scanning, individual scans are crossing at right angle, giving a lot of overlapping scans. A frequent change of directions of scanning is apparent. In chaotic scanning there are frequent changes of directions of the scan but the individual scans overlap minimally. The fourth strategy called parallel with joints is the same as parallel but with smooth movements in joints and the last strategy parallel-roll is the same as parallel but with roll of laser head.

Fig. 3.6: Measuring strategies: a) parallel, b) cross, c) chaotic [46]

Straightness of cross sections were analysed for all strategies. The cross strategy has about twice the value of the straightness compared to the parallel and chaotic strategies showing the significance of overlapping scans. Straightness in different sections for the parallel with joints strategy is close to the cross strategy and to the parallel and chaotic strategies. It can be explained with the axis of rotation, around which cyclical turns of joints were being made. It is recommended, if it is possible, to limit overlapping of scans and also frequent changes in the scanning direction.

The influence of point cloud processing on the accuracy of results was presented in [42]. The experiment was conducted on data from the measurement of an element with small diameter and simple geometry – a ceramic ball. The data was obtained from the non-contact measuring method – laser triangulation. The point cloud (results of non-contact measurement) were processed in different ways: creating a mesh of triangles, and filtered with the median filter, and the average filter. The parameters taken into account in the analysis were the radius of the sphere (nominal value of 3.5 mm) and sphericity error (nominally less than 0.13 μm). Results are presented in Table 3.1.

Table 3.1 : The values of the determined radius for different ways of data processing [42]

	raw data	**mesh of triangles**	**average filter**	**median filter**
mean, mm	3.410	3.385	3.372	3.406
st. dev. μm	16.3	23.7	16.3	16.3
max. value, mm	3.442	3.419	3.403	3.437
min. value, mm	3.381	3.335	3.345	3.377

The first issue to note is comparison of the determined radius value with the nominal value. For the raw point cloud the value of radius is of 90 μm smaller than the nominal value. This may be due to a small radius of curvature but also due to absorption of the laser beam by the material of the ball. Referring to the effects of average and median filters on the "raw" point clouds it can be seen that the average filter decreases the mean value of the determined radius by about 30 μm more than the median filter. It should also be noted that the mesh of triangles, which is a routine procedure in most software for the analysis of point clouds resulted in an increase of dimension error from 90 μm (for raw data) to about 120 μm. It is therefore important that actions used to process point clouds were individually selected to the specific data.

The values of sphericity error for all types of data were also analyzed. Results are presented in Table 3.2.

Table 3.2 : The values of sphericity error for the point clouds [42]

	raw data	**mesh of triangles**	**average filter**	**median filter**
mean, μm	346	230	292	338
st. dev. μm	81.8	55.0	44.2	70.9
max. value, μm	524	332	402	477
min. value, μm	233	145	232	226

Taking into account the sphericity error it can be seen that the mesh triangles reduces the error to the greatest extent. Creating a mesh of triangles also reduces the volume of data. It is however primarily improvement in visual look of a point cloud representing the ball, which is not connected with the accuracy of measurements. Considering Table 3.1 and Table 3.2 it can be concluded that for small parts when it is important to determine their diameter it is preferable to work on raw point cloud or to improve the look of a cloud, for computer graphic, to use median filter. In general the use of filters to measurements of small parts disrupts the results. Based on this conclusion in all research, whenever small balls were measured, the raw data was used.

In non-contact measurements the properties of the measured surface are very important. The influence of the roughness, determined by the roughness standards, and of reflectivity was analysed. The research was fully described in [43]. Sample standards of roughness are presented in Fig. 3.7.

Fig. 3.7: Sample standards of roughness

Standards of roughness were divided into scattering and reflective (both can be seen in Fig. 3.7). From both groups four standards with different parameters of roughness were chosen. As a roughness parameter Ra was used. An effort has been made to choose sample with similar Ra parameters from both reflective and scattering standards. Selected eight samples were measured using contact surface profilers and parameters are presented in Table 3.3.

Table 3.3 : Selected standards of roughness [43]

Reflective surface (Ra, µm)	**Scattering surface (Ra, µm)**
33.0	26.7
9.1	9.4
4.7	5.1
0.9	1.4

Measurements were performed in the perpendicular and parallel direction to the surface roughness profile. In each direction for each surface a series of 10 measurements were performed. Sections perpendicular to roughness profile were measured. The non-linear trend was removed, similarly as measuring roughness using contact profiler, and straightness of these lines were determined. From ten values of straightness for each section their averages and standard deviations were calculated.

Results are presented in the Tables 3.4 and 3.5. Table 3.4 includes the mentioned parameters for reflective surfaces, while Table 3.5 includes the parameters for scattering surfaces.

Table 3.4 : Straightness of cross-sections for reflective surfaces [43]

	perpendicular		**parallel**	
Ra, µm	**straightness, µm**	**st. dev., µm**	**straightness, µm**	**st. dev., µm**
33.0	225	25.7	184	59.6
9.1	64	12.6	113	59.3
4.7	68	22.1	64	47.1
0.9	68	28.4	69	30.7

Table 3.5: Straightness of cross-sections for scattering surfaces [43]

	perpendicular		**parallel**	
Ra, µm	**straightness, µm**	**st. dev., µm**	**straightness, µm**	**st. dev., µm**
26.7	116	18.6	91	5.1
9.4	60	12.1	48	4.6
5.1	54	7.2	45	3.9
1.4	53	5.8	43	3.8

Results are also presented in graphs. Straightness for reflective and scattering surfaces are shown in Fig. 3.8 and Fig. 3.9 respectively.

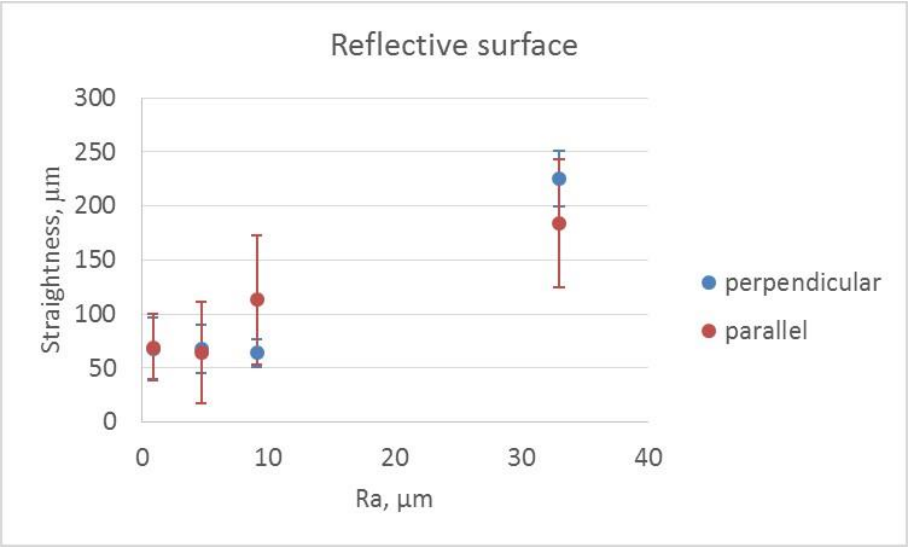

Fig. 3.8: Straightness of cross-sections for reflective surfaces

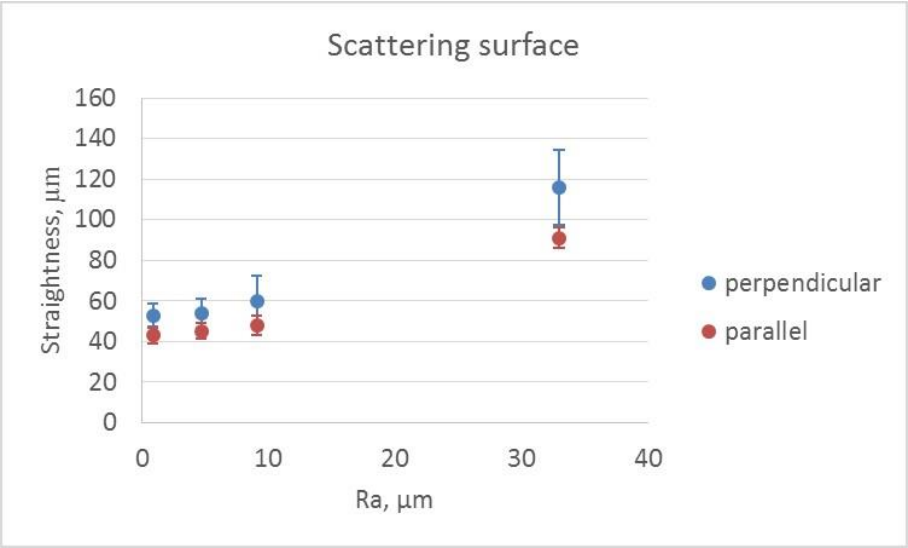

Fig. 3.9: Straightness of cross-sections for scattering surfaces

The first thing, which should be noted, is that straightness of sections is higher in case of reflective surfaces than for scattering. It shows how reflective surfaces are improper for non-contact measurements. For this type of surfaces standard deviation of conducted measurements is higher in case of parallel scanning.

Much better results were obtained for scattering surfaces. It can be noted that with decrease of the roughness both straightness and standard deviation decrease. For scattering parts the measured surface is better reproduced by the scanner. Higher roughness reflects the laser beam so standard deviation is higher. For scattering surfaces more accurate and stable results are obtained when the part is measured in the direction parallel to the roughness profile.

It can be concluded that in order to reduce the impact of the measured surface properties on the results part should be prepared for measurement, for example by applying appropriate coating.

The presented results helped to understand the nature of non-contact measurements and to conduct in future this type of measurements in the best manner, to achieve as high accuracy as possible.

CHAPTER 4 PROPOSED METHOD OF DATA FUSION

4.1 Theory

The general idea of data fusion method is presented in Fig. 4.1. The inspected part is measured using a non-contact method. It covers the whole part with high density and high coverage point cloud. Then using a contact method a set of characteristic points is gathered from the part (A). They will be used to correct the point cloud from non-contact measurement. These characteristic points can be represented by material or virtual markers. Both methods were developed and presented below. Then having a set of characteristic points from contact method a corresponding set (B) is sought in point cloud from non-contact method. Before this, it is ensured that both data are in the same coordinate system. Having two sets of characteristic points a matrix relation functions between them is determined (correcting vectors). It says how much and in which direction points from the B set should be transformed to be at the positions of corresponding points from A set. All pairs of points are considered separately, so relation between them changes. Then based on correcting vectors, correction vectors are determined. These are vectors which should be added to all points from the initial cloud to correct it. Their values depend on correcting vectors and their distances to each point from the cloud. Detailed equations are presented in the following subchapters.

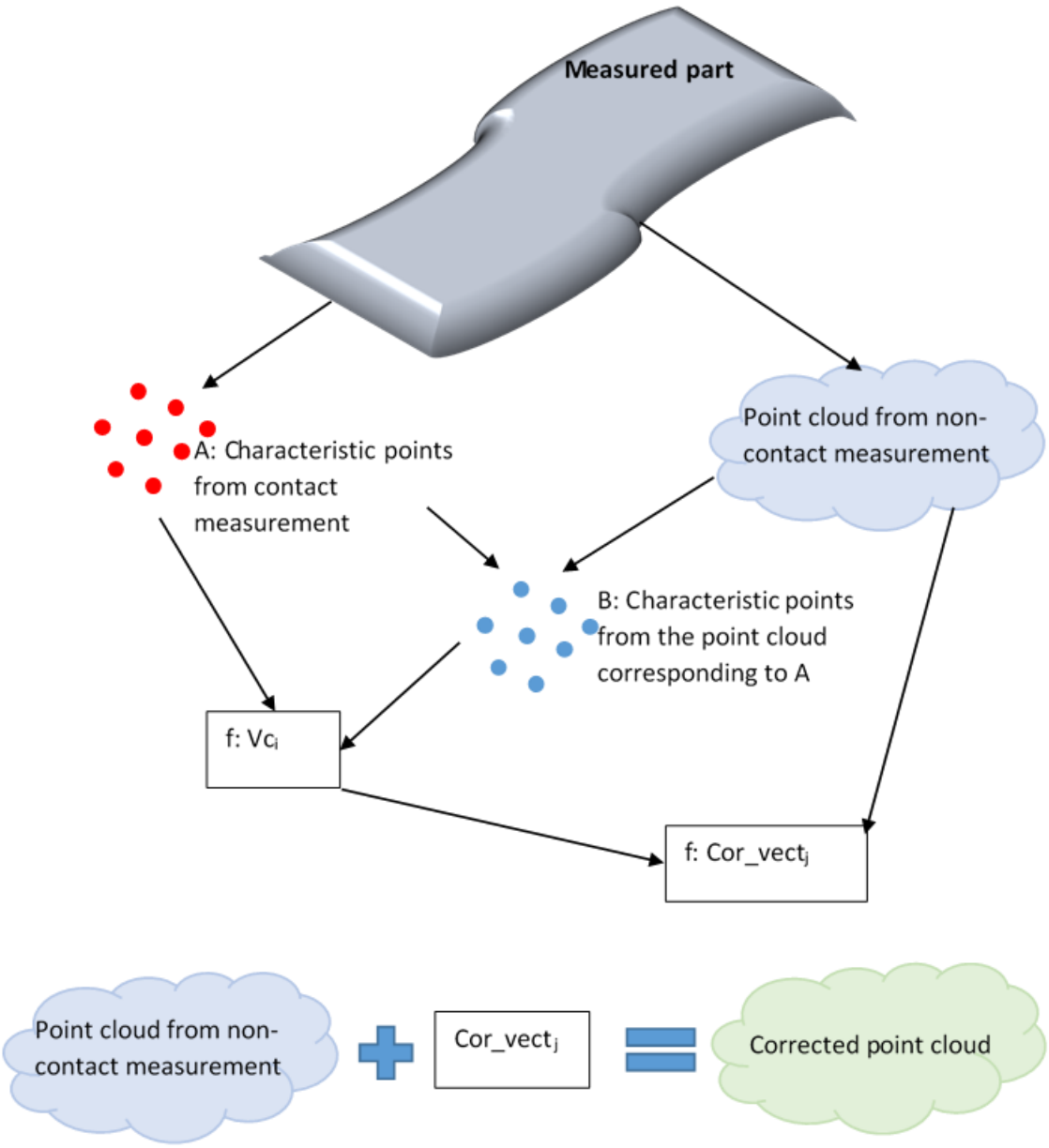

Fig. 4.1: General idea of data fusion method

The point cloud from non-contact measurement should be corrected because as it was already mentioned resulting point cloud is distorted by systematic errors. This property of non-contact measurement was presented in Fig. 1.3. A reference planar surface with low flatness error was measured using a measuring arm equipped with a laser scanner. From the whole point cloud from the measurement cross-sections were analysed.

The amplitude and frequency of changes depend on many factors from which the most important is measuring equipment. As in my tests I mainly used measuring arm fitted with a laser scanner

systematic errors of non-contact measurement were simulated based on data from this device. The amplitude of systematic changes was set as 100 µm. Their frequency depends on measuring strategy and experience of the operator. For the testing of presented method the assumed frequency of 1/200 mm.

For the purpose of testing various fusion approaches a sine shape was used for the simulation of systematic errors coming from non-contact measurements as shown in Fig. 4.2.

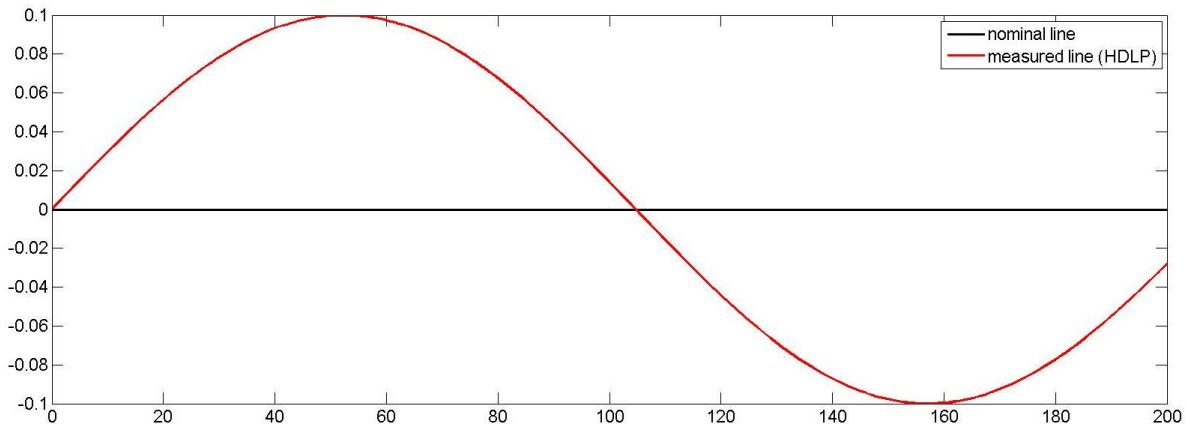

Fig. 4.2: Simulation of systematic errors from non-contact measurements

Results from non-contact measurement were presented as continuous line to show the high density of points from inspection using this method.

4.1.1 Determination of characteristic points using material markers

To determine characteristic points which could be measured using both contact and non-contact methods special features were used. As non-contact measurements are burdened with systematic errors but also with noise single points used as characteristic one would not be relevant. From this reason it was decided to use balls which are attached to the measured surface. For both methods determination of characteristic points is similar.

Contact method (for each ball):

- single points are gathered from the surface of a ball,

- to these points a Gaussian sphere (with known diameter) is fitted,

- centre of the Gaussian sphere is a characteristic point,

- procedure is repeated for all balls attached to the surface which gives the first set of characteristic points (from contact method).

Non-contact method:

- the whole surface of the part is measured together with the surfaces of the attached balls,

- the points belonging to each ball are segregated,

- to all points belonging to one ball a Gaussian sphere (with known diameter) is fitted,

- centre of the Gaussian sphere is a characteristic point,

- procedure is repeated for all balls attached to the surface which gives the second set of characteristic points (from non-contact method).

In this procedure a characteristic point is an average value from many gathered points. This way, the errors of individual points are averaged and positions of characteristic points are more reliable. It is particularly important for the non-contact measurements.

In order not to introduce additional errors the used balls should have high precision. Among many materials ceramic balls were chosen, as they are manufactured with small sphericity errors.

The first thing to do was to select a material with the best optical properties. The chemical composition of the ball should ensure that the laser beam is neither scattered nor absorbed by the surface. In the research four materials were tested: silicon nitride, tungsten carbide, zirconium oxide and aluminium oxide. They are presented in Fig. 4.3.

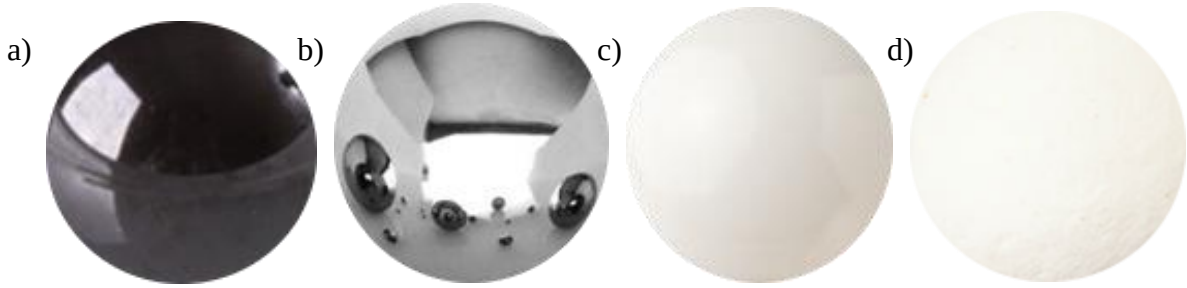

Fig. 4.3: Different materials of ceramic balls: a) silicon nitride, b) tungsten carbide, c) zirconium oxide, d) aluminium oxide

A simple test was performed. It was checked whether the laser beam intersects with the real surface of the ball. Location of measuring points outside the ball demonstrates significant surface

reflectivity, and gathering points inside the ball demonstrates absorptivity of ball's material. Balls of different materials were measured and their diameters were determined and compared to nominal values. The comparison is presented in Table 4.1.

Table 4.1 : Results of measurements of balls made of different materials [44]

Material	**Nominal diameter, mm**	**Measured diameter, mm**	**Measured-nominal, mm**
silicon nitride	12.700	12.765	0.065
tungsten carbide	6.350	7.910	1.560
zirconium oxide	15.875	15.451	-0.424
aluminium oxide	12.700	12.417	-0.283

Comparing the difference between the measured and nominal diameter it can be seen that material with the best optical properties is silicon nitride. Tungsten carbide has high reflective properties, while zirconium oxide and aluminium oxide absorb the laser beam.

Further studies were performed on balls made of silicon nitride. Balls with a diameter ranging from 12 mm to 5 mm were used to determine the smallest one which position can be measured with relatively high accuracy using non-contact method. Small diameter is desired not to obscure the measured surface. The first tested parameter was sphericity error. Its value for each diameter was shown in Fig. 4.4.

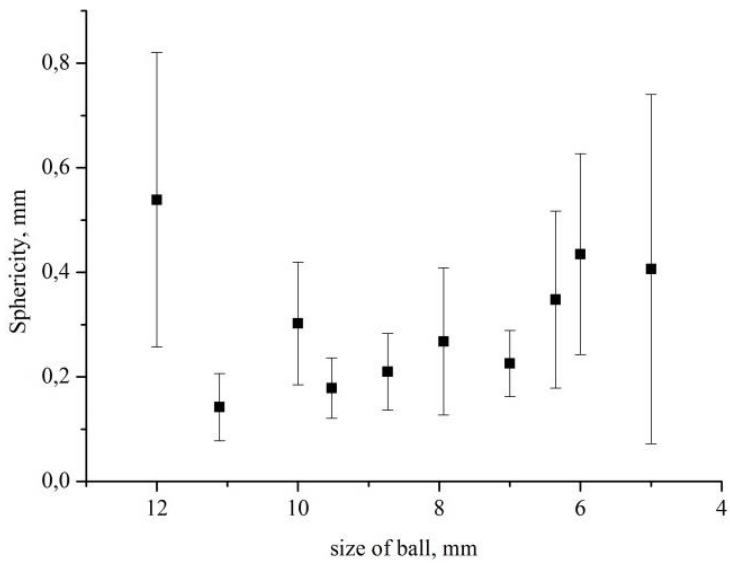

Fig. 4.4: Sphericity error for different diameters [44]

The curve of sphericity as a function of balls diameter may indicate a negligible effect of the radius of curvature on values of sphericity. It is rather due to properties of surfaces, environmental conditions and errors of the measuring device.

More important parameter is the stability of the position of the centre of the ball. Results are presented in Fig. 4.5. 3D centre deviation was calculated from the following equation:

$$3D_dev = \sqrt{\sigma_x^2 + \sigma_y^2 + \sigma_z^2} \qquad 4.1$$

where σ_x, σ_y, σ_z are standard deviations from a series of 20 measurements of the fixed ball, separately for each direction.

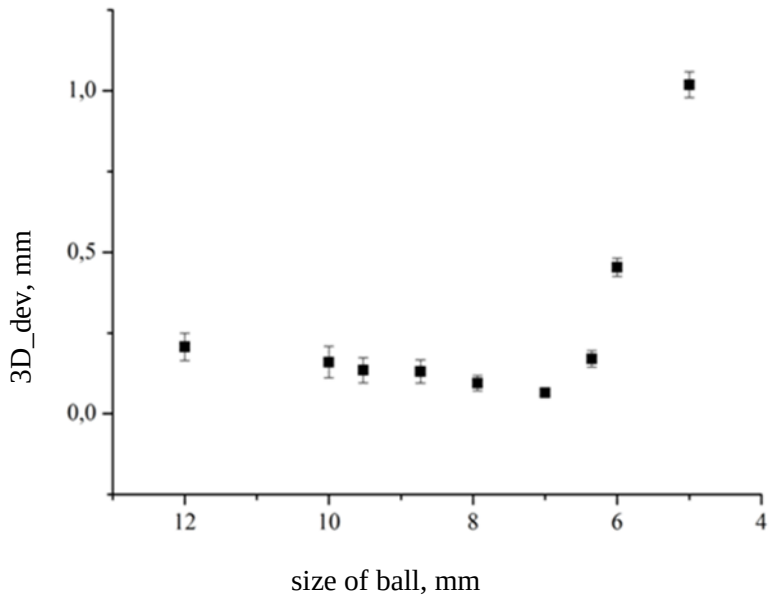

Fig. 4.5: Determination of ball's position [44]

It can be seen that the stability of centres of balls determination is maintained at a similar level up to the ball with a diameter of 7 mm. Subsequently a rapid increase is noticeable. This is due to the fact that in smaller balls percentage of random points and noise is much higher. From the smaller surface smaller number of points is collected so that any noise is more significant.

Based on the presented research ceramic balls with a diameter of 7 mm made of silicon nitride were used to make material markers. Being aware that gluing of markers to the surface is troublesome and can damage the measured surface markers were designed and made that can be fixed to the surface magnetically. For this purpose metal sleeves presented in Fig. 4.6 were used.

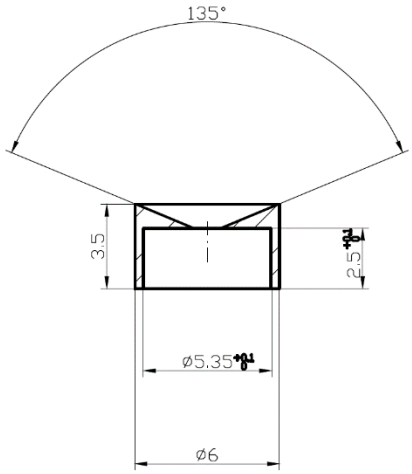

Fig. 4.6: Metal sleeve for material markers

From one end a neodymium magnet was glued, from the other the ceramic ball. The made markers are presented in Fig. 4.7.

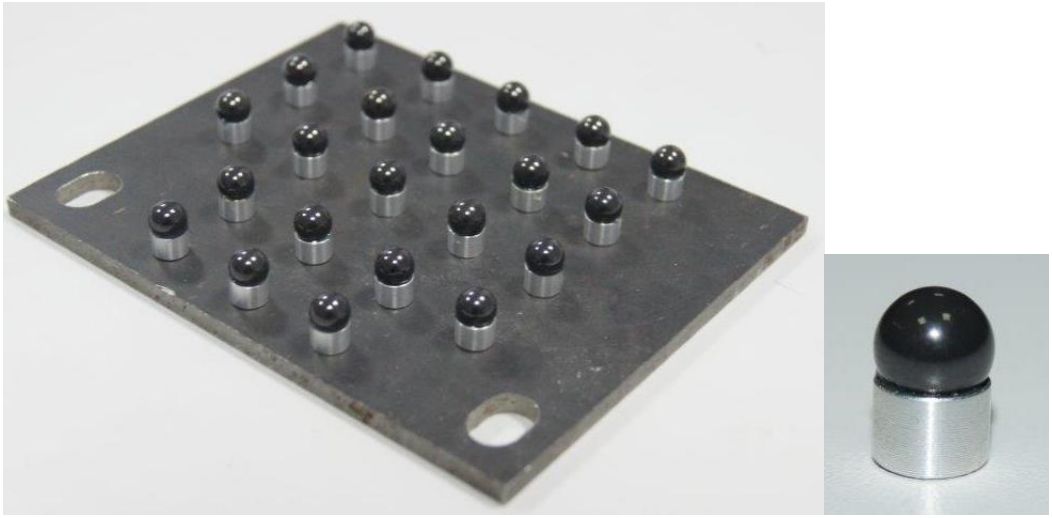

Fig. 4.7: Material markers

The next thing to examine was the influence of coverage of data on positioning of material markers. In low data coverage measurement only the upper area of the surface is measured as in Fig. 4.8a while in high data coverage measurement all available area of the ball's surface is measured as in Fig. 4.8b.

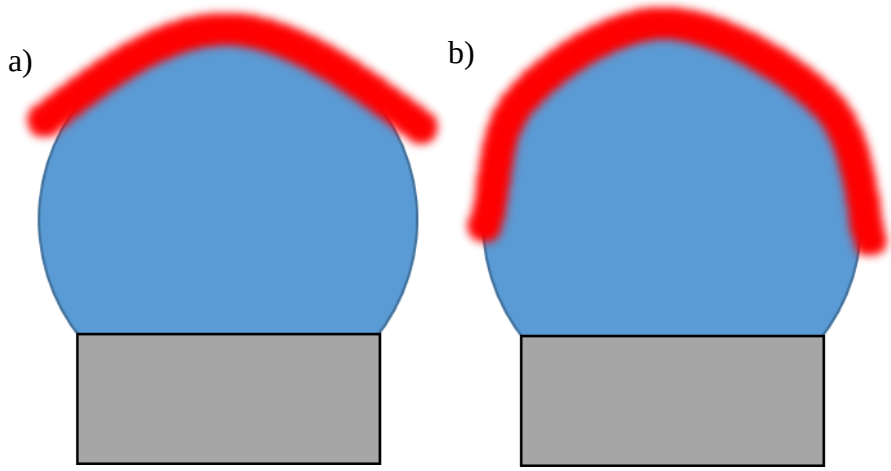

Fig. 4.8: Ball's data coverage (2D view)

For the ceramic ball made of silicon nitride with higher diameter (12.700 mm) it was checked whether high cover data, obtained from more scans that overlap each other, has better accuracy. As comparison parameters sphericity, sphere diameter and stability of the centre position were chosen. Results are presented in Table 4.2.

Table 4.2 : Parameters of the measured ball - data coverage [46]

parameter	**Low data coverage**	**High data coverage**
sphericity, µm	176	394
diameter, mm	12.758	12.751
σ_x, µm	34	10
σ_y, µm	37	19
σ_z, µm	61	24

Sphericity error is more than twice as large for high coverage measurements as a result of overlapping scans. The difference between the calculated diameters for both manners of measurement is insignificant and smaller than 8 µm. It also does not differ much from the nominal value which is 12.700 mm. It can be concluded that low coverage measurement gives

enough information to determine the diameter, so for economic reasons this strategy is recommended.

Problem of ball's accurate measurements was also considered by [28]. Authors found generation of profiles and their matching as very important issue.

In case of determination of position it is better to gather more coverage data. Instability of the centre calculated on the basis of standard deviations in each direction is 79 μm and 33 μm for low and high density measurements respectively.

This research has proven the significance of the measurement strategy and therefore the tremendous influence of the operator.

The final step was to check the influence of scanning strategy for a grid of material markers attached to the surface. A special artefact presented in Fig. 4.9 was created.

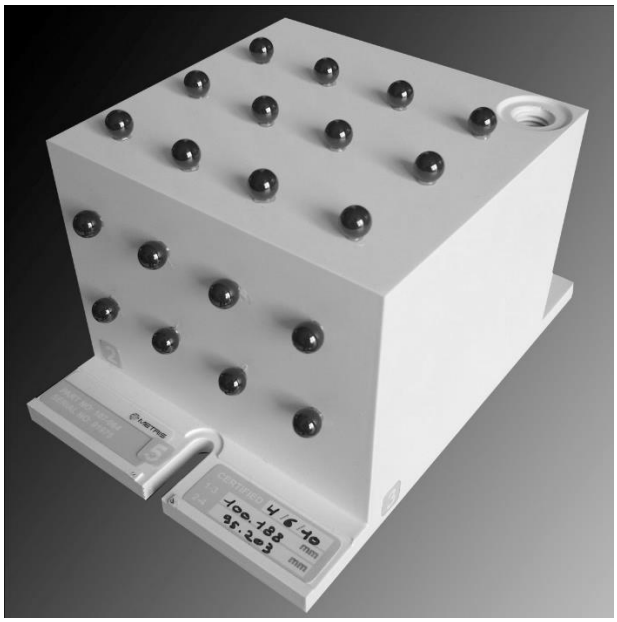

Fig. 4.9: Artefact with material markers

Using the artefact the impact of the measuring strategy on ball artefact measured geometry was analysed. The reason to consider this case was to explore how selected measurement strategies affect the measured positions of the material markers. Measurements were performed using a measuring arm equipped with a laser scanner with five different strategies. These strategies were:

- S1. single scan,

- S2. perpendicular scans,
- S3. chaotic scan,
- S4. single scan with intensive work of joints,
- S5. high coverage scan.

Strategies were similar to those performed on a plane and presented in [44]. They are presented in Fig. 4.10.

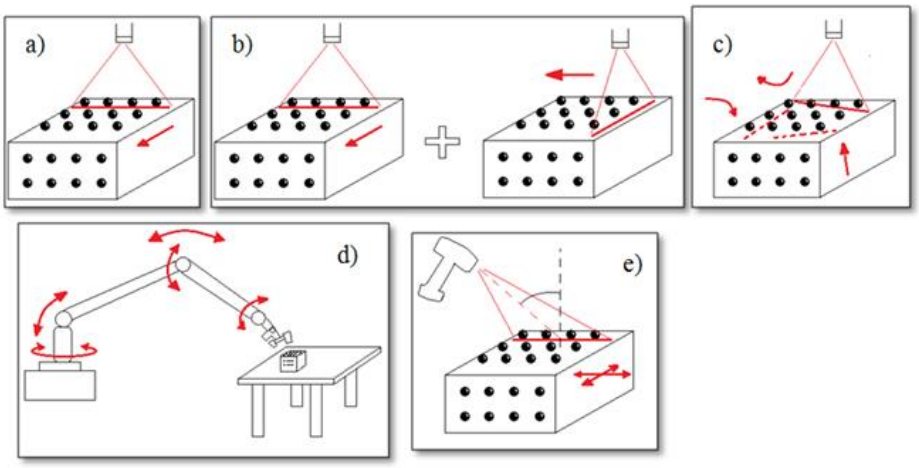

Fig. 4.10: Measuring strategies: a) single scan, b) perpendicular scans, c) chaotic scan, d) single scan with intensive work of joints, e) high coverage scan [41]

The artefact was measured on a Zeiss Accura CMM to obtain positions of the markers represented by the centres of the balls and to treat them as true values. From point clouds gathered from non-contact measurements for each strategy, the centres of balls were determined. Then centres of balls from laser scanning were aligned to centres of balls from CMM on the basis of the least sum of squares. Deviations between positions of the markers from non-contact measurement and contact measurement for all strategies are presented in Fig. 4.11. For deviations amplification factor of four was applied to make them more readable.

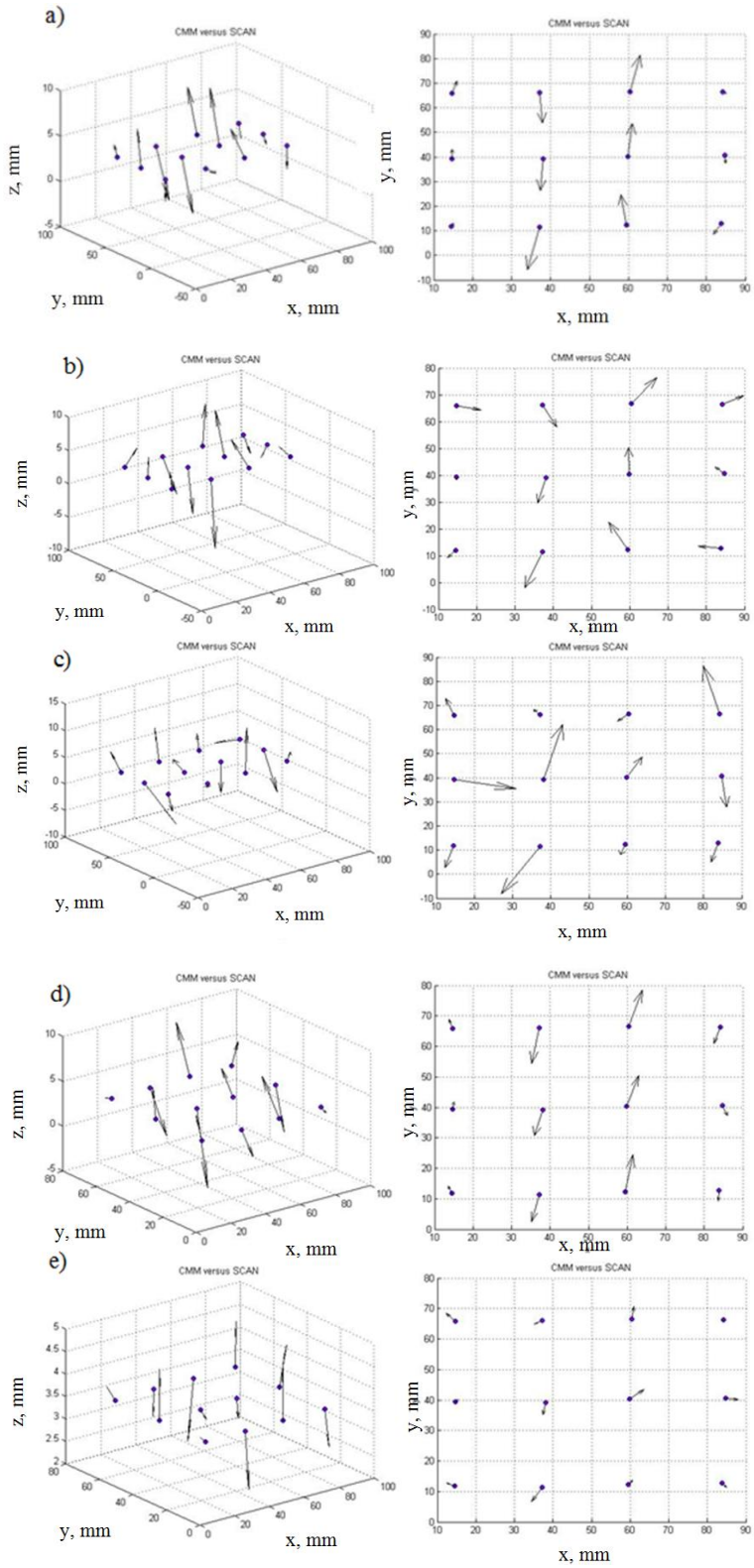

Fig. 4.11: 3D and 2D deviation diagrams for strategies: a) single scan, b) perpendicular scans, c) chaotic scan, d) single scan with intensive work of joints, e) high coverage scan [41]

Table 4.3 shows values of deviation for all strategies for the analysed markers.

Table 4.3 : Total deviations for each strategy [49]

strategy	Max. dev., mm	Min. dev., mm	Mean of dev., mm
single scan	3.509	0.408	1.864
perpendicular scans	3.397	0.661	1.807
chaotic scan	4.711	1.122	2.665
single scan with intensive work of joints	2.647	0.628	1.628
high coverage scan	1.130	0.231	0.619

Where: max. dev. is maximal difference between position from contact and non-contact measurement, min. dev. is minimal difference between position from contact and non-contact measurement, mean of dev. is mean value of this difference.

From the above table it can be seen that the highest deviations are for the chaotic scan strategy and the smaller deviations for the high coverage scan strategy. It is observed that coverage of data should be high to improve the accuracy, but often changes of scanning direction are not recommended as they can affect the measuring process. All further experiments with the use of material markers were performed respecting these directives.

4.1.2 Determination of characteristic points using virtual markers

The second method of determination of characteristic points uses so called virtual markers. This method eliminates the necessity of fastening additional features to the surface. These features cover the measured surface and a gap in information of the measured surface appears. The flowchart for the virtual markers method is presented in Fig. 4.12.

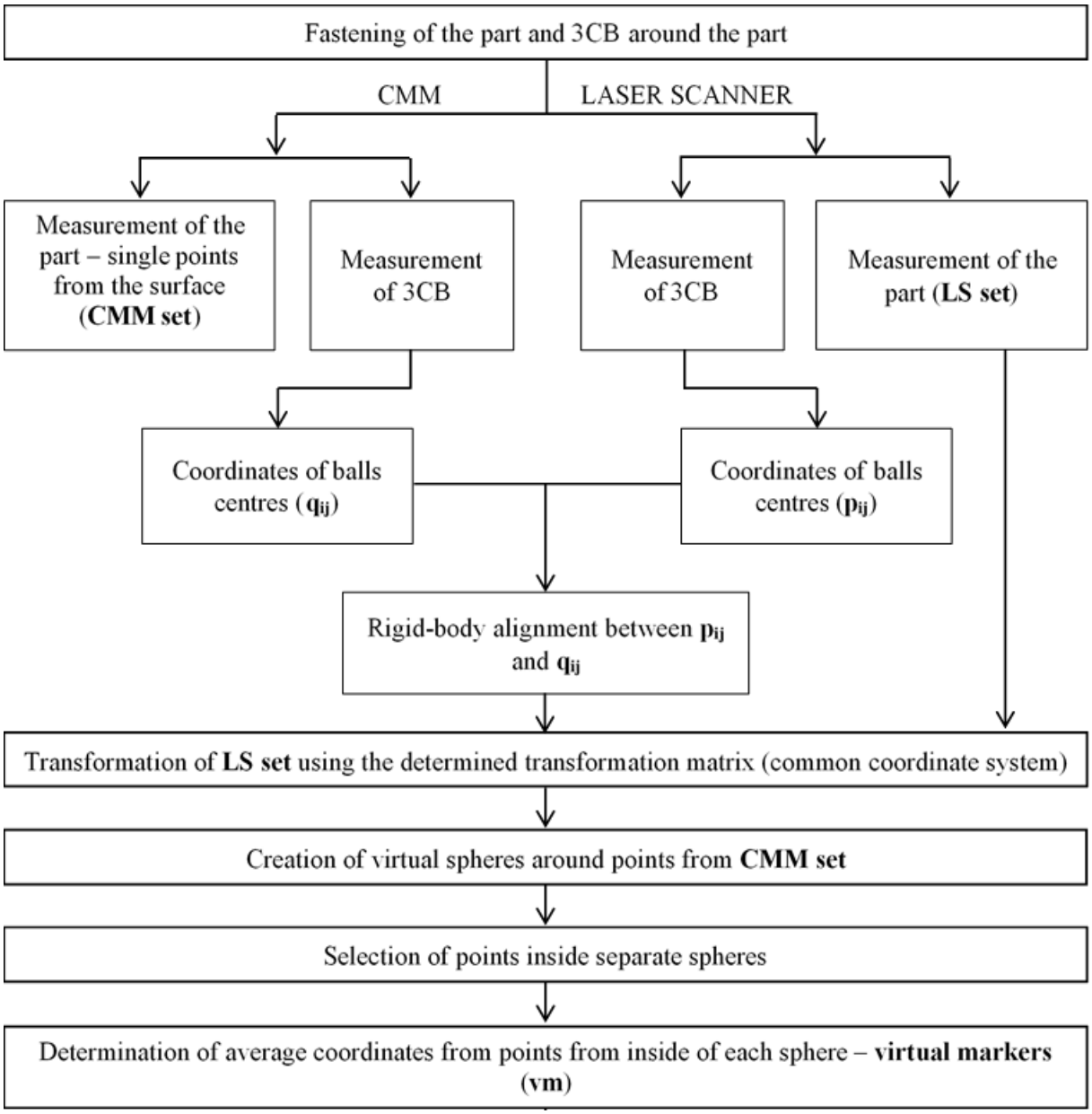

Fig. 4.12: Flowchart of virtual markers method [48]

First, the measured part to avoid movement when the probe contacts with the surface. Three precision balls (3CB) are fixed around the part on the measuring table to which the part was fixed, so as not to hinder the measurement of the part. Those balls ensure a common coordinate system for the two sets of data coming from the sensors. Then, the part and the 3CB are measured using the laser scanner or more generally using non-contact sensor, and the coordinate measuring machine (CMM) or other equipment measuring in the contact manner. The contact points are gathered on a regular grid in order to have evenly distributed data.

The relation between the balls centres from both sensors is analysed and characterized by a rigid-body transformation. This transformation matrix is then applied to the whole point cloud from the non-contact measuring system.

After these operations the main part of the virtual markers method can begin. The first set of characteristic points comes from contact measurements. A regular grid of points was gathered. Then around these points virtual spheres are defined. As both measurements were in a common coordinate system, each sphere includes points from the point cloud – non-contact measurement. For all spheres separately, the average coordinates from these points are computed. This gives a second set of characteristic points coming from the non-contact method and corresponding to the data from the contact method. The diameter of the spheres is determined to be minimal but enclose at least fifteen points from non-contact method. Bigger diameter would make the method insensitive to the curvature of the measured surface. Smaller diameter would not give reliable average value. The process of determination of the second set of characteristic points is illustrated in Fig. 4.13.

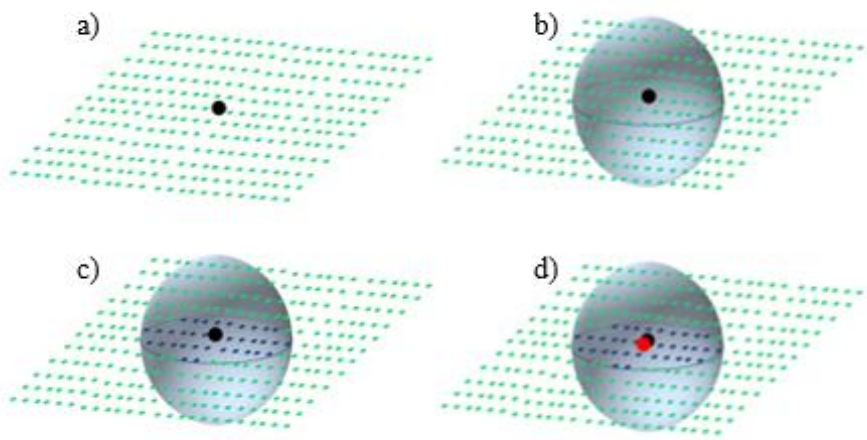

Fig. 4.13: Determination of a characteristic point pair: a) • - point cloud from laser scanner, ● - point from the CMM; b) determination of virtual sphere around the point from the CMM; c) selection of points inside the sphere (•); d) average of points from inside the sphere ● - characteristic point, corresponding to the point from the CMM (●) [48]

4.1.3 Description of the data fusion method

The concept for combining of data from different measurement methods is to determine in both types of data corresponding characteristic pairs of points. It can be done using the two methods described above – material or virtual markers. In each pair the coordinates of the point from (LDHP) low density high precision measurement (contact measurement) is treated as a reference for the corresponding point from (HDLP) high density low precision (non-contact) measurement. These pairs of points are presented in Fig. 4.14 for simulated data.

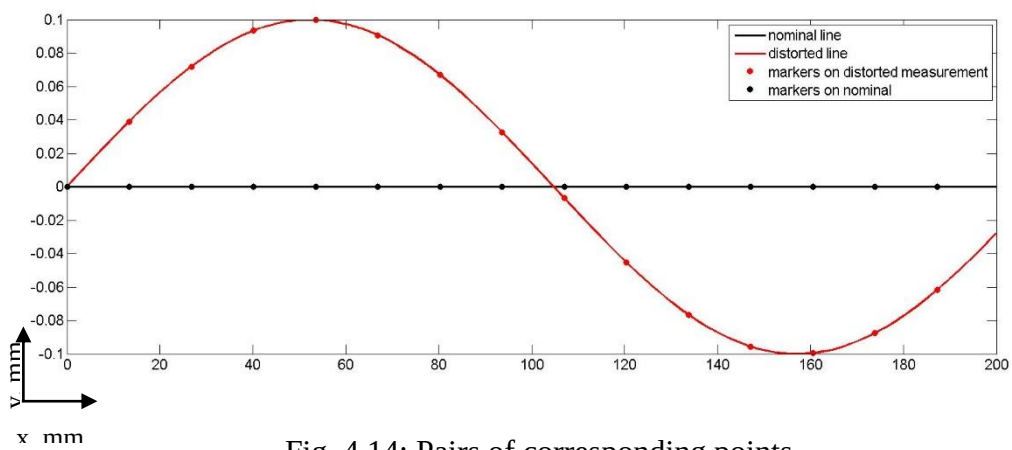

Fig. 4.14: Pairs of corresponding points

Nonetheless, in real measurements the uncertainty of these characteristic points, for both contact and non-contact methods, is non-zero. The larger the ratio of non-contact measurement uncertainty to contact measurement uncertainty, the influence of contact measurement on non-contact measurement is larger.

Therefore it was decided to treat two points from a pair as two measurements of the same quantity performed using two devices with different uncertainty. A typical behaviour in this case is the use of weighted average, where the weights are dependent on the uncertainty of each measurement. It is calculated according to the equation:

$$x_{avg} = \frac{\sum_{i=1}^{N} w_i \cdot x_i}{\sum_{i=1}^{N} w_i} \qquad 4.2$$

where x_{avg} is a weighted average of N measurements, x_i are subsequent measurements and w_i are the weights dependent on the uncertainties of each measurement.

To minimize the variance of the weighted average the inverse-variance weighting method known from statistics was used. Inverse-variance weighting is typically used in statistical meta-analysis to combine the results from independent measurements. The advantage of this method is that the inverse-variance weighted average has the least variance among all weighted averages. According to this method $w_i = \frac{1}{\sigma_i^2}$, where σ_i^2 is the variance of the *i*th measurement.

The uncertainty of the weighted average can be calculated from the equation:

$$\sigma_{ave} = \frac{1}{\sqrt{\sum_{i=1}^{N} w_i}} \qquad 4.3$$

The behaviour of the inverse-variance weighting method can be illustrated through the example of two measurements of the same quantity using devices with different uncertainties as in a pair of corresponding points as shown in Fig. 4.15.

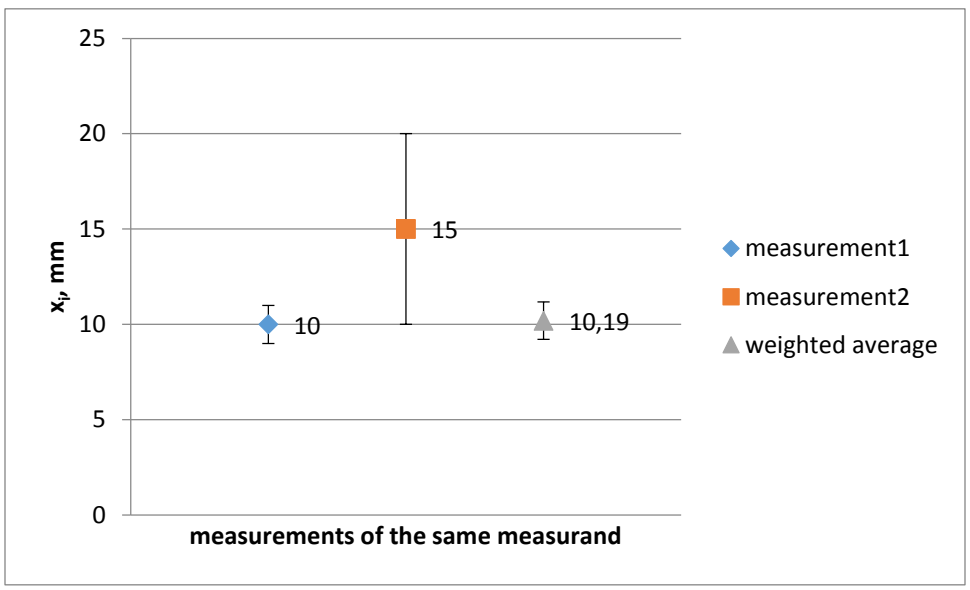

Fig. 4.15: Inverse-variance weighting method for a pair of points

As it can be seen from the graph the weighted average differs little from the measurement having five times lower uncertainty and also has lower uncertainty than each separate measurement. Therefore this point is taken as a point from low density high precision measurement instead of the initially gathered point. This approach allows taking into account the situation when the uncertainty of a LDHP measurement is not much lower the uncertainty of HDLP measurement. Then the information from low precision method influence more on the measurement result.

After finding corresponding pairs of points in both types of data, fusion is performed. As characteristic points from low density high precision measurements (the weighted average from two points as described above) are considered as a reference, the transformations are being performed in such a way to transform points from high density low precision measurements as close as possible to the position of corresponding points from the LDHP measurements, considering the fact that the shape of the surface/curve between characteristic points should not be deformed as a result of the merger.

The direction and value of the correction is described by correcting vectors. The correcting vectors are computed as a difference in the coordinates of characteristic points from LDHP measurements and corresponding points from HDLP measurements. The transformations of all points from the point cloud are calculated based on all correcting vectors and distances from them, according to the equation:

$$Cor_vect_j = \frac{\Sigma Vc_i \cdot w_i}{\Sigma w_i} \qquad 4.4$$

where Vc_i are correcting vectors at characteristic points (difference between points from LDHP and HDLP measurements), Cor_vect_j are correction vectors at each point of the point cloud, w_i are weights dependent on the distances D_i from each characteristic point to the points from the cloud. Closer vectors should have a bigger influence but still for each point from the point cloud, all correction vectors (from characteristic points) should be used. Each point from a point cloud is treated as a separate object, which means it is transformed in its own direction by its own value. Thus the relations between the points from the cloud change. The explanatory scheme is presented in Fig. 4.16.

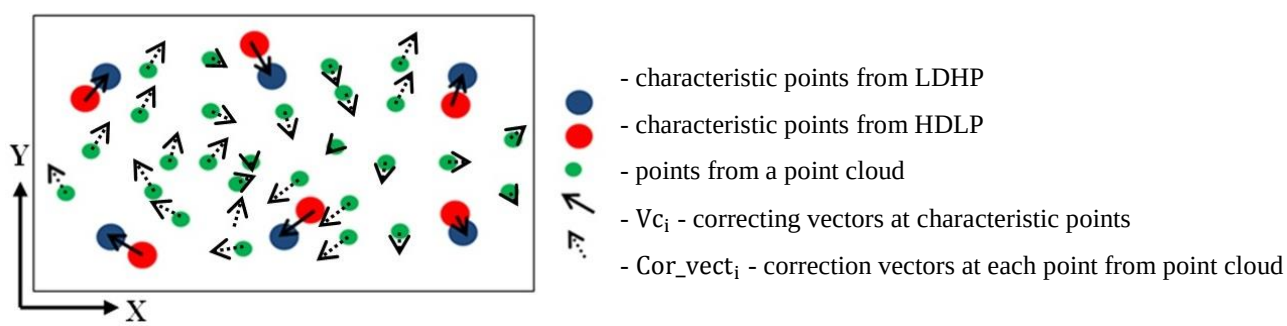

Fig. 4.16: Concept of correcting vectors [47]

In the next step different ways of determination the weights w_i were studied to choose the one having the best properties. To make the operation of the fusion algorithm more visible tests on weights were performed on a planar curve. Initial distortion was increased to make improvement provided by data fusion method more visible. Eight different methods for weights determination were selected: $\frac{1}{\sqrt{D}}$, $\frac{1}{D}$, $\frac{1}{D^2}$, $\frac{1}{D^3}$, $\frac{1}{1+D^2}$, $\frac{1}{1+D^3}$, $\frac{1}{1+D^4}$, $e^{-\lambda D}$. The results was presented in Fig. 4.17

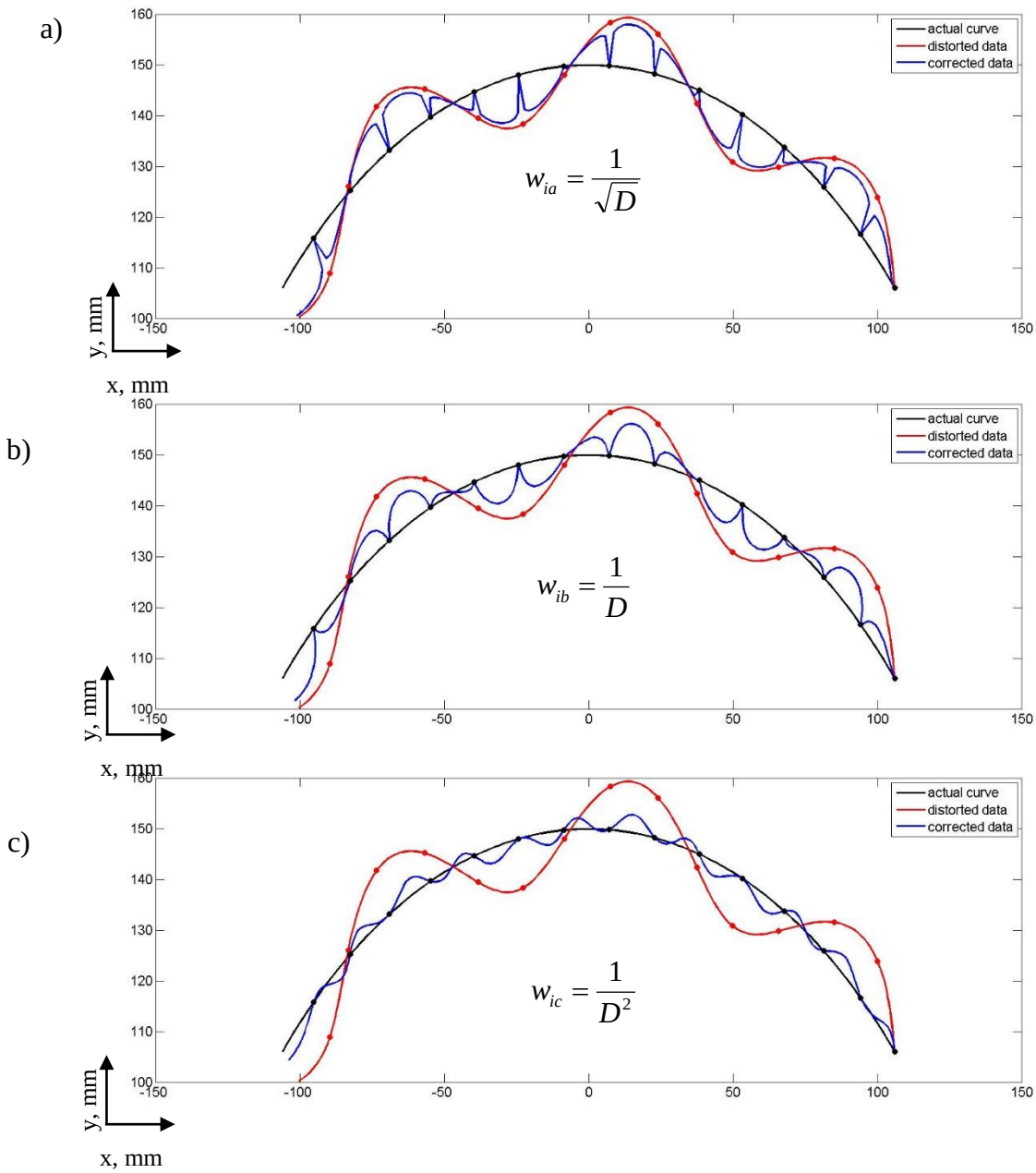

Fig. 4.17: Test on different methods of weight determination

d)

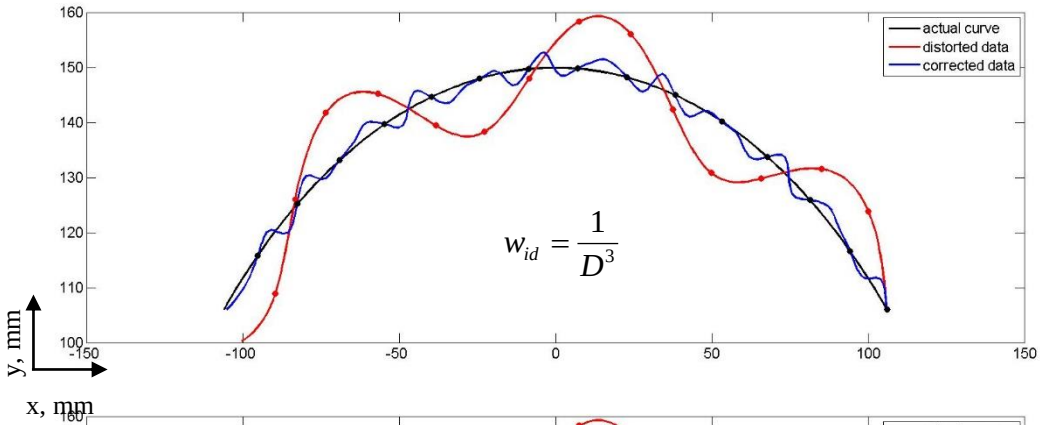

e)

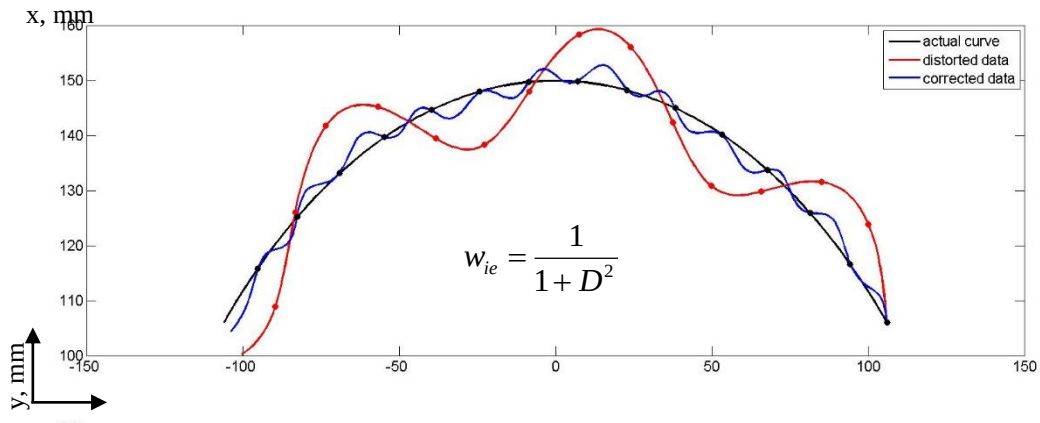

f)

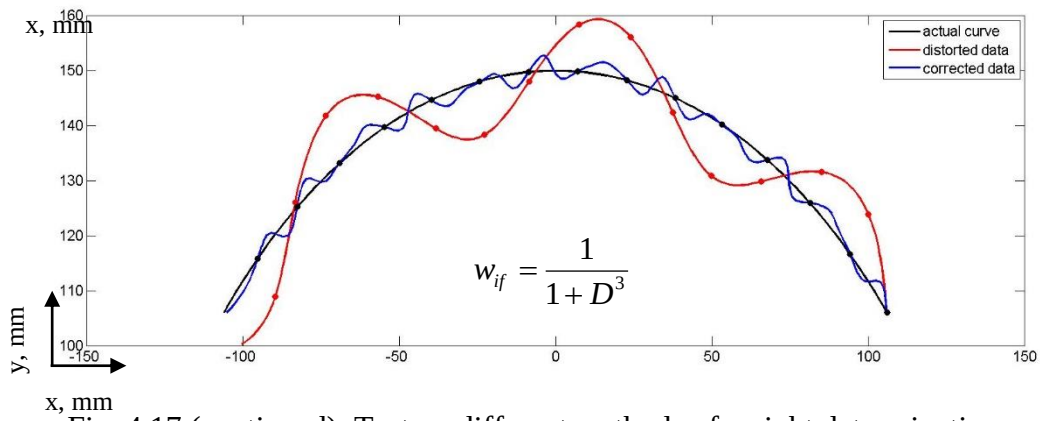

Fig. 4.17 (continued): Test on different methods of weight determination

g)

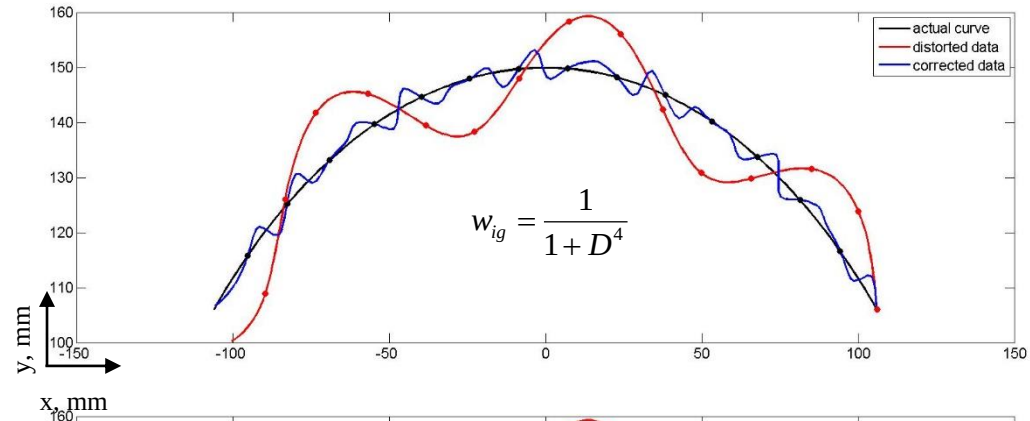

h)

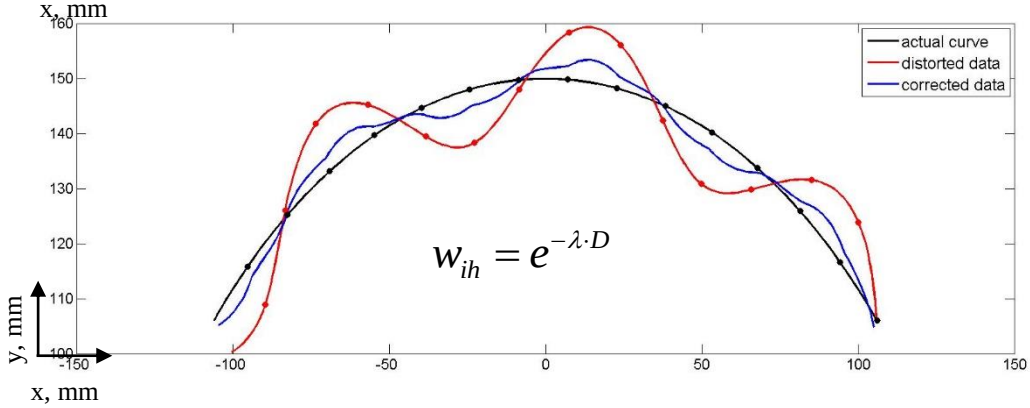

Fig. 4.17 (continued): Test on different methods of weight determination

As can be seen from Fig. 4.17a and Fig. 4.17b for those weights the curve after correction is discontinuous at the positions of characteristic points. Curves from Fig. 4.17c-g are continuous and at the places of characteristic points, these points from distorted data (HDLP marked red) after the fusion (blue curve) are exactly at positions of corresponding points from low density high precision method (black dots). The black curve reflects the actual shape of the tested curve. For these weights (Fig. 4.17c-g) the initial distortion coming from HDLP method is corrected perfectly at the characteristic points. It can be seen that the mean distance between corrected and actual curve is much lower than the distance between initially distorted and actual curve. Nevertheless between characteristic points low amplitude ripples appear. And also some parts of the waves from initial distortion being on one side of the actual shape are dragged to the other side. Summarizing, the initial distortion (HDLP data) having low frequency and high amplitude is transformed to high frequency distortion with lower amplitude.

A different situation occurs in the case presented in Fig. 4.17h. Here an improvement comparing to the initial distortion is achieved but the obtained curve is smooth. The function used here for weights determination is called the reliability function known from reliability theory.

4.1.4 The reliability function

In reliability theory the reliability function *Re(t)* is used in life data analysis. This function gives the probability of an item operating for a certain amount of time without failure. It is a function of time. The function is presented as a probability distribution function i.e. x % reliability at t hours. A commonly used in reliability engineering distribution is the exponential distribution. This type of distribution is used to model the lifetime of units that have a constant failure rate. The probably distribution function (pdf) of the exponential distribution is given by the following formula:

$$f(t) = \lambda e^{-\lambda t} \qquad 4.5$$

where λ (lambda) is the sole distribution parameter.

From the above equation, formula for the reliability function for the exponential distribution can be determined as follows:

$$Re(t) = 1 - \int_0^t \lambda e^{-\lambda s} ds = 1 - \left[1 - e^{-\lambda \cdot t}\right] = e^{-\lambda \cdot t} \qquad 4.6$$

The reliability function for the exponential distribution for different λ is presented in Fig. 4.18.

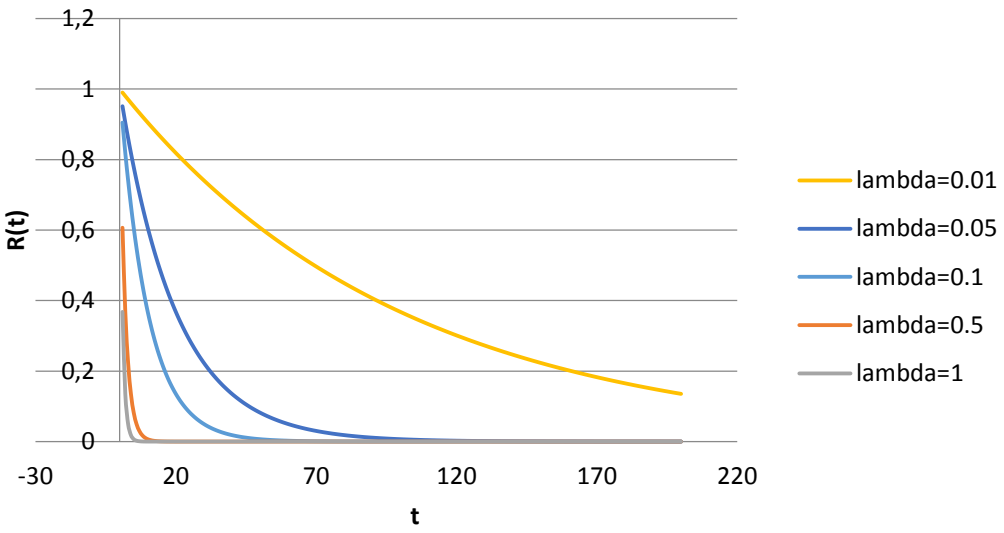

Fig. 4.18: Reliability function

It can be noted that with the decrease of the λ parameter the rate of change of the function decreases. The characteristics of the 1-parameter exponential distribution were discussed by Kececioglu [13]. Some of them are:

- The scale parameter is $\frac{1}{\lambda} = \mathrm{m}$, where m is mean time between failures, or to failure.
- With the decrease of λ, the distribution is stretched out to the right.
- The distribution starts at $\mathrm{t} = 0$ and decreases thereafter exponentially and monotonically with time. It is convex.

The initial research showed that this function for weights determination has good properties for the data fusion but appropriate value for λ parameter must be set. It cannot be constant for all cases. It should be connected with the distance between characteristic points. If they are spaced less frequently the influence of each one on the surrounding part of the point cloud should have a wider range. To ensure this λ should be small and its value will be determined in the next subchapter.

4.1.5 Determination of λ parameter

To establish how to determine the λ parameter depending on the distances between characteristic points, first the developed method of data fusion was applied to a line and an arc. At first the distance between characteristic points was constant and λ was changed. For the best case the

dependency between this distance and λ was determined. Tests performed for a line are presented in Fig. 4.19. Dots represent pairs of characteristic points.

$$w_i = e^{-\lambda \cdot D} \qquad 4.7$$

where w_i is the weight, D is the distance between characteristic points and the paired point from the point cloud and λ is the reliability function for the exponential distribution.

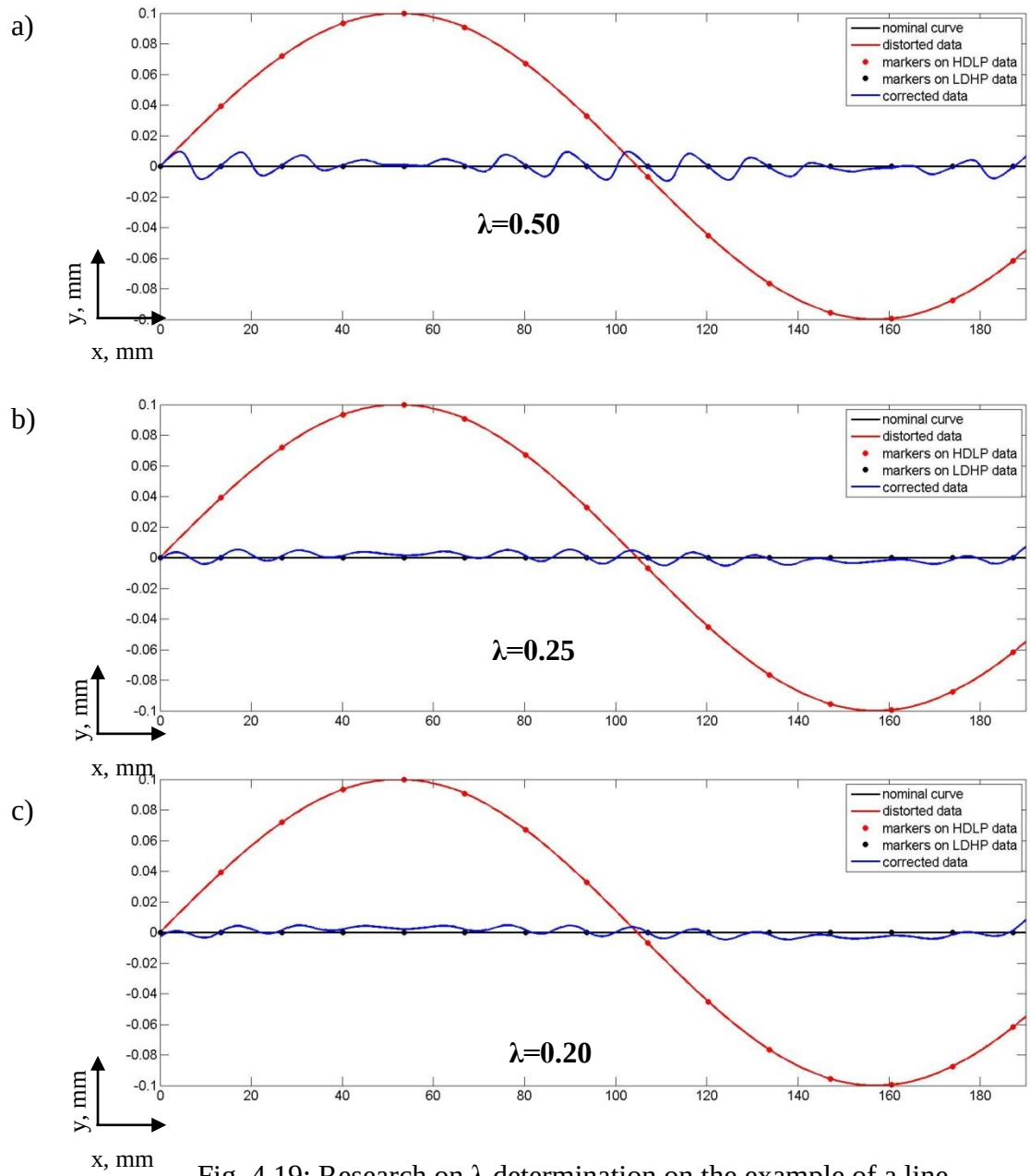

Fig. 4.19: Research on λ determination on the example of a line

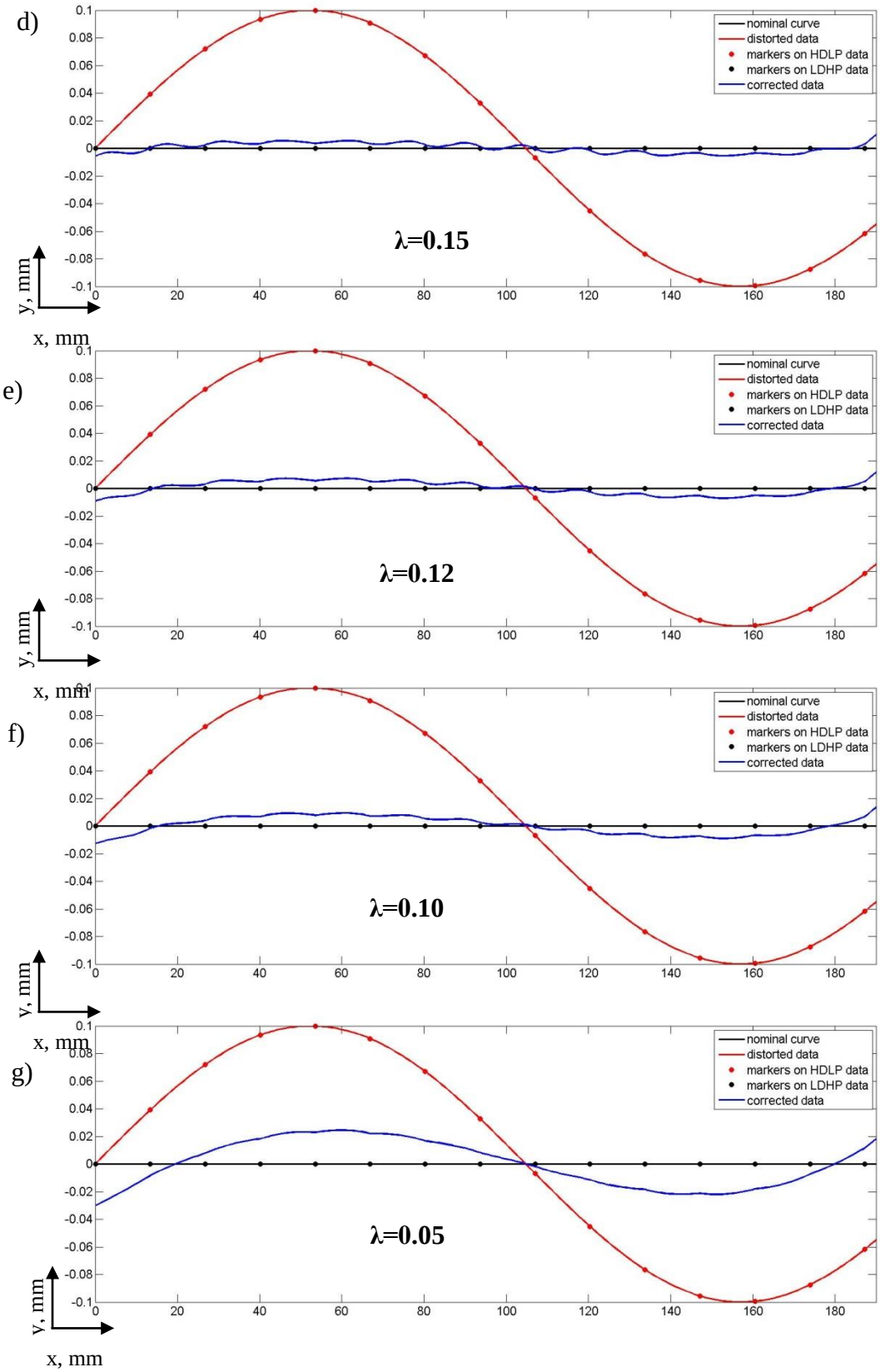

Fig. 4.19 (continued): Research on λ determination on the example of a line

As can be seen from Fig. 4.19a-c if the λ parameter is to big the curve obtained after fusion contains ripples between characteristic points which did not exist on the initial distortion. On the other hand Fig. 4.19f and g show that if the λ parameter is too small, the performed fusion is not efficient. From the above graphs Fig. 4.19e for $\lambda=0.12$ shows that for this function the initial distortion is retained as the best and also the ratio of improvement is high and exceeds 90%.

According to the already presented information about characteristics of reliability function for the exponential distribution for less dense distribution of characteristic points the λ parameter should be bigger. It can be selected using the following formula:

$$\lambda = \frac{C}{dist} \qquad 4.8$$

where C is a constant and $dist$ is the distance between characteristic points. Using the information about the distance and λ parameter from the simulation presented in Fig. 4.19e, $C \approx 1.8$.

This constant was also calculated for the arc, which is presented in Fig. 4.20. Initial distortion was increased to make improvement provided by data fusion method more visible. Dots represent pairs of characteristic points.

a)

b)

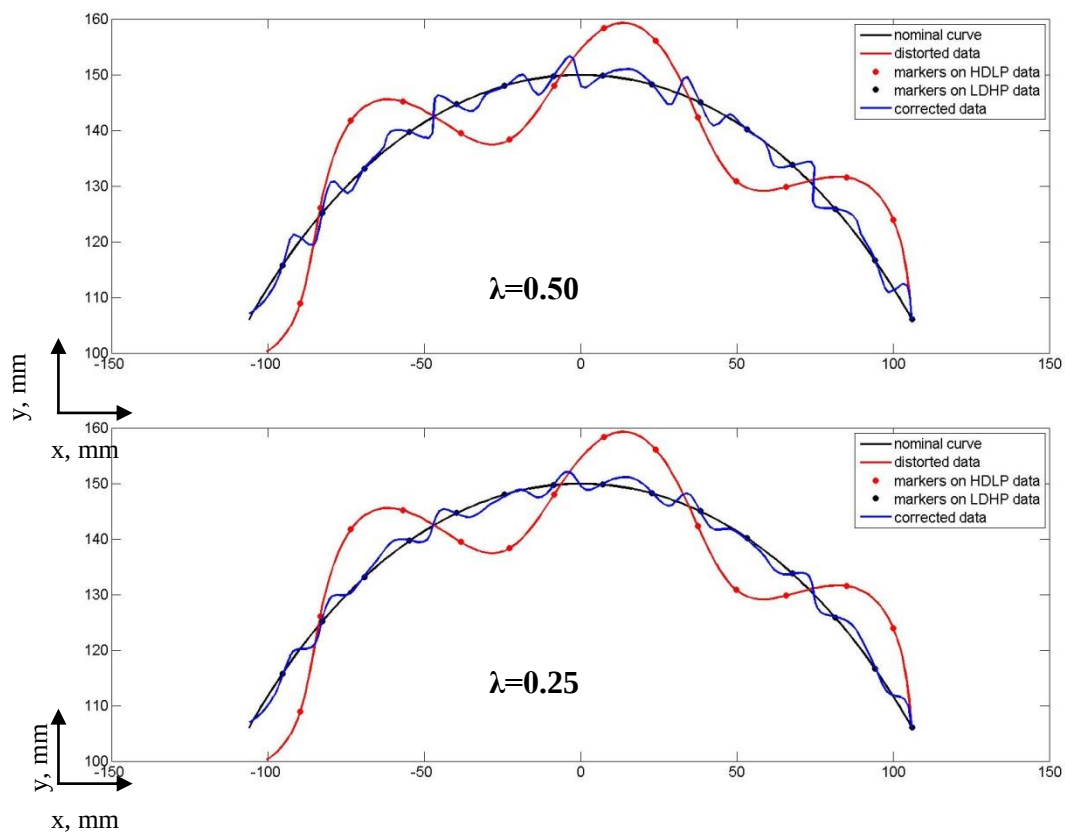

Fig. 4.20: Research on λ determination on the example of an arc

c)

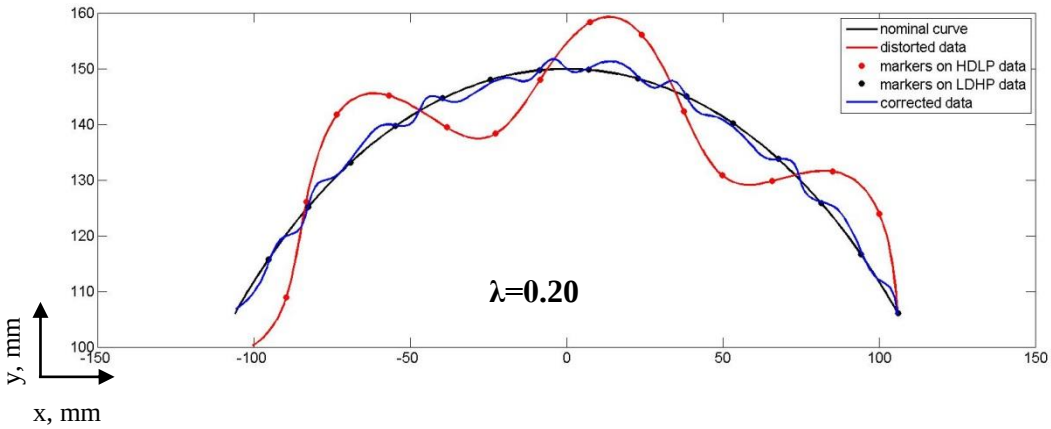

d)

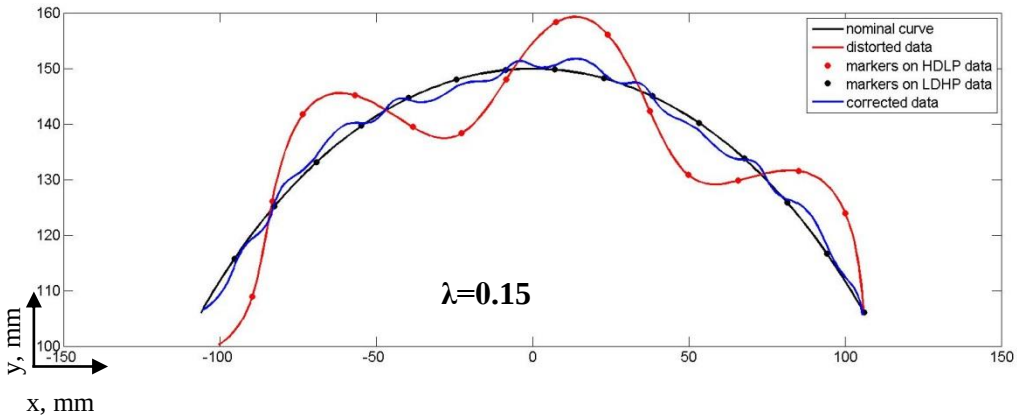

e)

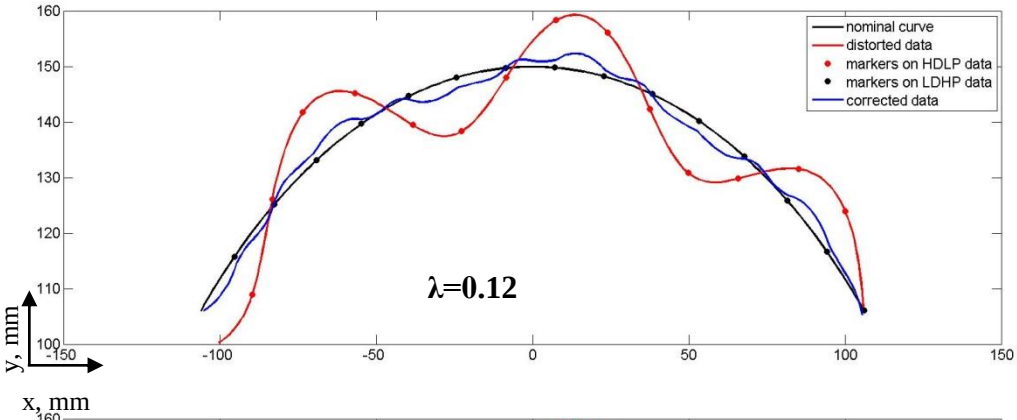

f)

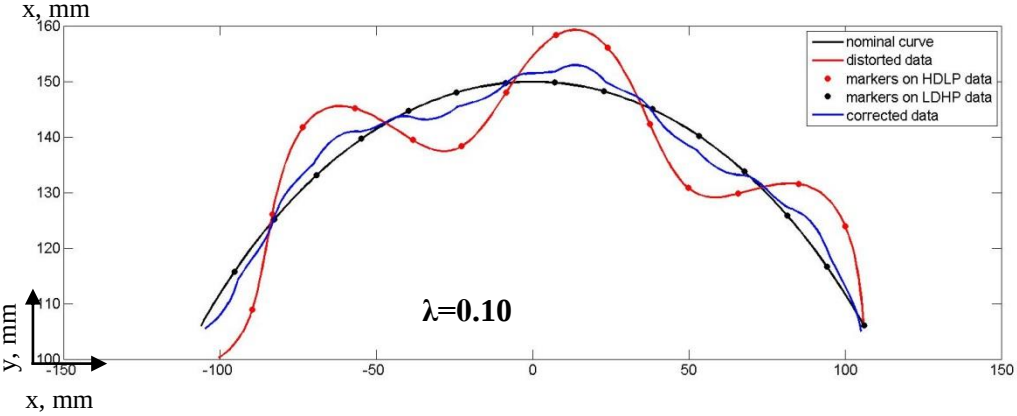

Fig. 4.20 (continued): Research on λ determination on the example of an arc

g)

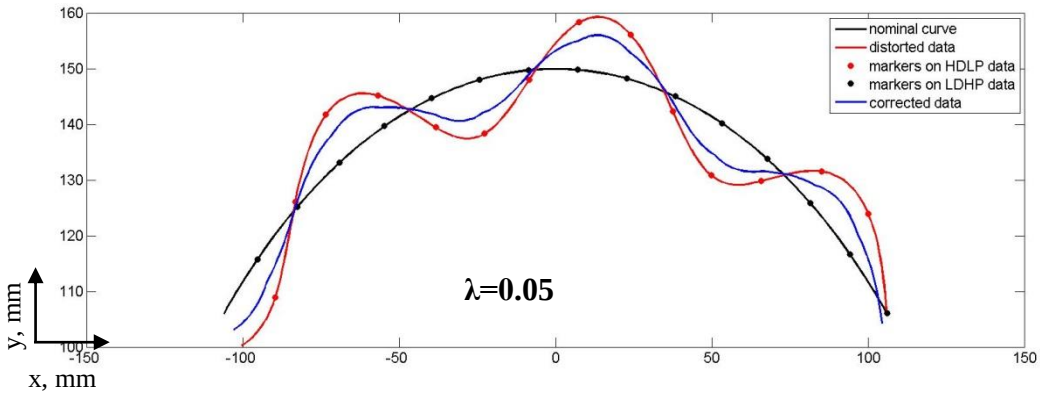

Fig. 4.20: (continued): Research on λ determination on the example of an arc

Here similarly as for the line for the first three values of λ (Fig. 4.20a-c) the curve obtained after fusion contains ripples between characteristic points which did not exist on the initial distortion. For small values of λ (Fig. 4.20f and g) the performed fusion is not efficient. Here the distances between characteristic points were of the same order as for the line. Also for $\lambda=0.12$ (Fig. 4.20e) the obtained results were the most satisfactory. For this case the value of the constant C is $C \approx 1.8$.

Based on these research the final form of the weights used for the determination of correction vectors in data fusion method is:

$$w_i = e^{-\frac{1.8}{dist} \cdot D_i} \qquad 4.9$$

This function was checked for different density of distribution of characteristic points. The evaluation of the method was also done numerically by determination of ratio of improvement. The ratio of improvement was calculated using equation *2.10*.

Results for different number of characteristic points and thus different distances between them are presented in Fig. 4.21 for a line and in Fig. 4.22 for an arc.

a)

b)

c)

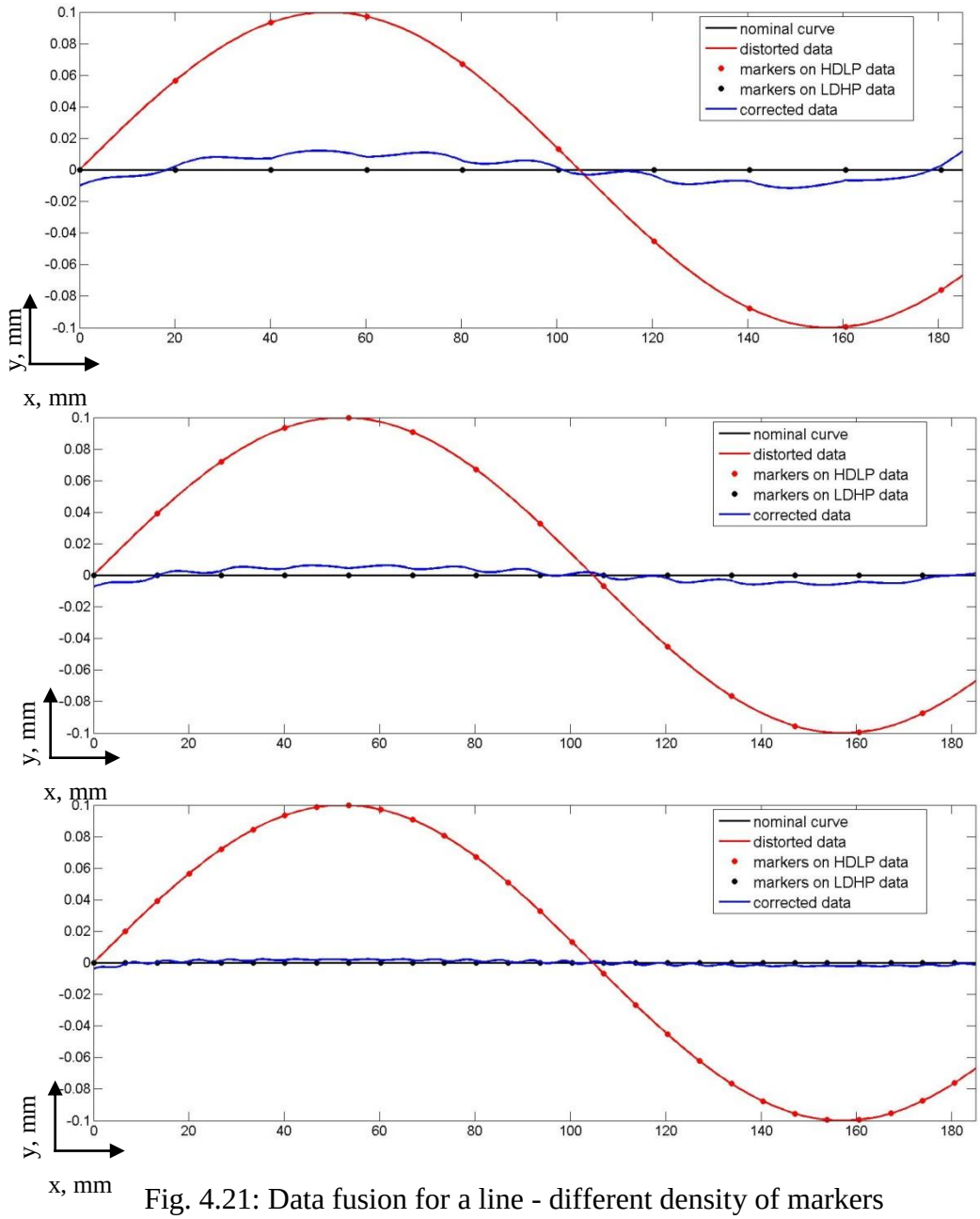

Fig. 4.21: Data fusion for a line - different density of markers

The results of data fusion for a line for different density of markers are presented in Table 4.4.

Table 4.4 : Results of data fusion for a line

No of characteristic points	**Mean distance between characteristic points, mm**	**Ratio of improvement, %**
10	20.0669	88.01
15	13.3779	93.63
30	6.6890	98.03

Then the simulation was performed for an arc. Initial distortion was increased to make improvement provided by data fusion method more visible.

a)

b)

c)

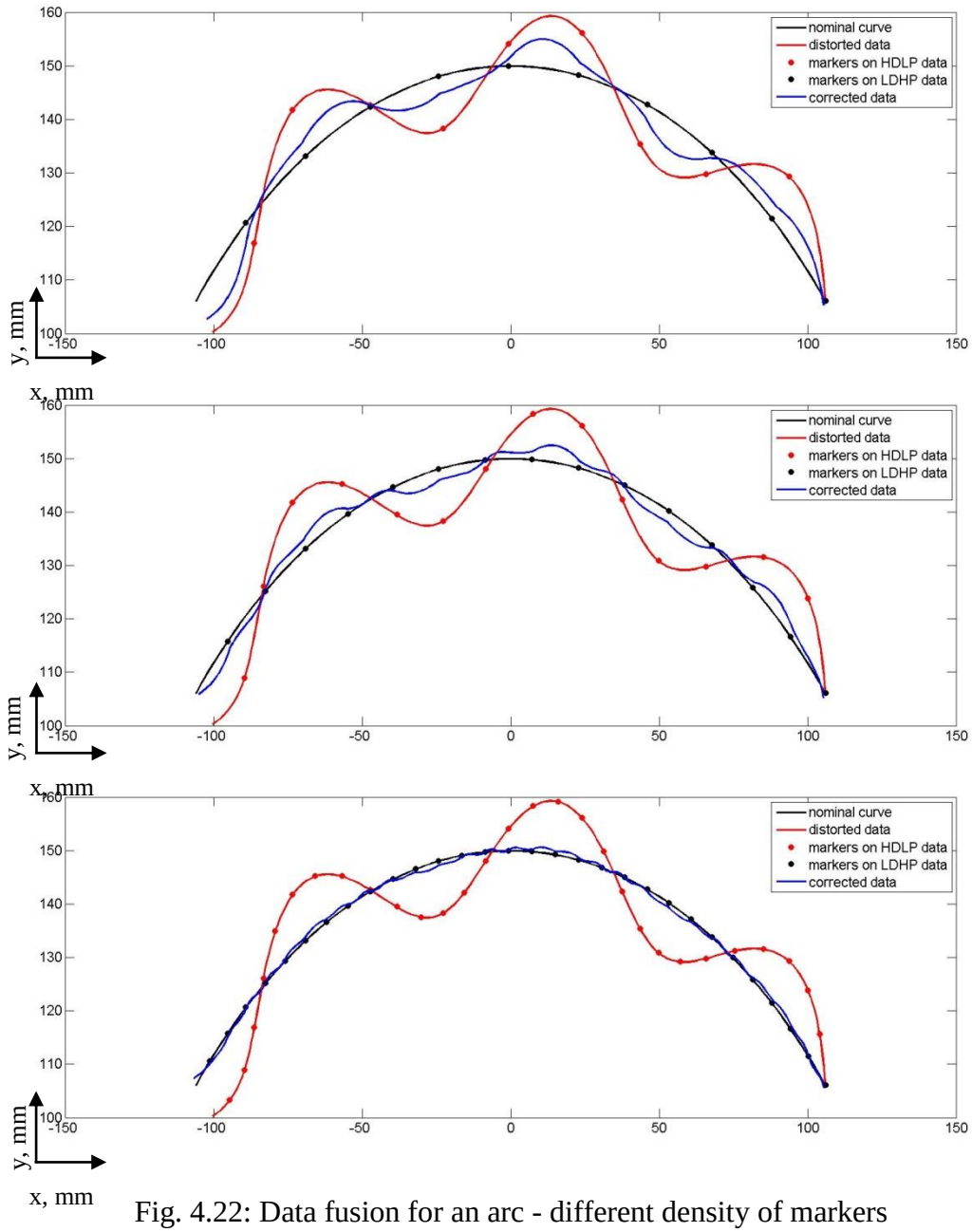

Fig. 4.22: Data fusion for an arc - different density of markers

Table 4.5 : Results of data fusion for an arc

No of characteristic points	Mean distance between characteristic points, mm	Ratio of improvement, %
10	23.6689	54.10
15	15.7885	75.22
30	7.8969	92.34

The results presented in Fig. 4.21 and Fig. 4.22 demonstrate the validity of the use of the proposed method of data fusion together with the described method of weights determination. As we can see for more characteristic points the ratio of improvement is higher. The data fusion method does not distort the shape of the initial errors for any number of characteristic points for none of the presented curves.

The next step is to take into account the uncertainties of the two types of measurements used to obtain LDHP and HDLP data. The uncertainty budged was done for data fusion method using virtual markers.

4.1.6 Uncertainty analysis

For each point from point cloud its position after fusion P_{a_f} is calculated from the following equation:

$$P_{a_f} = P_{b_f} + Cor_vect \qquad 4.10$$

where: P_{b_f} is a position of this point before data fusion, Cor_vect is a correction vector determined for this point.

Correction vectors for each point from a cloud are calculated separately from the equation *4.4*.

<u>1) Uncertainty of correcting vectors Vc_i:</u>

$$V_c = P_{CMM} - P_{LS} \qquad 4.11$$

where P_{CMM} is position of characteristic point from LDHP method (CMM-coordinate measuring machine), P_{LS} is position of characteristic point from HDLP method (LS-laser scanner.

As it was mentioned before, the position of characteristic point from LDHP method is replaced by the weighted average and takes the following form.

$$V_c = P_{AVE} - P_{LS} \qquad 4.12$$

According to equation 4.3 uncertainty of P_{AVE} depends on weights associated with the positions P_{CMM} and P_{LS}. Weights are inversely proportional to the variances of P_{CMM} and P_{LS}.

$$u(P_{AVE}) = \frac{1}{\sqrt{\frac{1}{u^2(P_{CMM})} + \frac{1}{u^2(P_{LS})}}} \qquad 4.13$$

$$u(P_{CMM}) = \frac{P_{MPE}}{\sqrt{3}} \qquad 4.14$$

(0.98 µm for Zeiss Accura used in tests)

where P_{MPE} is a maximum permissible probing error [24].

$$u(P_{LS}) = \frac{u(LS)}{\sqrt{n}} \qquad 4.15$$

where *u(LS)* is uncertainty of a measuring system with a laser scanner, *n* is an average number of points used to calculate characteristic point from HDLP method, for used scanner n=20.

$u(P_{LS})$ = 10.76 µm

$u(P_{AVE})$≈ 0.98 µm

The uncertainty of correcting vectors can be expressed by the following equation:

$$u(V_c) = \sqrt{u^2(P_{AVE}) + u^2(P_{LS})} \qquad 4.16$$

For used devices:

$u(V_c)$ = 10.80 µm

<u>2) Uncertainty of correction vectors Cor_vect:</u>

Correction vectors are calculated as a weighted average from correcting vectors. Uncertainty of weighted average is equal to weighted average of uncertainties of the individual values, so:

$$u(Cor_vect) = \frac{\sum u(Vc_i) \cdot w_i}{\sum w_i} \qquad 4.17$$

As uncertainties for all correcting vectors are the same, uncertainty of each correction vector is equal to uncertainty of correcting vectors:

$u(Cor_vect)$ = 10.80 µm

3) Total uncertainty of the point cloud after fusion:

$$u(P_{a_f}) = \sqrt{u^2(P_{b_f}) + u^2(Cor_{vect})} \qquad 4.18$$

$u(P_{b_f}) = u(LS)$ = 48.10 µm

$u(P_{a_f})$ = 49.30 µm

The uncertainty introduced by the proposed method is 1 µm which constitutes 2% of the uncertainty of the device having the highest uncertainty. Fig. 4.23 presents three curves. Red is the distorted line (representation of HDLP data), black curve represents the nominal curve and blue is the distorted line after correction. Dots represent characteristic points named as markers and rounds around them are the uncertainties.

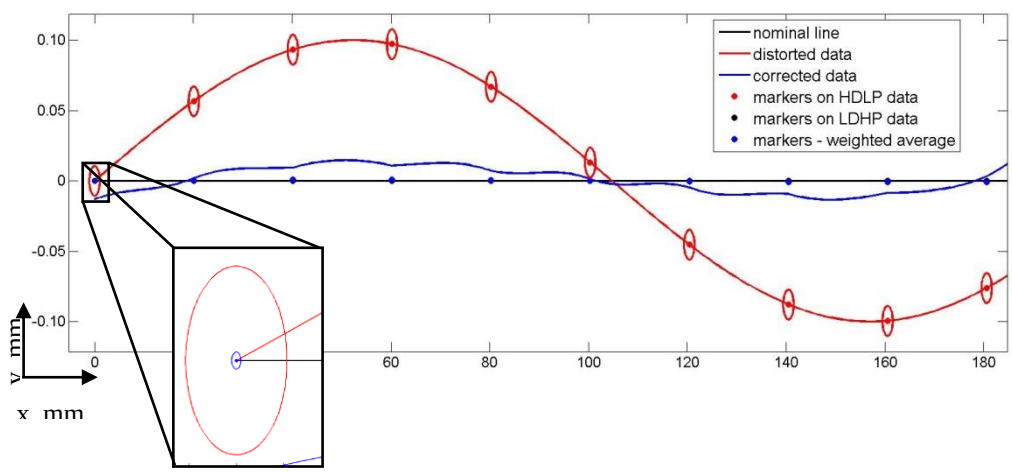

Fig. 4.23: Data fusion with uncertainties of characteristic points

4) Uncertainty after taking systematic errors into account:

According to ISO standard [25] the expanded measuring uncertainty should contain apart from uncertainties coming from the used devices or measuring method also systematic error. Based on the quoted standard the uncertainty of the proposed method takes the following form:

$$U = K \times u(P_{a_f}) + |b| \qquad 4.19$$

where K is a coverage factor (k=2 for coverage probability of 95%), $u(P_{a_f})$ is the final uncertainty of the proposed method, b is a systematic error.

As it can be seen from Fig. 4.23 the systematic error changes but its maximal value is equal to 100 μm before data fusion and 14.67 μm after data fusion. As it was mentioned the data fusion method introduces uncertainty of 1 μm but benefits from decrease of systematic errors are much more significant. From equation *4.19* the maximal expanded uncertainties U_{b_f} and U_{a_f} before and after data fusion respectively are equal to:

$$U_{b_f} = 2 \times 48.10 + 100 = 196{,}20 \text{ μm}$$

$$U_{a_f} = 2 \times 49.30 + 14.67 = 113{,}27 \text{ μm}$$

It means a reduction of uncertainty of more than 40% is achieved.

The uncertainties of the whole distorted curve and the corrected curve are presented as dashed lines in Fig. 4.24. Green dashed line is the uncertainty of HDLP data while the orange one is the uncertainty of corrected line after fusion of HDLP and LDHP data. Having known the nominal shape we could determine the systematic error for each single point and it varies from 0 to the maximal value.

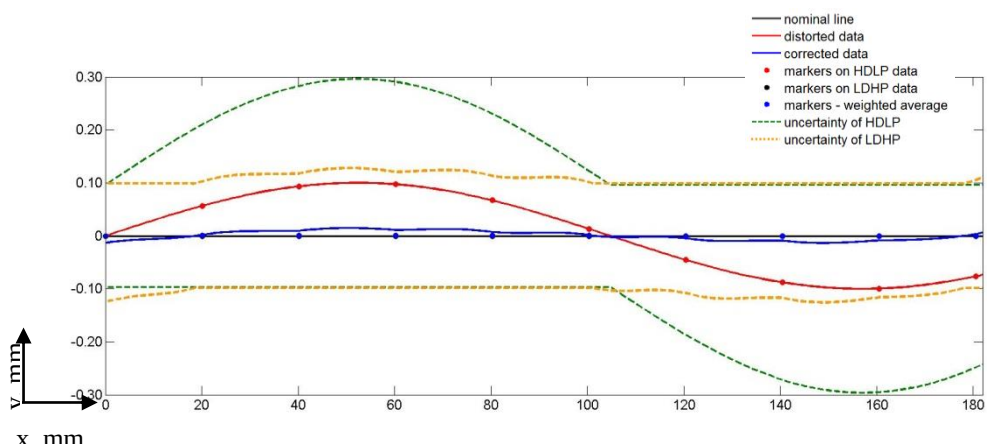

Fig. 4.24: Results of data fusion taking expanded uncertainty into account

Fig. 4.24 shows that the proposed data fusion method improved precision of HDLP data but also decreased its uncertainty. The high density of points a characteristic of HDLP measurement method, was maintained. The presented results showed that from two types of data HDLP and

LDHP data with main pros of both was obtained. The output data has high density of points and their precision is high - HDHP.

4.2 Methodology

The experiment was conducted using two types of measuring devices from the field of coordinate metrology. The first type enables gathering measuring points using contact method and the other enables gathering high density of points in a non-contact way. To obtain LDHP data two CMMs were employed. First one is a Legex 9106 with basic parameters listed in Table 4.6. Its full specification is included in ANNEX A.

Table 4.6 : The specification of Legex 9106

Accuracy	
E_{MPE}, µm	(0.50+L/1000)
P_{MPE}, µm	0.45

The second model of CMM used for research was Accura 7 by Zeiss. The full specification is included in ANNEX B.

Table 4.7 : The specification of Accura 7

Accuracy	
E_{MPE}, µm	(1.7+L/333)
P_{MPE}, µm	1.7

To provide HDLP data two non-contact systems working on the principle of triangulation were used. First was a Creaform Handyscan REVscan, which is a self-positioning system. The second one was a Metris Laser scanner MMC80 fixed to a measuring arm. The main parameters of the REVscan are presented in Table 4.8 and the parameters of the MMC80 are in Table 4.9. The full specification is included in ANNEX C

Table 4.8 : The specification of REVscan

Measurement Rate, measures/s	18 000
Resolution, mm	0.100 mm
Accuracy, mm	Up to 0.050
Volumetric Accuracy[1]	0.020 mm + 0.200 mm/m
Volumetric Accuracy[1] (with MaxSHOT 3D)	0.020 mm + 0.025 mm/m

[1] Based on the ISO 10360 standard, volumetric accuracy is defined as a size-dependent value.

Table 4.9 : The specification of MMC80

Stripe width (Y), mm	80
Accuracy (2σ), μm	35
Max data rate, real pts/sec[2]	24
Points per stripe[2]	800
Max speed, stripes/sec	30

[2] Metris points-per-second and points-per-stripe specifications state real scan points only. No interpolation techniques are used to oversample the point clouds.

All research were conducted using the following methodology.

<u>For material markers it consists of following steps:</u>

1. the inspected part is rigidly fixed to the measuring table,
2. material markers are evenly distributed on the measurand,
3. material markers are measured using a CMM,
4. centres of balls measured using a CMM are determined based on Gaussian fitting – first set of characteristic points,

5. for the evaluation of the method mutually perpendicular lines are measured from the part's surface using a CMM - the lines create a net,
6. the whole part together with material markers are measured using non-contact method,
7. centres of balls measured using non-contact method are determined based on Gaussian fitting – second set of characteristic points before alignment,
8. using equation *2.4* a rigid body transformation between points from step 4 and step 7 is determined,
9. rigid body transformation is applied to points from step 7 which gives second set of characteristic points,
10. the same rigid body transformation is applied to point cloud from non-contact method (step 6),
11. using two sets of characteristic points the data fusion method described above in this chapter is applied,
12. for the evaluation, point clouds before and after data fusion are compared to a net of mutually perpendicular lines from step 5.

<u>For virtual markers it consists of following steps:</u>

1. the inspected part is rigidly fixed to the measuring table,
2. three coordinate balls are fixed around the measurand, assuring their maximal separation (for big inspected parts, the balls were fixed directly to the surface of the part),
3. coordinate balls are measured using a CMM,
4. centres of balls measured using a CMM are determined based on Gaussian fitting,
5. a grid of evenly distributed points are gathered from the surface of a measurand using a CMM – first set of characteristic points,
6. for the evaluation of the method mutually perpendicular lines are measured from the part's surface using a CMM - the lines create a net,
7. the whole part together with three coordinate balls are measured using non-contact method,
8. centres of balls measured using non-contact method are determined based on Gaussian fitting,

9. using equation *2.4* a rigid body transformation between points from step 4 and step 8 is determined,
10. the rigid body transformation is applied to point cloud from non-contact method (step 7),
11. second set of characteristic points is determined using a method of virtual markers described above in this chapter,
12. using two sets of characteristic points the data fusion method described above in this chapter is applied,
13. for the evaluation, point clouds before and after data fusion are compared to a net of mutually perpendicular lines from step 6.

All calculations needed to perform the data fusion method were coded and calculated using Matlab environment. Comparison of point clouds before and after fusion with reference data were performed using Catia CAD software.

4.3 Results and discussion

The experiment was conducted for two methods used for determination of characteristic points: material markers and virtual markers. The results were presented in [47, 48].

4.3.1 Results and discussion for material markers

Preliminary results of developed data fusion method with the use of material markers were presented in journal paper [47]. Then, after improvement in the weights w_i from equation *4.4* results were updated and presented in this sub-chapter. As a first part to evaluate the proposed method of data fusion the reference cube was used. The cube is made of aluminium and painted white. Its size is (100x95x100) mm. The cube's upper surface flatness was measured as 26 μm on the ACCURA 7 CMM. The cube with material markers is presented in Fig. 4.25. In this case markers were glued to the surface because aluminium is not a magnetic material.

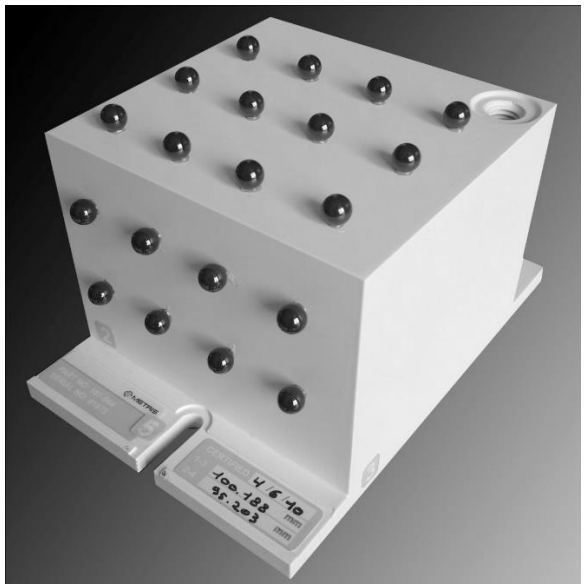

Fig. 4.25: The cube with material markers [47]

As it was described in the methodology, for the evaluation, a few lines on point cloud were measured and compared with corresponding lines measured on a CMM – reference data. Numerical results are presented in Table 4.10. They show the average values of distances between point clouds before and after fusion and reference data from a CMM. The shortest distances between two sets are sought.

Table 4.10 : The cube - results of data fusion with material markers

No of section	**Average distance (non-contact – reference) before fusion, mm**	**Average distance (non-contact – reference) after fusion, mm**	**Ratio of improvement, %**
S1	0.0407	0.0221	45.7
S2	0.0183	0.0008	95.6
S3	0.0027	0.0003	88.9
S4	0.0111	0.0038	65.8

From Table 4.10 it can be seen that the data fusion method decreased the average distance between point cloud and the reference data from the CMM. It can also be concluded that for these sections improvements of average distances are between around 46 % and 96%.

The proposed method of data fusion was also evaluated using freeform surfaces. As a first example of this type of surface, a turbine blade with dimensions (200x120) mm was used. The blade offers a realistic industrial freeform however given the size of the markers the sharp radii of curvature such as those found on the leading and trailing edges are excluded from the study. Material markers were distributed on its surface forming a regular grid as presented in Fig. 4.26.

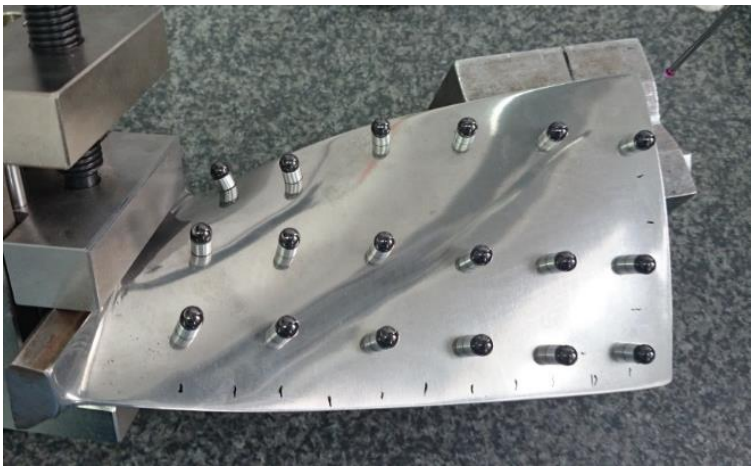

Fig. 4.26: Turbine blade with material markers [47]

Similarly to previous part as reference data mutually perpendicular lines creating a net were measured on a CMM additionally to the measurements of the balls. Then both point clouds, before and after data fusion were compared with the net. For point clouds obtained from the non-contact device two types of input data were used: raw point cloud and cloud after creation of mesh of triangles which decreases the number of points. For both point clouds, before and after fusion, an analysis on statistical distribution of distances between these clouds and reference data was performed. Always the closest point was searched. For all distances, weights based on frequency of appearance were assigned. Next a weighted average was calculated. Results are presented in Table 4.11.

Table 4.11 : Turbine blade - results of data fusion with material markers

Form of point cloud	**Average distance (non-contact – reference) before fusion, mm**	**Average distance (non-contact – reference) after fusion, mm**	**Ratio of improvement, %**
mesh	0.3705	0.3106	16.2
raw	0.2236	0.2112	5.5

Analysing the above table we notice that for raw point cloud the obtained ratio of improvement is around three times lower than in case of mesh of triangles. It is caused by the fact that in raw point cloud the ratio of random errors to systematic errors is higher. What can also be noticed is a higher average distance between point cloud and reference data before fusion for mesh of triangles. It is the effect of formation of mesh of triangles. As in measurements of ceramic balls, where for example creation of mesh of triangles from raw data resulted in an increase of dimension error from 90 μm to about 120 μm.

Table 4.11 shows that the maximum value of improvement is by 59.9 μm. This is about 80 % of the accuracy of the measuring system: scanner plus arm (40 μm + 34 μm = 74 μm). It was obtained for the mesh. In case of raw point cloud, the improvement is lower which is caused by noise in unprocessed data.

Another example of freeform surface used to evaluate the proposed method was the engine cover of a car. As it is an element which comprises openings, only a continuous surface with a dimension of (600x180) mm was used to perform data fusion. The engine cover with markers on its surface is presented in Fig. 4.27.

Fig. 4.27: Engine cover with material markers [47]

For the engine cover similar actions as for the turbine blade were performed. From the surface mutually perpendicular lines creating a net of reference data were measured on a CMM additionally to the measurements of the balls. Then both point clouds, before and after application of the proposed method, were compared with the net. For point clouds obtained from the non-contact device two types of input data were used: raw point cloud and cloud after creation of mesh of triangles which decreases number of points.

Similarly as in case of turbine blade for point clouds before and after application of the data fusion, an analysis on statistical distribution of distances between points from these clouds and closest points from reference data was performed. Then a weighted average was calculated.

Table 4.12 : Engine cover - results of data fusion with material markers

Form of point cloud	**Average distance (non-contact – reference) before fusion, mm**	**Average distance (non-contact – reference) after fusion, mm**	**Ratio of improvement, %**
mesh	0.0825	0.0794	3.8
raw	0.0740	0.0727	1.8

The engine cover is much bigger than a turbine blade but its curvature is lower. Similar comparisons as for the blade were performed. Table 4.12 shows improvement in the accuracy of the point cloud from laser scanner after application of data fusion. The improvement is lower than for turbine blade but also input data is burdened with smaller error, by one order of magnitude. Also the distances between each markers were higher which is due to the size of the part.

Analysing the above table we can notice that, similarly as for turbine blade, for raw point cloud the obtained ratio of improvement is lower than in case of mesh of triangles. It is caused by the fact that in raw point cloud the ratio of random errors to systematic errors is higher. Also here the higher average distance between point cloud and reference data before fusion for mesh of triangles was noticed. It is the effect of formation of mesh of triangles. As in measurements of ceramic balls, where for example creation of mesh of triangles from raw data resulted in an increase of dimension error from 90 μm to about 120 μm.

Analysing the above results the following conclusions are inferred. Better results are obtained when the distance between characteristic points is smaller – the same number of characteristic points distributed on a smaller surface. It was also presented in the results from the computer simulation.

The initial average distance between point cloud and reference data is higher for mesh of triangles as creation of triangles distorts the shape of a point cloud.

Lower improvement is obtained for raw data. It is caused by the fact that in this type of data ratio of random errors to systematic ones is higher.

The obtained results are worse than results from simulation. It is caused by instability of determination of positions of balls. This research were presented in sub-chapter 4.1.1.

Next part includes results for evaluation of the data fusion method using virtual markers, where the problem of instability in determination of position of the marker does not appear.

4.3.2 Results and discussion for virtual markers

The results of developed data fusion method with the use of virtual markers were presented in the journal paper [48]. To evaluate the developed method of data fusion three parts were selected.

The first test part was a planar surface represented by a granite table to which four balls were attached using a peripheral frame to ensure a common coordinate system for optical measurement and CMM data. This part is shown in Fig. 4.28.

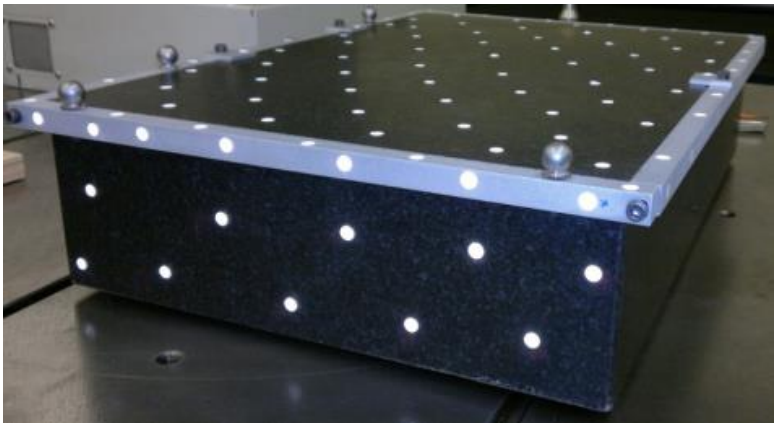

Fig. 4.28: Planar test part. White markers are used for self-positioning. They enable to determine scanner's relative position to the part [48]

The planar part was measured together with the reference ball frame using the Legex 9106 and the Creaform Handyscan. The CMM measured two sets of parallel lines mutually perpendicular to create a grid. This reference data was used for validation of the method. Then, at the intersections of all lines single points were gathered, which gave 754 points. These points were considered to be characteristic points from contact measurements and the basis to find corresponding points on the point cloud, using the virtual markers method. The principle of CMM measurements is shown in Fig. 4.29. The orange dots represent reference data from a CMM. They were gathered from the surface for evaluation of the method. Point clouds (data from non-contact measurement) before and after fusion were compared with this data. Blue dots, gathered separately from the surface by single points CMM measurement, were used to perform data fusion.

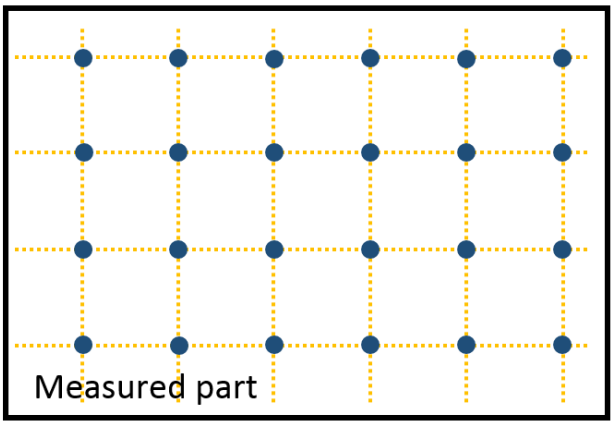

Fig. 4.29: Principle of CMM measurements of the part (the actual number of points varies for different part geometry). • - reference data for evaluation of the method, • - characteristic points used for data fusion [48]

Before application of the proposed method a mesh of triangles was created from the non-contact point cloud to limit the number of points and so the computing time. As it was described for previous parts the point clouds before and after application of the proposed method were compared with data obtained from calibration of the surface performed with the CMM. The comparison was performed in the Catia CAD software. An example of comparison between data from the CMM and the point cloud from the optical measurement is presented in Fig. 4.30.

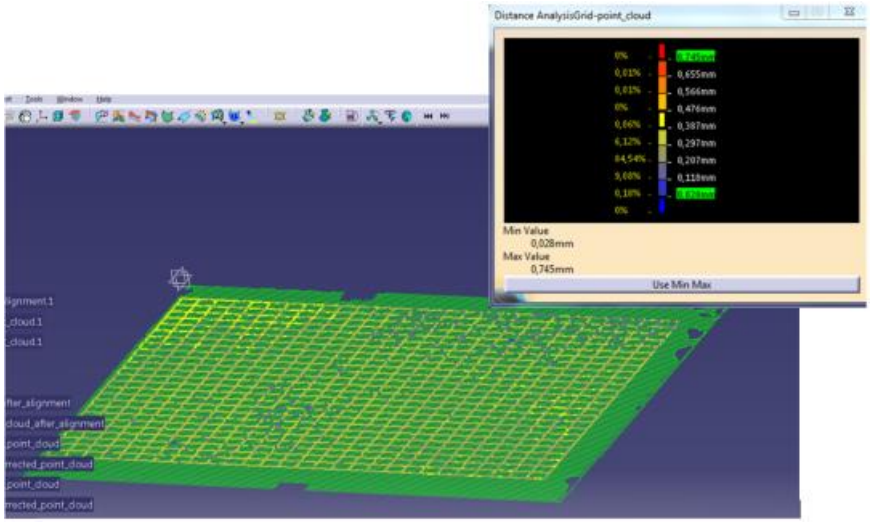

Fig. 4.30: Comparison between data from a CMM and a point cloud [48]

For point clouds before and after data fusion their distances to the reference data were determined. Also, statistical distributions of these distances were calculated. For all distances, weights based on frequency of appearance were assigned. Next for the whole point cloud a weighted average was calculated. The weighted average is calculated from following equation *4.2* , where weights depend on frequencies of appearance of distances (left column of the colour bar from Fig. 4.30)

For comparison with a point cloud the closest points to these from a CMM were searched. To check the influence of the size of selected virtual markers, three diameters were selected 10 mm, 20 mm and 30 mm. Numerical results are presented in Table 4.13.

Table 4.13 : Planar surface - comparison of point clouds with data from the CMM [48]

Φ – diameter of virtual marker, mm	**Average distance (non-contact – reference) before fusion, mm**	**Average distance (non-contact – reference) after fusion, mm**	**Ratio of improvement, %**
10	0.20429	0.00028	99.86
20	0.20429	0.00034	99.83
30	0.20429	0.00054	99.74

The above table shows that before application of the proposed method the average distance between the point cloud (aligned using four coordinate balls) and data from CMM was higher than 0.200 mm. It was caused by both misalignment between the two sets of data and errors in the positions of points in the point cloud. The results show how for a very simple feature non-contact measurement can be inaccurate. The application of the developed fusion method decreased the weighted average of distances by three orders of magnitude. In the evaluation weighted average was used as some distances repeat. If a certain value of distance repeats more often it has bigger influence on the calculated average, as in Fig. 4.30. It can also be noted that for a smaller size of the virtual marker sphere, a smaller average distance is obtained.

The proposed method was also evaluated on freeform surfaces which are common in modern products. The same parts as for material markers were used. The freeform surface test parts were measured using the Accura 7 and the Metris laser scanner MMC80 fixed to a measuring arm.

The first example of freeform surface is a turbine blade with dimensions (200x120) mm. The part together with the 3CB is presented in Fig. 4.31.

Fig. 4.31: Turbine blade with the 3CB for referencing [48]

First the part was measured on a CMM. It relied on measurements of two sets of parallel lines mutually perpendicular to create a net. Similarly as for the part in Fig. 4.29. This net was treated as reference data for evaluation of the method. Then, from the whole surface 113 points, arranged in a regular grid were gathered. These points were considered to be characteristic points from contact measurement and the basis to find corresponding points on the point cloud using the already described virtual markers method.

Since the turbine blade is an element with high curvature a small diameter for the virtual markers was chosen. The diameter was 6 mm. Data from the non-contact device had two forms: raw point cloud and mesh of triangles with fewer points.

A statistical analysis of the distances between point cloud and data from the CMM was performed in the Catia CAD software for point clouds before and after application of the method. The distance is between a point from a CMM and the closest point from the point cloud. For all distances, weights characterizing frequency of appearance, of a particular distance in the whole point cloud, were assigned. Subsequently a weighted average was determined. Results are presented in Table 4.14.

Table 4.14 : Turbine blade - comparison of point clouds with data from the CMM [48]

Form of point cloud	**Average distance (non-contact – reference) before fusion, mm**	**Average distance (non-contact – reference) after fusion, mm**	**Ratio of improvement, %**
mesh	0.2770	0.0743	73.18
raw	0.2085	0.0492	76.40

To visualise the obtained results cross-sections of point clouds in the places of the part where reference data were gathered were made. Cross-sections were made for point clouds before and after data fusion. These point clouds were in the coordinate system of CMM data. A sample results for one cross-section are presented in Fig. 4.32.

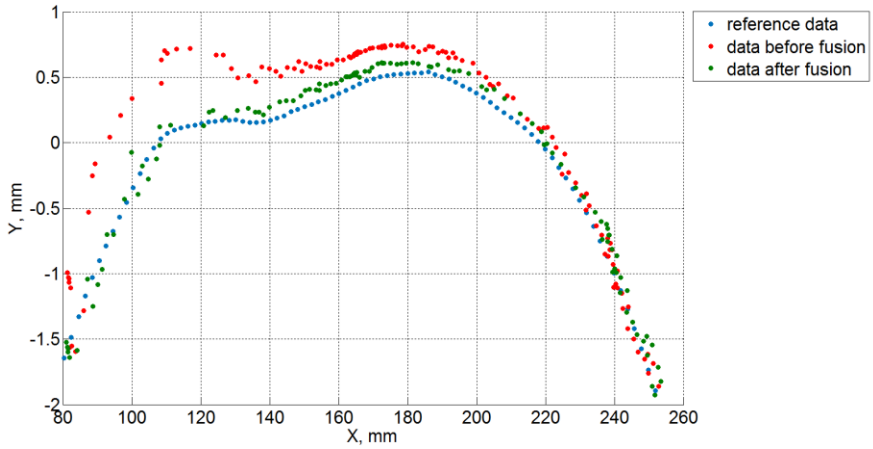

Fig. 4.32: Comparison of cross-sections of point clouds before and after fusion with reference data [48]

Table 4.14 shows the usefulness of the proposed method for a freeform surface. For both forms of data the obtained ratio of improvement was similar. For mesh of triangles it was about 73% and for raw point cloud about 76% compared to the data before data fusion. For this part the average distance between characteristic points was 12 mm. Based on Table 4.5 it can be assumed that the dependency between ratio of improvement and distance between markers for simulation data is linear. If the distance between markers was 12 mm then the ratio of improvement should be around 80 %.

This shows the ability to transfer the method tested on simulation data onto real data.

As for all previous examples the initial (before data fusion) average distance between point cloud and reference data is higher for mesh of triangles, comparing to raw data.

Analysing Fig. 4.32 it can be noted how the fusion pulled the point cloud from non-contact method closer to the reference, which proves improvement in precision.

Another example of freeform surface used to evaluate the proposed method was the engine cover of a car. As this element contains openings, only a continuous area with dimensions of (600x180) mm was used to perform data fusion. The engine cover together with the 3CB on its surface are presented in Fig. 4.33.

Fig. 4.33: Engine cover with the 3CB [48]

First the part was measured on a CMM along two sets of parallel lines mutually perpendicular to create a net. This net was treated as data for evaluation of the method, similarly to previous parts. Then, 62 points, arranged in a regular grid were gathered. These points were considered to be characteristic points from contact measurement and the basis to find corresponding points on the point cloud, using the virtual markers method described in sub-chapter 4.1.2.

For the engine cover similar actions as for the turbine blade were performed. The engine cover has higher curvature than a plane so a small diameter for the virtual markers was chosen. Similarly as in previous case, mutually perpendicular lines creating a net, measured on a CMM

were treated as reference data. Both point clouds, before and after application of the proposed method were compared with this reference. Data from the non-contact device had two forms: a raw point cloud and mesh of triangles with fewer points.

An analysis on statistical distribution of distances between point cloud and data from the CMM was performed for point clouds before and after application of the data fusion method in Catia software. Distance is determined from a point from a CMM to the closest point from a point cloud. For all distances, weights based on frequency of appearance were assigned. Subsequently a weighted average was determined. Results are presented in Table 4.15.

Table 4.15 : Engine cover - comparison of point clouds with data from the CMM [48]

Form of point cloud	**Average distance (non-contact – reference) before fusion, mm**	**Average distance (non-contact – reference) after fusion, mm**	**Ratio of improvement, %**
mesh	0.0638	0.0341	46.55
raw	0.0575	0.0327	43.13

Here the number of gathered characteristic points with regard to the size of the part was smaller than for the turbine blade but also the shape of this part was less complicated. The mean distance between characteristic points was about 110 mm. Also in this case ratio of improvement was similar for both forms of input data. It was about 47 % and 43 % for mesh and raw data respectively. We should also pay attention to the distance before application of data fusion. It is much smaller than for turbine blade. It is due to good optical characteristics of the measured surface and simplicity of the shape. For this part again higher distance between point cloud before fusion and reference data was observed for mesh of triangles.

The developed method of data fusion was also evaluated based on data from measurements of big part from aircraft industry – fuel tank, which was not included in [48]. The plane part had a length of around 1000 mm and a maximal diameter of 450 mm. The reason to use such part was to show how big parts can be measured fast and with sufficient accuracy, which is highly desirable from economic point of view. Fig. 4.34 shows the selected part mounted on the measuring table of a CMM.

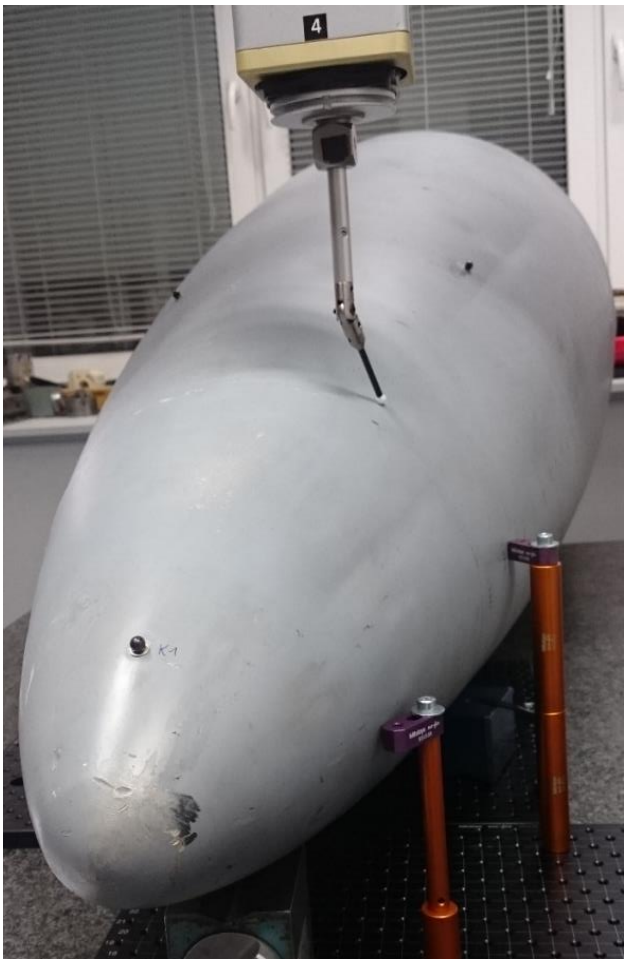

Fig. 4.34: Measurand – plane part

To the part, three coordinate balls were glued to ensure a common coordinate system for data from both contact and non-contact measurements. They were distant from each other as far as possible to make the determination of coordinate system more stable.

From the surface of the fuel tank 456 characteristic points were measured using a CMM with a tactile probe. The mean distance between these points was 40 mm – this value was used as one of the parameters in the data fusion method. Then, keeping the same rule as for previous parts, the whole surface was measured using the CMM creating an additional net of mutually perpendicular lines. This was the reference data for the data fusion method evaluation. Both point clouds, before and after application of the proposed method were compared with this reference. In this case to limit processing time only mesh of triangles was used for analysis.

An analysis on statistical distribution of distances between point cloud and data from the CMM was performed for point clouds before and after application of the data fusion method in Catia CAD software. Distance is determined from a point from a CMM to the closest point from a point cloud. For all distances, weights based on frequency of appearance (more distances with the same value give higher frequency) were assigned. Subsequently a weighted average was determined. Results are presented in Table 4.16.

Table 4.16 : Plane part - comparison of point clouds with data from the CMM

Average distance (non-contact – reference) before fusion, mm	**Average distance (non-contact – reference) after fusion, mm**	**Ratio of improvement, %**
0.0801	0.0356	55.56

To visualize changes presented in the above table a graphical comparison from Catia CAD software is given. Comparison before data fusion is presented in Fig. 4.35 while comparison after fusion in Fig. 4.36.

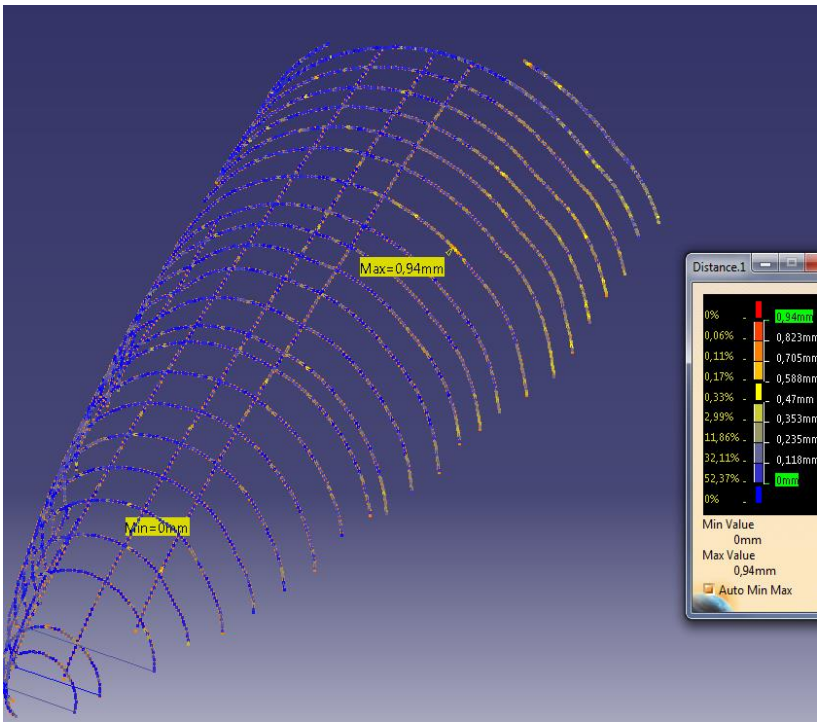

Fig. 4.35: Distances between point cloud from non-contact measurement and reference data before data fusion

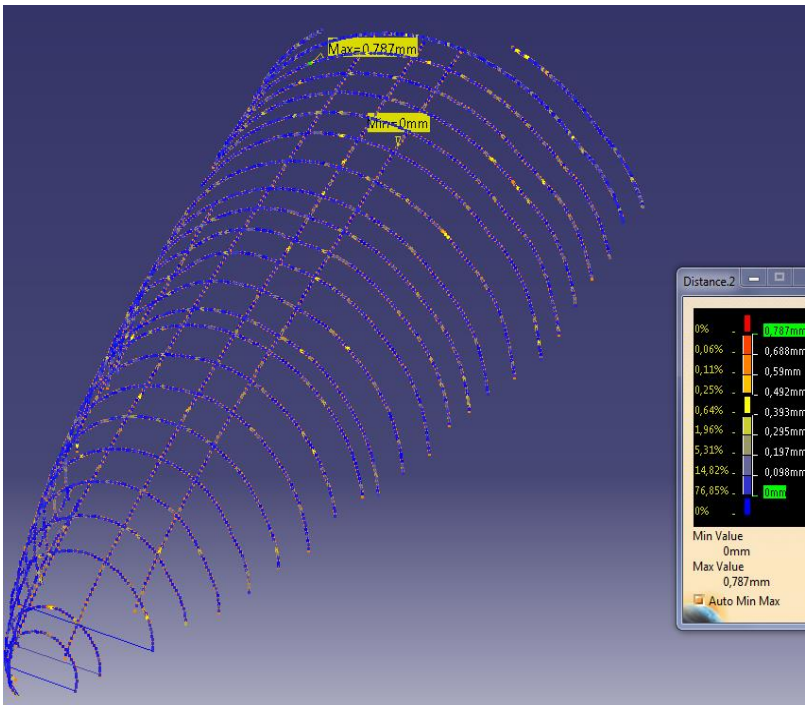

Fig. 4.36: Distances between point cloud from non-contact measurement and reference data after data fusion

It can be noted that the maximal distance was decreased by more than 150 µm. Data fusion also decreased the average distance. The biggest improvement can be observed in areas where the initial distortion was the highest – right area of Fig. 4.35.

I also wanted to analyse the character of the changes. An important issue is whether systematic errors were corrected or only inaccuracy of alignment was removed. For this purpose in Fig. 4.37 I presented one of the lines from Fig. 4.35 and Fig. 4.36. It can be observed how data fusion moved the points from the point cloud closer to the reference data.

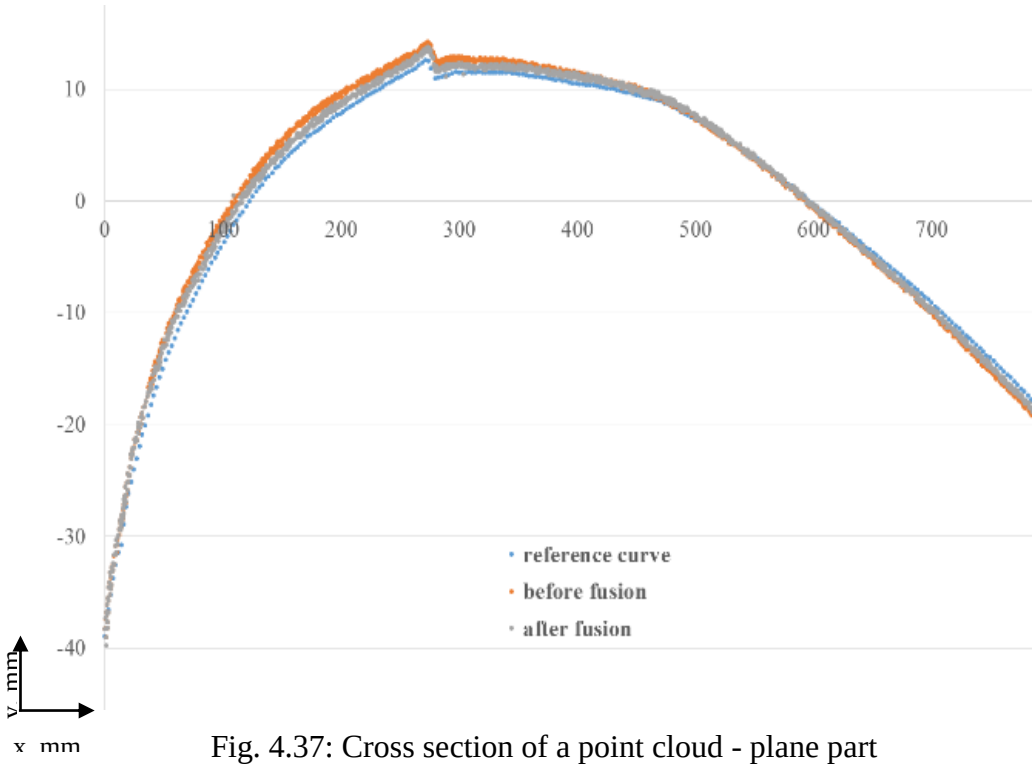

Fig. 4.37: Cross section of a point cloud - plane part

As it is presented in Fig. 4.37 the initial cross-section of the point cloud (orange dots) has not undergone only rigid body transformation which would shift, rotate or scale it. Areas which are on one side of the reference data (blue dots) stay on the same side but are much closer to the true value. The initial distortion has been decreased. Corrected data is marked grey.

To make the improvement more visible, the most susceptible area of the curve, the area of the edge was magnified and presented in Fig. 4.38.

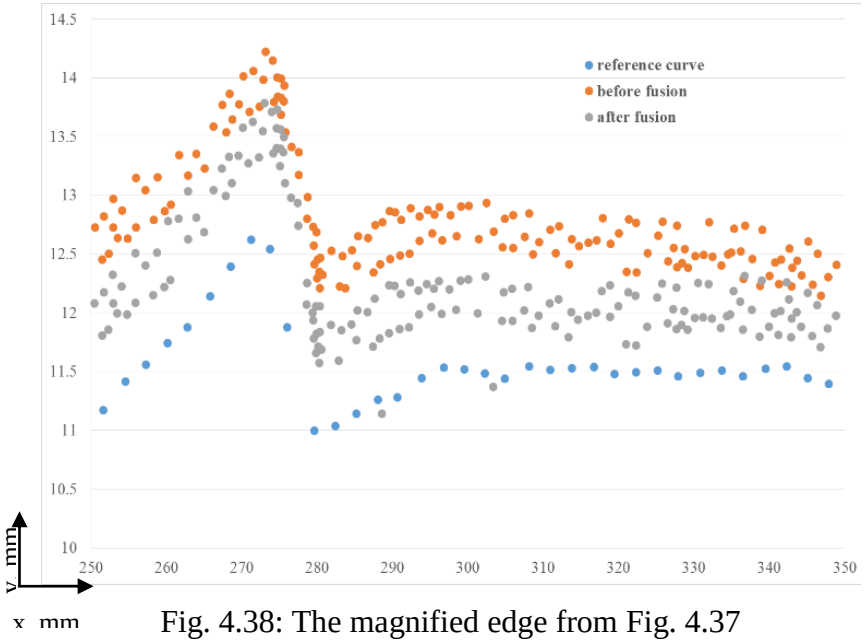

Fig. 4.38: The magnified edge from Fig. 4.37

As we can see from Fig. 4.38 the random error represented by noise was not removed. However, the main goal of the method was achieved, the systematic error was decreased.

An important advantage of the presented data fusion method is visible when we want to characterize the curve, which is magnified in Fig. 4.38, using only characteristic points from contact method – not the additional, reference measurement. It is shown in Fig. 4.39.

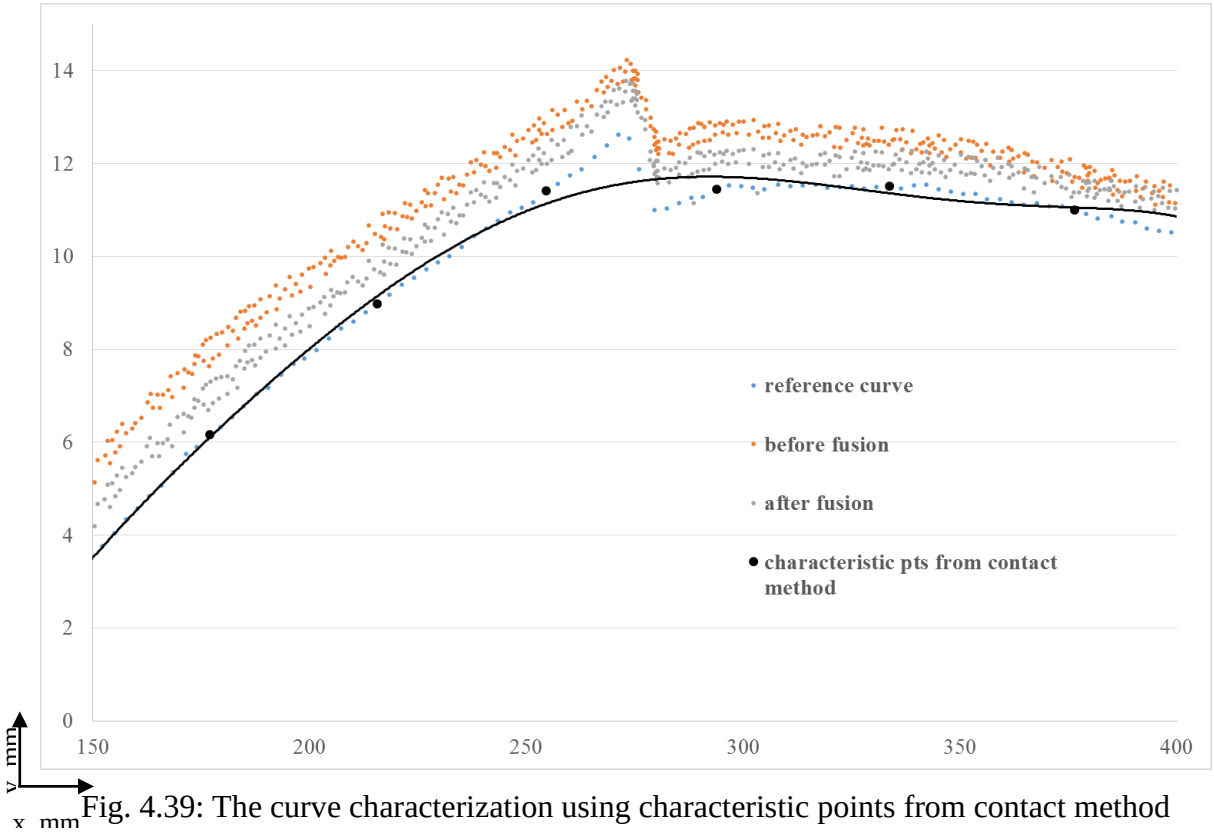

Fig. 4.39: The curve characterization using characteristic points from contact method

Big, black dots are the characteristic points from contact method used for fusion. If we had only this data the reconstructed curve would look like the black curve. The important information about the edge would be lost. The edge was detected by non-contact measurement, so after data fusion information about the inspected part is complete and more precise than only non-contact measurement.

The developed method of data fusion was also evaluated based on results from CMM and CT scanner measurements of the plano-parallel plate presented in Fig. 1.4.

To show utility of the data fusion method described in this thesis it was assessed how systematic errors from the CT measurement process can be reduced. To perform fusion I chose some points from measurements on a CMM, from data used for the CAD model creation. 20 points for each planar surfaces and 15 points from the cylinder were used.

To analyse improvement of the accuracy of data from non-contact measurement provided by the use of contact measurement, the resulting point cloud was compared with the reference model. Comparison of geometrical parameters before and after data fusion is presented in Table 4.17.

Table 4.17 : Comparison of geometrical parameters for the plano-parallel plate.

	Reference (CMM)	**CT measurement**	**Data after fusion**
distance between planes, mm	16.139	16.745	16.140
radius of the cylinder, mm	23.417	22.436	23.383

Table 4.17 shows that these two parameters from data after fusion tend to the value represented by reference data. When the parameter for non-contact measurement were higher than the reference, it stayed higher but much closer to this reference and when before fusion it was lower it stayed lower but more accurate. To make the nature of changes more visible then for the cross-section from Fig. 1.5 a second cross-section in the same location but for data after fusion was added. It is presented in Fig. 4.40.

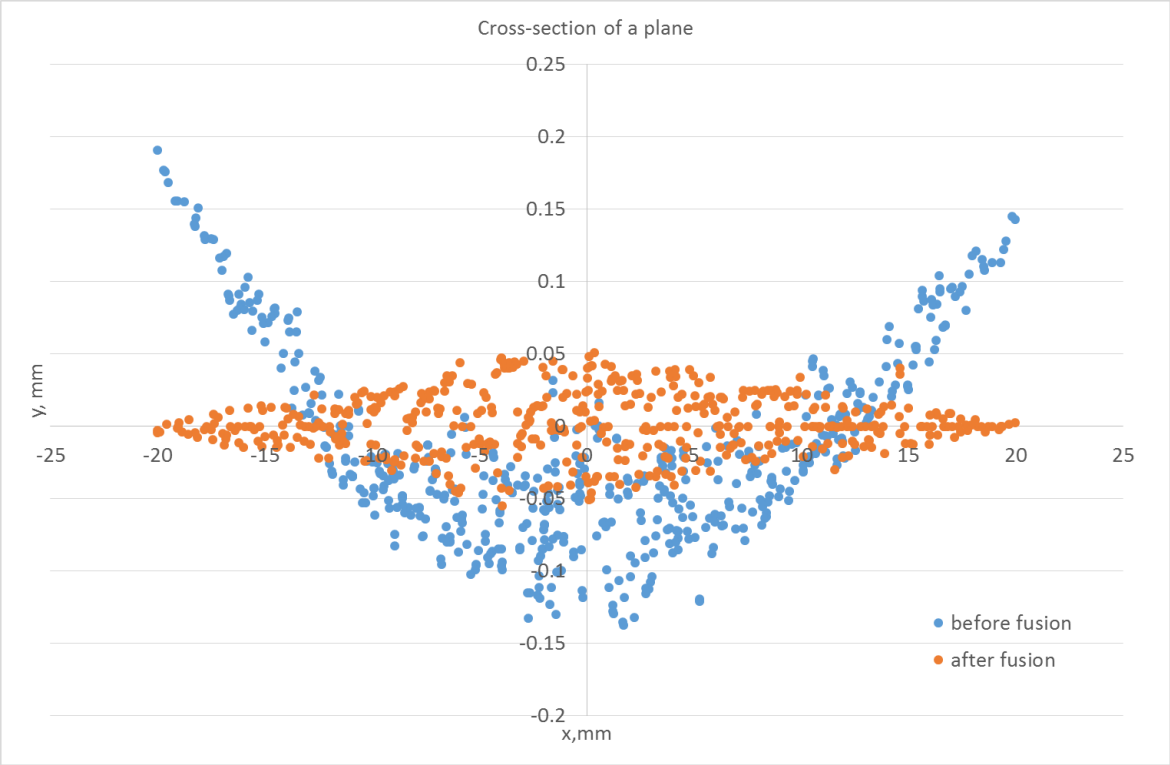

Fig. 4.40: Comparison of cross-sections before and after data fusion

The graph shows that the proposed fusion method decreased the systematic error represented by the original U-shaped distortion. The improvement is also apparent from the 3D comparison with the CAD model depicted in Fig. 4.41.

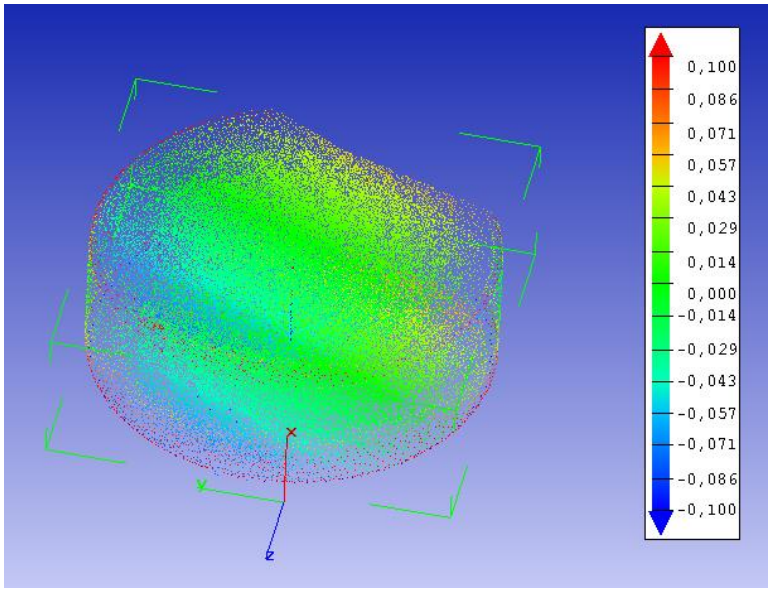

Fig. 4.41: Comparison between data after fusion and CAD model

The most evident observation is that the scale of the difference form reference data is reduced by a factor of 4. On the edges we can see the highest difference between the point cloud and the CAD model, which was also apparent for data before fusion. This is the feature of many non-contact measurements like laser triangulation or CT scanning. In these areas strong noise occurs and also reconstruction algorithms have segregation problems; attributing points to particular surfaces. Also, in the central part of the plate there are many points lying on both sides of the fitted planes, which is caused by noise.

Table 4.18 shows how the data fusion method influences the range of points coordinates for geometric features fitted to specific areas of point clouds – two planes and cylinder.

Table 4.18 : Range of points coordinates for fitted features

	CT measurement	**Data after fusion**
upper plane, mm	0.339	0.104
lower plane	0.321	0.096
radius of the cylinder, mm	0.155	0.153

Range for the cylinder remained unchanged while for both planes it was decreased three times. This is caused by the fact that in CT measurements distortions representing systematic errors appear in surfaces parallel to the measuring table of a CT scanner. So, for the cylinder which axis were perpendicular to the measuring table, systematic errors did not occur, they were not limited by data fusion method and the range is caused by noise.

This shows that proposed method of data fusion can be used for data from different measuring devices.

CHAPTER 5 CONCLUSIONS

This thesis presents a novel method of data fusion. All data comes from coordinate measurements. In these techniques point coordinates gathered on the part surface are processed to characterise the measured surface or feature. More points are measured more complex information about the measurand is provided.

In coordinate metrology points can be collected using contact and non-contact sensors. In the case of contact measurements high precision coordinates are obtained. The main disadvantages of this approach are the small number of measurement points and the long measuring time. Faster and more thorough inspection of machined parts in order to shorten product process development time is required by modern industry. Non-contact methods are attractive solutions. In this way much data over the whole object is gathered in a short time albeit with lower precision.

Every method has its advantages and disadvantages. Therefore it is often desirable to combine data from two measuring techniques. In such a way that cons are limited and pros are maintained. Methods of data fusion from literature were presented. Many of them are not applicable to freeform surfaces, which are very common. Even the methods of data fusion dedicated to freeform surfaces have many limitations. ICP algorithm is often used. It is a rigid transformation. Therefore point cloud modelling is not complete and no real improvement is obtained.

The main objective of this dissertation was to fuse data of the same surface but obtained from different types of measuring methods. The proposed approach is suitable for freeform surfaces. The main goal was to increase the precision of the non-contact HDLP set of data, using the contact LDHP set.

In the data fusion method first, the part was measured using a non-contact method. Then using a contact method a set of characteristic points was gathered from the part. These characteristic points can be represented by material or virtual markers. Then a set of corresponding points was sought in point cloud from non-contact method. Based on these two sets a matrix relation functions between them was determined. It was used to determine correction vectors for all points from the cloud needed for correction.

Based on research, as material markers, ceramic balls made of silicon nitride with the diameter of 7 mm were used. The balls were glued into specially designed magnetic fixture. Thanks to this they could be put on the measured surface and materialise characteristic points.

The next method developed for determination of characteristic points is the method called virtual markers. In this method, after ensuring a common coordinate system, a regular grid of points is gathered using contact method. Then around these points virtual spheres were created. Each sphere included points from the point cloud – non-contact measurement. For all spheres separately, the average coordinates from these points were computed. This gives a second set of characteristic points coming from the non-contact method. The diameter of the spheres is determined to be minimal but enclose at least fifteen points from non-contact method. Bigger diameter would make the method insensitive to the curvature of the measured surface.

Characteristics on non-contact measuring methods were analysed. It was shown that data form non-contact type of measurement is burdened with random and systematic errors. The systematic errors cause distortion of the point cloud and are the ones which are intended to be corrected by the developed method.

Non-contact measurements are susceptible to many factors like: projected angle, scanning depth, environmental effects, influence of the operator and measuring strategy, data processing or measured surface properties. The factors were analysed to develop the best manner of non-contact measurements conduction.

Most of the research was conducted on laser scanner working on the principle of triangulation. It was shown that higher resolution is obtained when the distance between the laser scanner and the measured surface is shorter. Concerning projected angle it is recommended to keep the triangulation plane orthogonal to the measured surface.

For environmental effects, the impact of external illumination was tested, using different types and different intensities of lighting. It was shown that stronger lighting yields better results from the same surface. This may be due to the fact that with higher lighting fewer data points are collected.

Also the influence of the measuring strategy was tested in details. Five strategies differing in the involvement of the arm’s joints, changes in scanning direction and overlapping of scans. The

tests results suggests to limit overlapping of scans and also frequent changes in the scanning direction.

Research on point cloud processing showed that for small parts when it is important to determine their diameter it is preferably to work on raw point cloud or to improve the look of a cloud to use a median filter. Creation of mesh of triangles, although it limits the number of points and thus decreases computing time, provides additional error in position and diameter of features and surfaces.

Knowing the nature of non-contact measurements the developed method of data fusion was evaluated. Both methods of characteristic points determination were tested. Fusion using material markers was tested on three surfaces: plane, turbine blade and engine cover. Fusion using virtual markers was tested on the same surfaces (as plane bigger part was used). Additionally big part from aircraft industry was used for evaluation of the method using virtual markers. Evaluation was also performed through computer simulation for two planar curves: line and arc.

First, the material markers method was applied at the planar part of the reference cube was used. Point clouds before and after fusion were compared with reference data by determination of average distance between them. Results showed that the data fusion method decreased the average distance between point cloud and the reference data. It can also be concluded that precision of measurement was improved from 46 % to 95%, depending on the selected reference line.

The proposed method of data fusion was also evaluated using freeform surfaces. First a turbine blade was used. It offers a realistic industrial freeform. As in previous case both point clouds, before and after data fusion were compared with the reference data. For point clouds obtained from the non-contact device two types of input data were used: raw point cloud and cloud after creation of mesh of triangles. For both point clouds, before and after fusion, an analysis on statistical distribution of distances between these clouds and reference data was performed. Always the closest point was searched. For all distances, weights based on frequency of appearance were assigned. Then a weighted average distance for evaluation of the method was calculated. It was noticed that for raw point cloud the obtained ratio of improvement is around three times lower than in the case of mesh of triangles. It is caused by the fact that in raw point cloud the ratio of random errors to systematic errors is higher. Also higher average distance

between point cloud and reference data before fusion for mesh of triangles was noticed. It is the effect of formation of mesh of triangles, which affects shape, diameter and position of surfaces and features. A similar situation occurred for measurements of ceramic balls, where for example the creation of mesh of triangles from raw data resulted in an increase of dimension error from 90 μm to about 120 μm. The maximal improvement for this part was higher than 16 %, less than for the plane. It is caused by higher curvature of the blade. Lower improvement was obtained for raw point cloud, which is caused by noise in the unprocessed data.

The next freeform surface was the engine cover of a car. For this part similar actions as for the turbine blade were performed. Both point clouds, before and after application of data fusion method, were compared with the reference. Both raw point cloud and cloud after creation of mesh of triangles were used. An analysis on statistical distribution of distances between points from these clouds and closest points from reference data was performed. Then a weighted average was calculated.

Results showed that in this case the improvement is lower than for turbine blade but also input data is burdened with smaller error, which is caused by smaller curvature of the part.

It was noticed that, as for turbine blade, for raw point cloud the obtained ratio of improvement is lower than in the case of mesh of triangles. It is caused by the fact that in raw point cloud the ratio of random errors to systematic errors is higher. Also here the higher average distance between point cloud and reference data before fusion for mesh of triangles was noticed. It is the effect of formation of mesh of triangles.

The method of data fusion was also tested using the virtual markers method.

First the method was evaluated using computer simulation for two planar curves: line and arc. Different density of characteristic points was tested. For the highest distance between characteristic points (~20 mm) the improvement was of almost 90 % and for the lowest (~7 mm) more than 98 %.

Then the simulation was performed for an arc. Here for similar distances between characteristic points the improvement was between 54 % and 92 %. The obtained results demonstrated the validity of the proposed method of data fusion. For more characteristic points the ratio of improvement is higher. The data fusion method does not distort the shape of the initial measurement error for any number of characteristic points for none of the presented curves.

Then for evaluation, the same parts as for material markers were used, although the plane was replaced by granite table with higher dimension than the reference cube. For all parts three coordinate balls were fixed on or around the measured part to ensure a common coordinate system. To have reference data the parts were measured by gathering a net of mutually perpendicular lines using contact method.

The first part was the plane represented by a granite table. Before application of the proposed method a mesh of triangles was created from the non-contact point cloud to limit the number of points and so the computing time. Similarly as in all previous parts the point clouds before and after application of the proposed method were compared with reference data. For point clouds before and after data fusion their distances to the reference data were determined and so statistical distribution of these distances were calculated. Then the weighted average distance was calculated. To check the influence of the size of selected virtual markers, three diameters were selected 10 mm, 20 mm and 30 mm. It was noted that for a smaller size of the virtual marker sphere, better results were obtained.

For all sizes of virtual markers the results showed that the application of the developed fusion method decreased the weighted average of distances by three orders of magnitude. It should be highlighted that the shape is simple and the number of characteristic points used for fusion was high.

The proposed method was also evaluated on freeform surfaces. The first example of freeform surface was a turbine blade. A net of lines was measured using contact method to get reference data for comparison. Both point clouds, before and after application of the proposed method were compared with this reference. Data from the non-contact device had two forms: raw point cloud and mesh of triangles with fewer points.

A statistical analysis of the distances between point clouds before and after fusion and reference data was performed and weighted average was determined.

Results show the usefulness of the proposed method for a freeform surface. For both forms of data the obtained ratio of improvement was similar. For mesh of triangles it was about 73% and for raw point cloud about 76% compared to the data before data fusion. It is few times more than for material markers. Simulation showed that the dependency between ratio of improvement and distance between markers for simulation data is linear. If the distance between markers was 12

mm then the ratio of improvement should be around 80 %. This shows the ability to transfer the method tested on simulation data onto real data.

Similarly as for all previous examples the initial (before data fusion) average distance between point cloud and reference data is higher for mesh of triangles, comparing to raw data.

Then the method was evaluated on the engine cover of a car. For the evaluation point clouds before and after fusion were compared with the reference data from contact measurements of the analysed surface. Based on statistical distribution of distances point cloud – reference data average distance was calculated. Data from the non-contact device had two forms: a raw point cloud and mesh of triangles with fewer points.

Here for bigger part but smaller curvature and smaller number of characteristic points the obtained improvement was of 47 % and 43 % for mesh and raw data respectively. It should be noted that the distance before application of data fusion was much smaller than for turbine blade. It is due to good optical characteristics of the measured surface and simplicity of the shape. For this part again higher distance between point cloud before fusion and reference data was observed for mesh of triangles.

The developed method was also evaluated based on data from measurements of big part from aircraft industry – fuel tank. Point clouds before and after fusion were compared with reference data from contact measurement and average distances point cloud – reference data were determined. In this case to limit processing time only the mesh of triangles was used for analysis. It was noted that data from non-contact measurement was improved by almost 56 % and the maximal distance point cloud – reference data was decreased by more than 150 μm. The biggest improvement can be observed in areas where the initial distortion was the highest.

Based on cross-section of point cloud it was observed how data fusion moved the points from the point cloud closer to the reference data. It was observed that the systematic error was decreased.

An important advantage was revealed be the presence of edge (wrinkle) on the surface. As this area was not measured when gathering points using the contact method (characteristic points), this detail would be lost. But the edge was detected by non-contact measurement, so after data fusion information about the inspected part is complete and more precise than only from non-contact measurement.

Based on uncertainty analysis presented in subchapter 4.1.6 it was shown that a reduction of uncertainty was achieved. For the devices used the uncertainty was decreased by more than 40%.

The presented results showed that the set objectives have been met. Two sets of data with fundamentally different nature were fused. A first set, from non-contact method, is characterized by a low precision but high density of points (HDLP). A second set comes from contact measurements and has low density of points but also higher precision (LDHP). Results showed that based on both sets one set with high precision and high density of points (HDHP) was achieved.

BIBLIOGRAPHY

1. Ascione, R., et al., *Adaptive inspection in coordinate metrology based on kriging models.* Precision Engineering, 2013. **37**(1): p. 44-60.

2. Besl, P.J. and N.D. McKay, *A method for registration of 3-D shapes.* IEEE Transactions on Pattern Analysis and Machine Intelligence, 1992. **14**(2): p. 239-256.

3. Blanco, D., et al. *Influence of surface material on the quality of laser triangulation digitized point clouds for reverse engineering tasks*. in *2009 IEEE Conference on Emerging Technologies and Factory Automation, ETFA 2009, September 22, 2009 - September 26, 2009*. 2009. Mallorca, Spain: IEEE Computer Society.

4. Boudjemaa, R. and A.B. Forbes, *Report to the National Measurement System Policy Unit, Department of Trade and Industry. From the Software Support for Metrology Programme. Parameter estimation methods for data fusion*. 2004, Nat. Phys. Lab., Teddington, UK: UK. p. ii+45.

5. Bracun, D., M. Jezerek, and J. Diaci, *Triangulation model taking into account light sheet curvature.* Measurement Science and Technology, 2006. **17**(8): p. 2191-2196.

6. Bradley, C. and V. Chan, *A Complementary Sensor Approach to Reverse Engineering.* J Manuf Sci Eng, 2001. **123**(1): p. 74-82.

7. Carbone, V., et al., *Combination of a vision system and a coordinate measuring machine for the reverse engineering of freeform surfaces.* International Journal of Advanced Manufacturing Technology, 2001. **17**(4): p. 263-71.

8. Chan, V.H., C. Bradley, and G.W. Vickers, *A multi-sensor approach to automating co-ordinate measuring machine-based reverse engineering.* Computers in Industry, 2001. **44**(2): p. 105-15.

9. Colosimo, B.M., G. Moroni, and S. Petro, *A tolerance interval based criterion for optimizing discrete point sampling strategies.* Precision Engineering, 2010. **34**(4): p. 745-54.

10. Colosimo, B.M., M. Pacella, and N. Senin, *Multisensor data fusion via Gaussian process models for dimensional and geometric verification.* Precision Engineering, 2015. **40**: p. 199-213.

11. Contri, A., P. Bourdet, and C. Lartigue, *Quality of 3D digitised points obtained with non-contact optical sensor.* CIRP Annals - Manufacturing Technology, 2002. **51**(1): p. 443-446.

12. Cuesta, E., et al., *Influence of roughness on surface scanning by means of a laser stripe system.* International Journal of Advanced Manufacturing Technology, 2009. **43**(11-12): p. 1157-66.

13. Dimitri, K., *Reliability Engineering Handbook.* Prentice Hall, Inc., Englewood Cliffs, New Jersey, 1991. **Vol. 1**.

14. Dumas, A., et al., *AK-ILS: An active learning method based on Kriging for the inspection of large surfaces.* Precision Engineering, 2013. **37**(1): p. 1-9.

15. Edgeworth, R. and R.G. Wilhelm, *Adaptive sampling for coordinate metrology.* Precision Engineering, 1999. **23**(3): p. 144-154.

16. ElMaraghy, W. and C. Rolls, *Design by quality product digitization.* CIRP Annals - Manufacturing Technology, 2001. **50**(1): p. 93-96.

17. Feng, H.-Y., Y. Liu, and F. Xi, *Analysis of digitizing errors of a laser scanning system.* Precision Engineering, 2001. **25**(3): p. 185-191.

18. Franca, J.G.D.M., et al. *A 3D scanning system based on laser triangulation and variable field of view*. in *IEEE International Conference on Image Processing 2005, ICIP 2005, September 11, 2005 - September 14, 2005*. 2005. Genova, Italy: Institute of Electrical and Electronics Engineers Computer Society.

19. Gelfand, N., et al. *Geometrically stable sampling for the ICP algorithm*. in *Proceedings Fourth International Conference on 3-D Digital Imaging and Modeling. 3DIM 2003, 6-10 Oct. 2003*. 2003. Los Alamitos, CA, USA: IEEE Comput. Soc.

20. Gruen, A. and D. Akca, *Least squares 3D surface and curve matching.* ISPRS Journal of Photogrammetry and Remote Sensing, 2005. **59**(3): p. 151-74.

21. Gunnarsson, K.T. and F.B. Prinz, *CAD model-based localization of parts in manufacturing.* Computer, 1987. **20**(8): p. 66-74.

22. Hannachi, A., et al. *Multi-sensor data fusion for realistic and accurate 3d reconstruction*. in *5th European Workshop on Visual Information Processing, EUVIP 2014, December 10, 2014 - December 12, 2014*. 2015. Paris, France: Institute of Electrical and Electronics Engineers Inc.

23. Huang, Y. and X. Qian. *A dynamic sensing-and-modeling approach to 3D point- And area-sensor integration*. in *International Conference on Manufacturing Science and Engineering, MSEC 2006, October 8, 2006 - October 11, 2006*. 2006. Ypsilanti, MI, United states: American Society of Mechanical Engineers.

24. ISO, *ISO 10360-5:2010, Geometrical product specifications (GPS) -- Acceptance and reverification tests for coordinate measuring machines (CMM)*. Part 5: CMMs using single and multiple stylus contacting probing systems. 2010.

25. ISO/TS, *ISO/TS 15530-3:2004, Geometrical Product Specifications (GPS) -- Coordinate measuring machines (CMM): Technique for determining the uncertainty of measurement*. Part 3: Use of calibrated workpieces or standards. 2004.

26. Jamshidi, J., A. Mileham, and G. Owen, *Rapid and Accurate Data Integration Method for Reverse Engineering Applications*, in *Advances in Integrated Design and Manufacturing in Mechanical Engineering II*, S. Tichkiewitch, M. Tollenaere, and P. Ray, Editors. 2007, Springer Netherlands. p. 163-175.

27. Jamshidi, J., G.W. Owen, and A.R. Mileham, *A new data fusion method for scanned models.* Journal of Computing and Information Science in Engineering, 2006. **6**(4): p. 340-348.

28. Janecki, D., K. Stępień, and S. Adamczak, *Sphericity measurements by the radial method: I. Mathematical fundamentals.* Measurement Science and Technology, 2016. **27**(1): p. 015005.

29. JCGM, *International vocabulary of metrology - basic and general concepts and associated terms (VIM)*. 2008: JCGM.

30. Kuang-Chao, F. and T. Tung-Hsien, *Optimal shape error analysis of the matching image for a free-form surface.* Robotics and Computer-Integrated Manufacturing, 2001. **17**(3): p. 215-22.

31. Lartigue, C., A. Contri, and P. Bourdet, *Digitised point quality in relation with point exploitation.* Measurement, 2002. **32**(3): p. 193-203.

32. Lee, K.H., H. Park, and S. Son, *A framework for laser scan planning of freeform surfaces.* International Journal of Advanced Manufacturing Technology, 2001. **17**(3): p. 171-180.

33. Li, Y. and P. Gu. *Free-form surface inspection techniques state of the art review*. 2004. Elsevier Ltd.

34. Li, Y.F. and Z.G. Liu, *Method for determining the probing points for efficient measurement and reconstruction of freeform surfaces.* Measurement Science & Technology, 2003. **14**(8): p. 1280-8.

35. Liang-Chia, C. and G.C.I. Lin, *A vision-aided reverse engineering approach to reconstructing free-form surfaces.* Robotics and Computer-Integrated Manufacturing, 1997. **13**(4): p. 323-36.

36. MacKinnon, D.K., V. Aitken, and F. Blais. *A comparison of precision and accuracy in triangulation laser range scanners*. in *2006 Canadian Conference on Electrical and Computer Engineering, 7-10 May 2006*. 2007. Piscataway, NJ, USA: IEEE.

37. Martinez, S., et al., *Analysis of laser scanning and strategies for dimensional and geometrical control.* Int J Adv Manuf Technol, 2010. **46**: p. 621-629.

38. Menq, C.H., H.T. Yau, and G.Y. Lai, *Automated precision measurement of surface profile in CAD-directed inspection.* IEEE Transactions on Robotics and Automation, 1992. **8**(2): p. 268-78.

39. Nafi, A., J.R.R. Mayer, and A. Wozniak, *Novel CMM-based implementation of the multi-step method for the separation of machine and probe errors.* Precision Engineering, 2011. **35**(2): p. 318-328.

40. Pedone, P., G. Vicario, and D. Romano, *Kriging-based sequential inspection plans for coordinate measuring machines.* Applied Stochastic Models in Business and Industry, 2009. **25**(2): p. 133-149.

41. Rak, M., et al., *The Effect of Scanning Strategy on a Ball Artifact Measured Geometry*, in *2nd International Conference on Virtual Machining Process Technology*. 2013: Hamilton, Canada.

42. Rak, M. and A. Wozniak, *Wpływ algorytmu przetwarzania chmury punktów na dokładność wyznaczenia wymiaru małych elementów* in *VI National Congress of Metrology*. Kielce, Poland.

43. Rak, M. and A. Wozniak, *The influence of properties of a measured object on the surface digitalization performed by a laser scanner integrated with measuring arm.* Measurement Automation and Robotics, 2012. **12/2012**: p. 76-81.

44. Rak, M. and A. Woźniak, *The influence of properties of a measured object on the surface digitalization performed by a laser scanner integrated with measuring arm.* Pomiary Automatyka Robotyka, 2012. **12/2012**: p. 76-81.

45. Rak, M. and A. Woźniak, *Systematic errors of measurements on a measuring arm equipped with a laser scanner on the results of optical measurements*, in *Advanced Mechatronics Solutions*, R. Jabłoński and T. Brezina, Editors. 2016, Springer International Publishing. p. 355-360.

46. Rak, M., A. Woźniak, and J.R.R. Mayer, *Influence of the scanning path on the surface digitalization*, in *Accuracy in coordinate metrology*, A. Woźniak, Editor. 2012, WYDAWNICTWO NAUKOWE AKADEMII TECHNICZNO-HUMANISTYCZNEJ. p. 86-95.

47. Rak, M.B., R. Mayer, and A. Wozniak, *Proximity weighted correction of high density high uncertainty (HDHU) point cloud using low density low uncertainty (LDLU) reference point coordinates.* Optics and Lasers in Engineering, 2015. **68**: p. 160-165.

48. Rak, M.B., A. Wozniak, and J.R.R. Mayer, *The use of low density high accuracy (LDHA) data for correction of high density low accuracy (HDLA) point cloud.* Optics and Lasers in Engineering, 2016. **81**: p. 140-150.

49. Santolaria, J., et al., *A one-step intrinsic and extrinsic calibration method for laser line scanner operation in coordinate measuring machines.* Measurement Science & Technology, 2009. **20**(4): p. 045107 (12 pp.).

50. Senin, N., B.M. Colosimo, and M. Pacella, *Point set augmentation through fitting for enhanced ICP registration of point clouds in multisensor coordinate metrology.* Robotics and Computer-Integrated Manufacturing, 2013. **29**(1): p. 39-52.

51. Seokbae, S., P. Hyunpung, and K.H. Lee, *Automated laser scanning system for reverse engineering and inspection.* International Journal of Machine Tools & Manufacture, 2002. **42**(8): p. 889-97.

52. Shen, T.-S., *Multiple-sensor integration for rapid and high-precision coordinate metrology.* IEEE/ASME Transactions on Mechatronics, 2000. **5**(2): p. 110-121.

53. Sitnik, R., et al. *New concept of fast hybrid contact and no-contact measurement for automotive industry*. 2006.

54. Sładek, J., et al., *The hybrid contact–optical coordinate measuring system.* Measurement, 2011. **44**(3): p. 503-510.

55. Tansky, D., et al. *Multi-sensor multi-resolution data fusion modeling*. in *24th CIRP Design Conference 2014: Mass Customization and Personalization, April 14, 2014 - April 16, 2014*. 2014. Milano, Italy: Elsevier.

56. Van Gestel, N., et al., *A performance evaluation test for laser line scanners on CMMs.* Optics and Lasers in Engineering, 2009. **47**(3-4): p. 336-342.

57. Vukainovic, N., et al., *The influence of incident angle, object colour and distance on CNC laser scanning.* International Journal of Advanced Manufacturing Technology, 2010. **50**(1-4): p. 265-274.

58. Vukainovic, N., J. Mozina, and J. Duhovnik, *Correlation between incident angle, measurement distance, object colour and the number of acquired points at CNC laser scanning.* Strojniski Vestnik/Journal of Mechanical Engineering, 2012. **58**(1): p. 23-28.

59. Vukasinovic, N., M. Korosec, and J. Duhovnik, *The Influence of Surface Topology on the Accuracy of Laser Triangulation Scanning Results.* Strojniski Vestnik, 2010. **56**(1): p. 23-30.

60. Wang, J., X. Jiang, and L. Blunt, *Simulation of Adaptive Sampling in Profile Measurement for Structured Surfaces* in *Future Technologies in Computing and Engineering: Proceedings of Computing and Engineering Annual Researchers' Conference 2010: CEARC'10*. 2010. p. 48-53.

61. Wang, L., H. Ding, and S. Wang. *Measurement error compensation using data fusion technique for laser scanner on AACMMs*. in *3rd International Conference on Intelligent Robotics and Applications, ICIRA 2010, November 10, 2010 - November 12, 2010*. 2010. Shanghai, China: Springer Verlag.

62. Weckenmann, A., et al., *Multisensor data fusion in dimensional metrology.* CIRP Annals - Manufacturing Technology, 2009. **58**(2): p. 701-721.

63. Wozniak, A. and J.R.R. Mayer, *Discontinuity check of scanning in coordinate metrology.* Measurement, 2015. **59**: p. 284-289.

64. Woźniak, A. and M. Dobosz, *Influence of measured objects parameters on CMM touch trigger probe accuracy of probing.* Precision Engineering, 2005. **29**(3): p. 290-297.

65. Xi, F., Y. Liu, and H.Y. Feng, *Error compensation for three-dimensional line laser scanning data.* International Journal of Advanced Manufacturing Technology, 2001. **18**(3): p. 211-216.

66. Zussman, E., H. Schuler, and G. Seliger, *Analysis of the geometrical features detectability constraints for laser-scanner sensor planning.* The International Journal of Advanced Manufacturing Technology, 1994. **9**(1): p. 56-64.

APPENDIX A – THE SPECIFICATION OF LEGEX 9106

Length standard	Ultra-high accuracy linear encoder (glass scale with virtually zero thermal expansion coefficient)
Guide system	Air bearing (linear guide: LEGEX 322)
Max. drive speed, mm/s	200
Max. acceleration, G	0.1 (0.06: LEGEX 322)
Range	
X-axis, mm	910
Y-axis, mm	1010
Z-axis, mm	605
Resolution, µm	0.01
Accuracy	
E_{MPE}, µm	(0.50+L/1000)
P_{MPE}, µm	0.45
Work Tabela	
Material	Cast iron
Size, mm	950 x 1050
Tapped insert, mm	M8 x 1.25
Work piece	
Max. height, mm	856
Max. load, kg	800
Mass (main unit), kg	6500

APPENDIX B – THE SPECIFICATION OF ACCURA 7

Length standard	Linear encoder (zero-dur scales with patented thermally neutral frame)
Guide system	Air bearings
Max. drive speed, mm/s	520
Max. acceleration, G	0.24
Range	
X-axis, mm	900
Y-axis, mm	1200
Z-axis, mm	700
Accuracy	
E_{MPE}, µm	(1.7+L/333)
P_{MPE}, µm	1.7
Work Tabela	
Material	Granite
Tapped insert, mm	M8 x 1.25
Work piece	
Max. height, mm	800
Max. load, kg	1300

APPENDIX C – THE SPECIFICATION OF REVSCAN

Weight, g	980
Dimensions, mm	160 x 260 x 210
Measurement Rate, measures/s	18 000
Laser Class	II (eye-safe)
Resolution, mm	0.100 mm
Accuracy, mm	Up to 0.050
Volumetric Accuracy[1]	0.020 mm + 0.200 mm/m
Volumetric Accuracy[1] (with MaxSHOT 3D)	0.020 mm + 0.025 mm/m
Stand-Off Distance, mm	300
Depth of Field, mm	± 150
Laser Cross Area, mm	210 x 210
Software	VXelements
Output Formats	.dae, .fbx, .ma, .obj, .ply, .stl, .txt, .wrl, .x3d, .x3dz, .zpr

[1] Based on the ISO 10360 standard, volumetric accuracy is defined as a size-dependent value.

APPENDIX D – THE SPECIFICATION OF MMC80

Stripe width (Y), mm	80
Start measuring range, mm	100
Measuring range (Z), mm	100
Accuracy (2σ), μm	35
Max data rate, real pts/sec[2]	24
Points per stripe[2]	800
Max speed, stripes/sec	30
Temperature compensation	No
Sensor weight, g	410
Laser power Class	Class 2M
Localiser compatibility	Metris MCA (6 and 7 axis) Metris K-Scan (all variants) Romer/Cimcore Infinite/Stinger (6 and 7 axis) Faro Platinum/Titanium/Fusion/Quantum (6 and 7 axis)

[2] Metris points-per-second and points-per-stripe specifications state real scan points only. No interpolation techniques are used to oversample the point clouds.